CONVECTIVE HEAT TRANSFER OF CATTANEO-CHRISTOV HEAT FLUX MODEL OVER A WEDGE

MUHAMMAD SOLLEH ASMADI

FACULTY OF SCIENCE
UNIVERSITY OF MALAYA
KUALA LUMPUR

2019

CONVECTIVE HEAT TRANSFER OF CATTANEO-CHRISTOV HEAT FLUX MODEL OVER A WEDGE

MUHAMMAD SOLLEH ASMADI

DISSERTATION SUBMITTED IN FULFILMENT OF THE REQUIREMENTS FOR THE DEGREE OF MASTER OF SCIENCE

INSTITUTE OF MATHEMATICAL SCIENCES
FACULTY OF SCIENCE
UNIVERSITY OF MALAYA
KUALA LUMPUR

2019

UNIVERSITI MALAYA

ORIGINAL LITERARY WORK DECLARATION

Name of Candidate: Muhammad Solleh Asmadi

Registration/Matric No.: SMA170010

Name of Degree: Master of Science

Title of Project Paper/Research Report/Dissertation/Thesis (“this Work”):

Convective Heat Transfer of Cattaneo-Christov Heat Flux Model Over a Wedge

Field of Study: Computational Fluid Dynamics

I do solemnly and sincerely declare that:

(1) I am the sole author/writer of this Work;
(2) This Work is original;
(3) Any use of any work in which copyright exists was done by way of fair dealing and for permitted purposes and any excerpt or extract from, or reference to or reproduction of any copyright work has been disclosed expressly and sufficiently and the title of the Work and its authorship have been acknowledged in this Work;
(4) I do not have any actual knowledge nor do I ought reasonably to know that the making of this work constitutes an infringement of any copyright work;
(5) I hereby assign all and every rights in the copyright to this Work to the University of Malaya (“UM”), who henceforth shall be owner of the copyright in this Work and that any reproduction or use in any form or by any means whatsoever is prohibited without the written consent of UM having been first had and obtained;
(6) I am fully aware that if in the course of making this Work I have infringed any copyright whether intentionally or otherwise, I may be subject to legal action or any other action as may be determined by UM.

Candidate’s Signature Date:

Subscribed and solemnly declared before,

Witness’s Signature Date:

Name:

Designation:

CONVECTIVE HEAT TRANSFER OF CATTANEO-CHRISTOV HEAT FLUX MODEL OVER A WEDGE

ABSTRACT

The convective boundary layer flow, heat and mass transfer of Cattaneo-Christov heat flux model over a wedge is investigated. The heat transfer of two-dimensional, steady, incompressible laminar flow of upper-convected Maxwell fluid and Carreau fluid past a horizontal plate and a horizontal wedge are studied by using Cattaneo-Christov heat flux model. The mathematical formulation of the governed equation is presented. Similarity transformation for local similarity solution is used to reduce the partial differential equations to nonlinear ordinary differential equations. The resulting nonlinear ordinary differential equations are solved numerically using second-order and third-order finite difference method. Comparisons of present result with previously published results are done and they are found to be in good agreement. The numerical values of local skin friction coefficient, local Nusselt number and local Sherwood number are tabulated. The effects of local Deborah number, Weissenberg number, wedge angle parameter, power-law index, Prandtl number, Schmidt number, suction parameter, heat generation/absorption parameter, heat radiation parameter and chemical reaction parameter on the fluid velocity, temperature and concentration profiles are presented graphically and discussed in details. Several dimensional forms of the system are provided and the heat map of the thermal boundary layer with different parameters are analysed.

Keywords: Cattaneo-Christov heat flux model, finite difference method, upper-convected Maxwell fluid, Carreau fluid, horizontal wedge.

PEMINDAHAN HABA BEROLAK DENGAN MODEL FLUKS HABA CATTANEO-CHRISTOV KE ATAS BAJI

ABSTRAK

Aliran lapisan sempadan berolak, pemindahan haba dan jisim dengan model fluks haba Cattaneo-Christov ke atas baji mendatar telah dikaji. Pemindahan haba bagi aliran dua matra, mantap, tak termampat, bendalir lamina berolak atas Maxwell dan bendalir Carreau melepasi satu permukaan mendatar dan satu baji mendatar dikaji dengan menggunakan model fluks haba Cattaneo-Christov. Perumusan matematik bagi persamaan menakluk dipaparkan. Transformasi keserupaan untuk penyelesaian keserupaan setempat digunakan untuk menurunkan persamaan pembezaan separa kepada persamaan pembezaan biasa tak linear. Persamaan pembezaan biasa tak linear yang terhasil diselesaikan secara berangka dengan menggunakan kaedah beza terhingga bagi peringkat kedua dan ketiga. Perbandingan keputusan sekarang dengan keputusan terdahulu yang telah diterbitkan dilakukan dan didapati sangat memuaskan. Nilai berangka pekali geseran kulit setempat, nombor Nusselt setempat dan nombor Sherwood setempat dipaparkan dalam bentuk jadual. Kesan nombor Deborah setempat, nombor Weissenberg, parameter sudut baji, indeks hukum kuasa, nombor Prandtl, nombor Schmidt, parameter sedutan, parameter penjanaan haba/penyerapan, parameter radiasi haba dan parameter reaksi kimia pada profil halaju, suhu dan kepekatan bendalir dibentangkan secara grafik dan dibincangkan secara terperinci. Beberapa bentuk dimensi sistem disediakan dan peta haba lapisan sempadan haba dengan parameter yang berbeza dianalisis.

Kata Kunci: model fluks haba Cattaneo-Christov, kaedah beza terhingga, bendalir berolak atas Maxwell, bendalir Carreau, baji mendatar.

ACKNOWLEDGEMENTS

I would like to thank my supervisors, Dr Zailan Siri and Dr Ruhaila Md. Kasmani, for their patient guidance, encouragement and advice they have provided throughout my time as their student. I have been extremely thankful to have supervisors who cared so much about my work, and who responded to my questions and thoughts regarding this work. I would also like to thank them for giving me the freedom to choose my topic, at the same time giving me precious advice to complete my work in this dissertation.

I would like to express my gratitude to the University of Malaya for the opportunity to be a Graduate Research Assistant during the period of this study is conducted. This experience makes me realised how a research should be done in an orderly manner.

I would like to thank my parents, Asmadi Mat Safar and Kamariah Md. Daril, and my family members for their great sacrifice materially and emotionally and giving support throughout my research period.

Finally, I am indebted to all my friends who helped me along my journey to complete this study especially my roommates and the juniors of my *kompang* team who are always there whenever I cannot cope with my research.

TABLE OF CONTENTS

Abstract iii

Abstrak iv

Acknowledgements v

Table of Contents vi

List of Figures xi

List of Tables xiv

List of Symbols and Abbreviations xv

CHAPTER 1: INTRODUCTION 1

1.1 Fluid Dynamics 1

1.2 Boundary Layer 1

1.3 Upper-Convected Maxwell Fluid Model 2

1.4 Carreau Fluid Model 3

1.5 Heat Transfer 4

1.5.1 Conduction 4

1.5.2 Convection 5

1.5.3 Radiation 5

1.6 Types of Convection 6

1.6.1 Natural Convection 6

1.6.2 Forced Convection 6

1.7 Cattaneo-Christov Heat Flux Model 7

1.8 Mass Transfer 8

1.9 Research Objectives 8

1.10 Problem Statement 9

1.11 Significane of research 9

1.12 Thesis Organisation 10

CHAPTER 2: LITERATURE REVIEW **12**

2.1 Boundary Layer Flow over a Horizontal Plate 13

2.2 Boundary Layer Flow over a Horizontal Wedge 15

2.3 Boundary Layer Flow of Upper-Convected Maxwell Fluid 17

2.4 Boundary Layer Flow of Carreau Fluid 19

2.5 Boundary Layer Flow with Cattaneo-Christov Heat Flux Model 21

2.6 Boundary Layer Flow with Magnetohydrodynamic 22

2.7 Boundary Layer Flow with Suction/Injection 23

2.8 Boundary Layer Flow with Heat Generation/Absorption 24

2.9 Boundary Layer Flow with Heat Radiation 26

2.10 Boundary Layer Flow with Chemical Reaction 27

CHAPTER 3: MATHEMATICAL FORMULATION **29**

3.1 Introduction 29

3.2 The Boundary Layer Flow Model 29

3.2.1 The Continuity Equation 30

3.2.2 The Momentum Equation 32

3.2.3 The Momentum Equation of Upper-Convected Maxwell Fluid 34

3.2.4 The Momentum Equation of Carreau Fluid 35

3.2.5 The General Thermal Energy Equation 36

3.2.6 The Thermal Energy Equation of Cattaneo-Christov Heat Flux Model . 38

3.2.7 The Concentration Equation 38

3.2.8 The Boundary Conditions 40

3.2.9 The Stream Function 41

3.3 Similarity Transformation for the Boundary Layer Equations 41

3.3.1 Similarity Transformation for a Horizontal Plate 42

3.3.2 Similarity Transformation for a Horizontal Wedge 44

3.3.3 The Dimensionless Boundary Conditions 46

3.3.4 Local Similarity Solution 46

3.3.5 Local Similarity Solution for Horizontal Plate...................................... 47

3.3.6 Local Similarity Solution for Horizontal Wedge.................................... 48

3.4 The Local Skin Friction Coefficient, Local Nusselt Number and Local Sherwood Number 49

3.5 Numerical Method 50

3.5.1 Second-Order Ordinary Differential Equation 51

3.5.2 Third-Order Ordinary Differential Equation 53

3.6 Code Validation.. 55

CHAPTER 4: NUMERICAL ANALYSIS OF MASS AND HEAT TRANSFER FOR SAKIADIS AND BLASIUS FLOWS OF UPPER-CONVECTED MAXWELL FLUID WITH CATTANEO-CHRISTOV HEAT FLUX MODEL OVER A HORIZONTAL PLATE... 58

4.1 Mathematical Formulation.. 58

4.2 Results and Discussion 61

CHAPTER 5: NUMERICAL STUDY OF MASS AND HEAT TRANSFER FOR SAKIADIS FLOW OF MAGNETOHYDRODYNAMIC CARREAU FLUID OVER A HORIZONTAL PLATE USING CATTANEO-CHRISTOV HEAT FLUX MODEL........................ 70

5.1 Mathematical Formulation... 70

5.2 Results and Discussion 73

CHAPTER 6: CONVECTIVE BOUNDARY LAYER OF UPPER-CONVECTED MAXWELL FLUID OVER A HORIZONTAL WEDGE WITH SUCTION AND HEAT GENERATION/ABSORPTION USING CATTANEO-CHRISTOV HEAT FLUX MODEL........................ 82

6.1 Mathematical Formulation... 82

6.2 Results and Discussion 84

CHAPTER 7: HEAT TRANSFER ANALYSIS OF UPPER-CONVECTED MAXWELL FLUID OVER A HORIZONTAL WEDGE IN THE PRESENCE OF HEAT GENERATION/ABSORPTION, CHEMICAL REACTION, SUCTION AND HEAT RADIATION USING CATTANEO-CHRISTOV HEAT FLUX MODEL........................ 93

7.1 Mathematical Formulation... 93

7.2 Results and Discussion 96

CHAPTER 8: CONCLUSIONS AND RECOMMENDATIONS 110

8.1 Conclusions 110

8.2 Recommendations for Future Study 112

References 113

LIST OF FIGURES

Figure 2.1: Several boundary layer geometries 12
(a) A horizontal wedge 12
(b) A horizontal plate when $\beta_w = 0$ 12

Figure 3.1: The control volume element in the boundary layer region 30

Figure 3.2: The control element in the boundary layer region with the mass flow across the element 31

Figure 3.3: The stresses exerted by the control element 32

Figure 3.4: The external forces exerting on control element and the momentum fluxes across the control element 33

Figure 3.5: The energy-transfer term for a control element 36

Figure 3.6: The mass transfer term for a control element 39

Figure 3.7: The flowchart of the algorithm for second-order finite difference method (FDM) to solve second-order ordinary differential equation (ODE) 52

Figure 3.8: The flowchart of the algorithm for third-order finite difference method (FDM) to solve third-order ordinary differential equation (ODE) 56

Figure 4.1: The velocity profile for different values of β with Pr = Sc = 1 and $\gamma = 0.25$ 61

Figure 4.2: The temperature profile for different values of: (a) Pr when $\gamma = 0.3$; (b) γ when Pr = 1; with $\beta = 0.5$ and Sc = 1 64

Figure 4.3: The concentration profile for different values of Sc with $\beta = 0.5$, Pr = 1 and $\gamma = 0.3$ 65

Figure 4.4: The effect of β on $-\phi'(0)$ for different values of Sc 66

Figure 4.5: The heat map of: (a) Sakiadis flow; (b) Blasius flow; for air at $T_\infty = 20°C$ with $U_\infty = 100$ cm/s, $T_w = 70°C$, $\beta = 0.5$, $\gamma = 0.3$ and Sc = 1 67

Figure 4.6: The heat map of Sakiadis flow with (a) $\gamma = 0$, (b) $\gamma = 0.5$; for air at $T_\infty = 20°C$ with $U_\infty = 100$ cm/s, $T_w = 70°C$, $\beta = 0.5$ and Sc = 1 69

Figure 5.1: The velocity profile, temperature profile and concentration profile for different values of: (a) We when $n = 0.5$; (b) n when We = 0.5; with Pr = Sc = 1 and $\gamma = 0.2$ 74

Figure 5.2: The temperature profile for different values of: (a) γ when Pr= 1; (b) Pr when $\gamma = 0.5$; with We = n = 1 and Sc = 0.2 77

Figure 5.3: The concentration profile for different values of Sc with We = n = 0.5, Pr = 1 and $\gamma = 0.2$ 78

Figure 5.4: The heat map of: (a) Air; (b) Pure water; at $T_\infty = 20°C$ with $U_\infty = 100$ cm/s, $T_w = 70°C$, We = 0.5, $n = 1$, $\gamma = 0.2$ and Sc = 1 80

Figure 5.5: The heat map of air at: (a) $T_\infty = 5°C$; (b) $T_\infty = 25°C$; with $T_w = 70°C$, $U_\infty = 100$ cm/s, We = 0.5, $n = 1$ and Sc = 1 81

Figure 6.1: The velocity profile and temperature profile for different values of: (a) m when $\beta = 0.2$; (b) β when $m = 0.0141$; with $\gamma = \delta = 0.2$ and Pr= 2 87

Figure 6.2: The temperature profile for different values of γ with $m = 0.0141$, $\beta = \delta = 0.2$ and Pr = 2 88

Figure 6.3: The temperature profile for different values of: (a) Pr when $\delta = 0.2$; (b) δ when Pr = 2; with $m = 0.0141$ and $\beta = \gamma = 0.2$ 89

Figure 6.4: The heat map of gaseous ammonia with: (a) $m = 0$; (b) $m = 0.2$; at $T_\infty = 25°C$ with $T_w = 75°C$, $U_\infty = 100$ cm/s, and $\beta = \gamma = \delta = 0.2$ 91

Figure 6.5: The heat map of gaseous ammonia with: (a) $\delta = -0.2$; (b) $\delta = 0.2$; at $T_\infty = 25°C$ with $U_\infty = 100$ cm/s, $T_w = 75°C$, $m = 0.0141$ and $\beta = \gamma = 0.2$ 92

Figure 7.1: The velocity profile, temperature profile and concentration profile for different values of m with $\beta = \gamma = \delta = 0.2$, $s = 0.1$, Pr = 2, $K = 0.5$, $R = 5$ and Sc = 1 96

Figure 7.2: The velocity profile, temperature profile and concentration profile for different values of: (a) β when $s = 0.1$; (b) s when $\beta = 0.2$; with $m = 0.0141$, $\gamma = \delta = 0.2$, Pr = 2, $K = 0.5$, $R = 5$ and Sc = 1 100

Figure 7.3: The temperature profile for different values of: (a) Pr when $\gamma = 0.2$; (b) γ when Pr= 2; with $m = 0.0141$, $\beta = \delta = 0.2$, $s = 0.1$, $K = 0.5$, $R = 5$ and Sc = 1 102

Figure 7.4: The temperature profile for different values of: (a) δ when $R = 5$; (b) R when and $\delta = 0.2$; with $m = 0.0141$, $\beta = \gamma = 0.2$, $s = 0.1$, Pr= 2, $K = 0.5$ and Sc = 1 103

Figure 7.5: The concentration profile for different values of: (a) Sc when K = 0.5; (b) K when Sc= 1; with $m = 0.0141$, $\beta = \gamma = \delta = 0.2$, $s = 0.1$, Pr= 2 and $R = 5$ 104

Figure 7.6: The heat map of gaseous ammonia with: (a) $T_w = 55°$C; (b) $T_w = 115°$C; at $T_\infty = 25°$C with $U_\infty = 100$ cm/s, $m = 0.0141$, $s = 0.1$, $R = 7$ and $\beta = \gamma = \delta = 0.2$ 106

Figure 7.7: The heat map of gaseous ammonia with: (a) $R = 1.5$; (b) $R = 5$; at $T_\infty = 25°$C with $T_w = 55°$C, $U_\infty = 100$ cm/s, $m = 0.0141$, $s = 0.1$ and $\beta = \gamma = \delta = 0.2$ 107

Figure 7.8: The heat map of gaseous ammonia with: (a) $U_\infty = 50$ cm/s; (b) $U_\infty = 200$ cm/s; at $T_\infty = 25°$C with $T_w = 55°$C, $m = 0.0141$, $s = 0$, $R = 7$ and $\beta = \gamma = \delta = 0.2$ 108

LIST OF TABLES

Table 3.1: Comparison of the value of $f''(0)$ with different values of m from Yih (1998), Khan et al. (2013), Ganapathirao (2013) and Khan et al. (2014) with the present results where $\beta = 0$ 57

Table 4.1: The values of $f''(0)$, $-\theta'(0)$ and $-\phi'(0)$ for various values of β, Pr, γ and Sc 62

Table 4.2: The physical properties for selected fluid.......... 67

Table 5.1: The values of $f''(0)$, $-\theta'(0)$ and $-\phi'(0)$ for various values of We, n, Pr, γ and Sc 75

Table 5.2: The physical properties for selected fluids 79

Table 6.1: The values of $f''(0)$ and $-\theta'(0)$ for various values of m, β, Pr, γ and δ 85

Table 6.2: The physical properties for selected fluid.......... 90

Table 7.1: The values of $f''(0)$, $-\theta'(0)$ and $-\phi'(0)$ for various values of m, β, s, Pr, γ, δ, R, Sc and K 97

Table 7.2: The physical properties for selected fluid.......... 105

LIST OF SYMBOLS AND ABBREVIATIONS

A_1	:	First Rivlin-Eriksen tensor
a, b	:	Constants
a_1, a_2	:	Arbitrary domain boundary
B_0	:	Magnetic field
C	:	Local fluid concentration
C_f	:	Local skin-friction coefficient
C_p	:	Specific heat capacity
C_w	:	Fluid concentration at surface
C_∞	:	Ambient fluid concentration
$\mathbf{D}_r$	:	Deformation rate tensor
D	:	Fluid diffusivity
E_c	:	Convection fluid energy
E_i	:	Internal fluid energy
F	:	Momentum source function
f	:	Dimensionless stream function
$\mathbf{G}$	:	Mass flux
G_x, G_y	:	Mass flux in x- and y-directions
h	:	Uniform stepsize
$\mathbf{I}$	:	Identity tensor
$\mathbf{J}$	:	Diffusion flux vector
K	:	Chemical reaction parameter
K_f	:	Flow consistency parameter
K_0	:	Chemical reaction coefficient
k	:	Thermal conductivity
k_1	:	Mean absorption coefficient
M	:	Magnetic field parameter
m	:	Wedge angle parameter
N	:	Number of domain division
Nu	:	Nusselt number
n	:	Power-law index
P	:	Fluid pressure
Pr	:	Prandtl number
Q	:	Heat generation/absorption coefficient
$\mathbf{q}$	:	Heat flux
q_r	:	Radiative heat flux
R	:	Radiation parameter
Re_x	:	Reynolds number
Sc	:	Schmidt number

Sh	: Sherwood number
s	: Suction parameter
T	: Local fluid temperature
$\mathbf{T}_s$	: Cauchy stress tensor
$\mathbf{T}_s^u$	: Upper-convected time derivative for tress tensor
T_w	: Fluid temperature at surface
T_∞	: Ambient fluid temperature
t	: Time
U_w	: Fluid velocity at surface
U_∞	: Free stream velocity
u, v	: Velocity component in x- and y-direction
$\mathbf{V}$	: Fluid velocity vector
v_0	: Suction
We	: Weissenberg number
x, y	: Cartesian coordinates

Greek symbols

α	: Thermal diffusivity
$\alpha_1, \alpha_2, \alpha_3, \beta_1, \beta_2$	: Arbitrary boundary conditions
β	: Local Deborah number for velocity profile
β_w	: Hartree pressure gradient
β_0	: Fluid separation point
Γ	: Relaxation time for Carreau model
γ	: Local Deborah number for thermal profile
γ_c	: Mass diffusion parameter
$\dot{\gamma}$	: Fluid shear rate
δ	: Heat generation parameter
η	: Similarity variable
Θ	: Thermal source function
θ	: Dimensionless temperature
λ_1	: Fluid relaxation time
λ_2	: Heat flux relaxation time
μ	: Fluid viscosity
μ_0	: Fluid viscosity at zero shear rate
μ_∞	: Fluid viscosity at infinite shear rate
ν	: Kinematic viscosity
ξ	: Dimensionless distance
ρ	: Fluid density
σ	: Fluid normal stress
σ_s	: Stefan-Boltzmann constant

σ_c	:	Electrical conductivity
τ	:	Fluid shear stress
Φ	:	Concentration source function
ϕ	:	Dimensionless concentration
ψ	:	Stream function
Ω	:	Wedge angle

Subscripts

w	:	Condition at the surface
∞	:	Free stream/ambient conditions

Abbreviations

Al_2O_3	:	Alumina/Aluminium oxide
Cu	:	Copper
FDM	:	Finite difference method
HAM	:	Homotopy analysis method
MHD	:	Magnetohydrodynamic
ODE	:	Ordinary differential equation
PDE	:	Partial differential equation
TiO_2	:	Titania/Titanium oxide
UCM	:	Upper-convected Maxwell

CHAPTER 1: INTRODUCTION

1.1 Fluid Dynamics

Fluid mechanics is a branch of physics that takes into account the mechanics of fluids (such as plasmas, liquids and gases) and the forces on that medium. Fluid mechanics has two seemingly compelling fields of study; fluid statics and fluid dynamics. Fluid statics deals with fluids at rest, while fluid dynamics deals with the forces on the motion of fluids. The aim in fluid dynamics is to construct a mathematical model that can represent the motion of fluid under certain conditions. The motion of the fluid is governed by the following principles:

1. Conservation of mass.
2. Conservation of momentum (Newton's second law of motion).
3. Conservation of energy (first law of thermodynamics).

Some examples of applications of fluid dynamics include air-conditioning system in a room, water heater and air flow around an aeroplane.

1.2 Boundary Layer

The term boundary layer was coined by Ludwig Prandtl (1904), who bridged the idea of ideal and real fluids. At that time, the classical theory of inviscid flow stated that viscous forces in a fluid are relatively negligible compared to the inertial forces of the fluid. This statement is considered true as the viscosity of many fluids are extremely low. But in many cases, Prandtl noticed that viscous forces are still important in some local regions of fluids flow. He found that there is a thin layer between surface and fluid where the fluid sticks to the surface, most probably due to the friction force exerted to the fluid. This thin layer is called boundary layer.

In this region, the viscous forces and inertial forces are comparable in magnitude. In direction of normal to the surface, the flow accelerates from zero velocity at the surface to a relatively high free stream value away from the surface. Based on this observation, Prandtl classified two regions in the fluid; the boundary layer and outside the boundary layer. In the boundary layer, the viscosity of the fluid and skin friction are dominant, while outside the boundary layer, the flow is inviscid.

This observation greatly reduced the complexity of Navier-Stokes equations. The equations which modelled the boundary layer can be solved numerically using existing numerical method.

1.3 Upper-Convected Maxwell Fluid Model

The power-law model is a general model to describe the thinning and thickening behaviour of fluids. The law is also called as Ostwald-de Waele power law, named after Wilhelm Ostwald and Armand de Waele, the scientists who developed it. The power-law for generalised Newtonian fluid states that:

$$\sigma = K_f \left(\frac{\partial u}{\partial y} \right)^n , \tag{1.1}$$

where σ is the shear stress of the fluid, K_f is the flow consistency parameter and n is the power-law index. This model has some drawbacks, to which it cannot be used to describe the viscoelastic characteristics of the fluid. In addition, the model cannot describe the behaviour of the real non-Newtonian fluid. Maxwell (1867) proposed a fluid model based on the power-law model. His model captures the viscoelastic characteristic that lacks from the power-law model. The model is useful because it shows both elasticity and viscosity properties of a material. The generalisation of Maxwell material for large deformations is proposed by Oldroyd (1950), and it is called upper-convected Maxwell (UCM) model, named after James Maxwell using upper-convected time derivative. The UCM model states that,

$$\mathbf{T}_s + \lambda_1 \mathbf{T}_s^u = 2\mu \mathbf{D}_r, \tag{1.2}$$

where $\mathbf{T}_s$ is the stress tensor, λ_1 is the relaxation time of the material, μ is the material viscosity, $\mathbf{D}_r$ is the deformation rate tensor and $\mathbf{T}_s^u$ is the upper-convected time derivative of stress tensor in the form of,

$$\mathbf{T}_s^u = \frac{\partial}{\partial t}\mathbf{T}_s + \mathbf{V} \cdot \nabla \mathbf{T}_s - \left[(\nabla \mathbf{V})^T \cdot \mathbf{T} + \mathbf{T}_s^u \cdot (\nabla \mathbf{V}) \right], \tag{1.3}$$

where $\mathbf{V}$ is the fluid velocity vector.

1.4 Carreau Fluid Model

The power-law model for generalised Newtonian fluid from Eq.(1.1) cannot describe the flow of a fluid for a very small or a very large shear rates. This is due to the model can only describe the fluid behaviour for a range of shear rates which fit the coefficients used. To overcome this problem, Pierre Carreau (1972) proposed a model which captures the above missing characteristics from the power-law model. Carreau fluid is a model of generalised Newtonian fluid with the viscosity of the fluid depends on the shear rate of the fluid. The general Carreau fluid model is as follows,

$$\mathbf{T}_s = -P\mathbf{I} + \mu \mathbf{A}_1, \tag{1.4}$$

with the viscosity of the fluid μ to be,

$$\mu = \mu_\infty + (\mu_0 - \mu_\infty) \left[1 + (\Gamma \dot{\gamma})^2 \right]^{\frac{n-1}{2}}, \tag{1.5}$$

where μ_0 is the viscosity of the fluid at zero shear rate, μ_∞ is the viscosity at the infinite shear rate, Γ is the relaxation time of Carreau fluid, $\dot{\gamma}$ is the shear rate of the fluid, n is the power-index law, P is the pressure of the fluid, $\boldsymbol{T_s}$ is the stress tensor, $\mathbf{I}$ is the identity tensor and $\mathbf{A}_1$ is the Rivlin-Ericksen tensor.

This model is suitable for free surface flows such as suspensions of polymer behaviour in some problems. This is because the situation requires the viscosity of the fluid to be finite as the deformation rate becomes zero. For most practical cases, $\mu_0 >> \mu_\infty$ (Boger, 1977). When μ_∞ approaches zero, Eq.(1.4) becomes,

$$\boldsymbol{T_s} = -P\mathbf{I} + \mu_0 \left[1 + (\Gamma\dot{\gamma})^2\right]^{\frac{n-1}{2}} \mathbf{A}_1. \tag{1.6}$$

1.5 Heat Transfer

The concept of heat transfer refers to the exchange of thermal energy due to a temperature difference. The energy flows from a higher temperature region to a lower temperature region. According to the first law of thermodynamics, the internal energy of the medium involved is changed by heat transfer. Since energy is neither created nor destroyed, energy in a system must flow. There are three main methods of heat transfer; conduction, convection and radiation.

1.5.1 Conduction

Conduction describes the energy transfer when two mediums are in a physical contact. It occurs when any two combinations of solid and liquid such as solid-solid, solid-liquid or liquid-liquid are in contact. The energy is transferred by collisions and vibrations of particles of the medium involved. Some examples of conduction are:

1. A thumbtack are glued with some candles to one end of a metal rod. Then the other end of the rod is heated with flames. Eventually, the heat transferred to the candled thumbtack and melt the candle.

2. Ice cubes are put into a hot cup of tea. The ice will melt and the hot tea will become cold.
3. A candle is lighted and the flame makes the candle melt.

1.5.2 Convection

Convection occurs through collective movement of particles in fluids (such as liquids and gases). Contrary to conduction, the molecules that are undergoing convection carry energy itself and moves from a higher temperature region to a lower temperature region. The direction of movement of the energy depends on the position where heat is applied. Some examples of the application of convection are:

1. A metal pot containing water at room temperature is heated at the bottom of the pot by a gas burner. This creates a circular pattern of the heat distribution.
2. The cold air from air conditioning system comes from an air conditioner located at the top of a room. The interaction of cold and hot air particles creates a circular motion of air inside the room.

1.5.3 Radiation

Radiation occurs when thermal energy is transmitted using electromagnetic waves. This method does not require particles to transfer the heat. Random movement of particles in a medium creates a radiation. All matter with temperature above absolute zero temperature (0 K) emit thermal radiation. Some of the examples of thermal radiation are:

1. A microwave oven heats up food by emitting thermal radiation.
2. A person's body emits heat after heavy exercise to the surroundings in the form of radiation. The effect is more visible in a cold weather.
3. The sun radiates heat waves in outer space, eventually reach the Earth which keeps the Earth warm and habitable.

1.6 Types of Convection

There are three types of convection:

1. Natural convection.
2. Forced convection.
3. Mixed convection.

1.6.1 Natural Convection

Natural convection is a mechanism of heat transfer where the fluid motion is not generated by any external force. It depends only on density difference in fluids due to temperature gradients. Examples of natural convection are:

1. Hot potato that laid down on a table will eventually be cooled down by surrounding air at room temperature.
2. Warm seawater around the equator circulate towards the poles and the cold seawater from the poles moves towards the equator.

1.6.2 Forced Convection

As a contrary to natural convection, forced convection is a heat convection which facilitated by external forces such as a pump, a suction and a fan. Some of the examples are air conditioning system, car radiator using coolant and a convection oven.

When natural and forced convections are combined to transfer the heat, mixed convection phenomenon occurs. It is a situation where both pressure and buoyant forces interact with each other. Examples of this phenomenon are electric cooling, nuclear reactor, and typical refrigerator.

1.7 Cattaneo-Christov Heat Flux Model

Heat transfer in a fluid has gained a considerable attention due to its application in industries such as heat dissipation in mobile phones and water heater. Fourier (1822) proposed a heat conduction model in a medium and it has been the best model to give a comprehensive knowledge on heat exchange mechanism in various situations. This Fourier law of heat conduction is used to describe heat transfer in simple problems, which the idea of heat transfer is revolved back then. Fourier law states that,

$$\mathbf{q} = -k\nabla T, \tag{1.7}$$

where $\mathbf{q}$ is the heat flux of the fluid, k is the thermal conductivity of the fluid and ∇T is the local temperature gradient.

The primary downside of the law is any initial disturbance to the system will affect the fluid instantly, which is not a representative to many complex cases. Cattaneo (1948) overcome this problem by including a thermal relaxation time parameter to present the thermal inertia into the equation. The law is known as Maxwell-Cattaneo law. The law is further refined by Christov (2009) by obtaining the material-invariant properties. He changed the time derivative in Maxwell-Cattaneo model with the Oldroyd upper convected derivative to obtain the material-invariant properties. The law from Eq.(1.7) becomes,

$$\mathbf{q} + \lambda_2 \left(\frac{\partial \mathbf{q}}{\partial t} + \mathbf{V}.\nabla \mathbf{q} - \mathbf{q}.\nabla \mathbf{V} + (\nabla.\mathbf{V})\mathbf{q} \right) = -k\nabla T, \tag{1.8}$$

where $\mathbf{V}$ is the velocity vector and λ_2 is the relaxation time for heat flux. Note that for $\lambda_2 = 0$, the model in Eq.(1.8) reduces to the classical Fourier law of Eq.(1.7).

1.8 Mass Transfer

Mass transfer occurs when there is a difference in the concentration of some types of chemicals present in a mixture. It commonly involves diffusion which occurs in solids, liquids and gases. Mass transfer is stronger in gases than in liquids and stronger in liquids than solids, since it depends on the molecular spacing of the medium. Some of the examples of mass transfer are:

1. Distillation of pure water from tap water.
2. Evaporation of seawater to the atmosphere to form clouds on a hot day.
3. Purification of blood in kidneys.

In year 1855, Fick (1855) proposed a simple model to describe diffusion of particles in matter. The law is called the Fick's law of diffusion which is useful to describe the behaviour of mass transfer in a medium. Fick's first law of diffusion states that,

$$\mathbf{J} = -D\nabla C, \tag{1.9}$$

where $\mathbf{J}$ is the diffusion flux vector, D is the diffusion coefficient or diffusivity of the fluid, and ∇C is the local concentration gradient of the fluid.

1.9 Research Objectives

The followings are the research objectives to be achieved at the end of the candidature:

1. To extend a mathematical model of convective heat transfer of Cattaneo-Christov heat flux model over a horizontal plate with
   a) Sakiadis and Blasius flow upper-convected Maxwell (UCM) fluid,
   b) Sakiadis magnetohydrodynamics (MHD) Carreau fluid.

2. To construct a mathematical model of convective heat transfer of Cattaneo-Christov heat flux model over a horizontal wedge with
    a) UCM fluid with suction and heat generation/absorption,
    b) UCM fluid in the presence of suction, heat generation/absorption, heat radiation, and chemical reaction.
3. To develop an algorithm for solution of Cattaneo-Christov heat flux model as stated in Objective 1 numerically.
4. To analyse the numerical solutions of heat transfer obtained as stated in Objective 1.

1.10 Problem Statement

The followings are the problem statements to be answered during candidature:

1. What are the effect of Cattaneo-Christov heat flux model to the heat transfer for Sakiadis and Blasius flow of upper-convected Maxwell (UCM) over a horizontal plate?
2. Is there any effect of magnetic field to the heat and mass transfer for Sakiadis flow of Carreau fluid over a horizontal plate if Cattaneo-Christov heat flux model are applied?
3. Is the boundary layer of UCM fluid over a horizontal wedge affected in the presence of suction and heat generation/absorption for Cattaneo-Christov heat flux model?
4. How does the heat and mass transfer of UCM fluid over a horizontal wedge with Cattaneo-Christov heat flux model varies if heat generation/absorption, chemical reaction, suction and heat radiation are present?

1.11 Significane of research

The direct beneficiaries of the research will be the scientific and engineering communities, as well as the industries. The following are the importance of the research:

1. The scientific community will gain better understanding in terms of the fundamental scientific knowledge of the phenomena-related subjects,
2. The research provides some theoretical results in the form of correlation so that the related group of people have better comparison with their physical experimental data, and
3. The existing labs and experiment facilities in the industry will be improved and better calibrated by this theoretical experiment and will eventually increase the efficiency.

1.12 Thesis Organisation

This thesis consists of seven chapters. The general introduction to fluid dynamics, upper-convected Maxwell (UCM) fluid, Carreau fluid, Cattaneo-Christov heat flux model and heat and mass transfer are presented in Chapter 1. The objectives of this study are also stated in this chapter.

Chapter 2 gives a comprehensive literature review regarding past research works on UCM and Carreau fluid, Cattaneo-Christov heat flux model and boundary layer flow past a horizontal plate and a horizontal wedge. Based on the literature background, it is found that there exist some important parts in boundary layer problems that to be covered in this study.

The detail of mathematical formulations are given in Chapter 3. In this chapter, derivation of the governing equations is provided. From the governed equations, a similarity transformation is done to transform the equations into a set of ordinary differential equations, which to be computed using some numerical methods. The numerical methods are then transformed into a mathematical programming code, which is also presented in this chapter. The comparisons between the present results with previously published results are performed to validate the methods and the programming code.

The next four chapters deal with the problems for this study. In Chapter 4, the numerical analysis of Sakiadis and Blasius flow of UCM fluid over a horizontal plate by using Cattaneo-Christov heat flux model are shown. Next, the numerical study of mass and heat transfer for Sakiadis flow of MHD Carreau fluid over a horizontal plate by using Cattaneo-Christov heat flux model is presented in Chapter 5. Chapter 6 deals with the convective boundary layer of UCM fluid over a horizontal wedge with suction and heat generation using Cattaneo-Christov heat flux model. Meanwhile, Chapter 7 presented the analysis of the heat and mass transfer of UCM fluid over a horizontal wedge in the presence of heat generation, suction, chemical reaction and heat radiation using Cattaneo-Christov heat flux model.

Chapter 8 presents the conclusions of this study and some recommendations for future work.

CHAPTER 2: LITERATURE REVIEW

Studies on various convective boundary layer flow past different types of geometries have been conducted extensively. The most frequent study has been the wedge flow. Wedge flow or Falkner-Skan flow has been associated with a horizontal wedge with wedge angle $\Omega = \beta_w \pi$ where β_w is the Hartree pressure gradient as shown in Figure 2.1(a). For $\beta_w = 0$ corresponds to the horizontal plate as in Figure 2.1(b). Some examples of boundary layer flow over a horizontal flat plate and horizontal wedge are:

1. Horizontal wedge
   a) Bow of a ship (The foremost part of the hull of a ship or a boat).
   b) Wingtip of an aeroplane.
   c) The overall shape of a Formula One car.
2. Horizontal flat plate
   a) Blades of a wind turbine.
   b) Spoiler at the back of a car.
   c) Rudder of a ship (a part of steering apparatus of a ship that is submerged in the water).

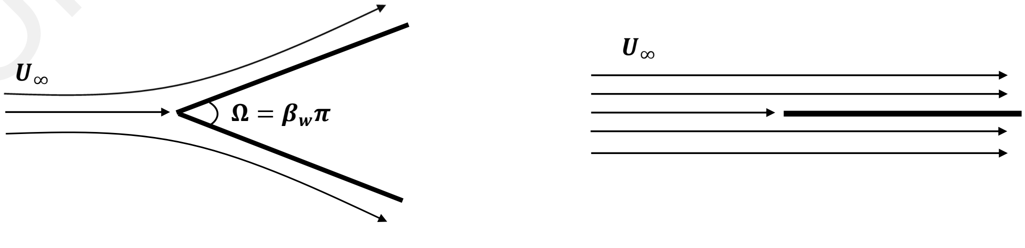

(a) A horizontal wedge (b) A horizontal plate when $\beta_w = 0$

Figure 2.1: Several boundary layer geometries

2.1 Boundary Layer Flow over a Horizontal Plate

The study of boundary layer flow past a horizontal plate has been going for a long time. Prandtl (1904) proposed that for the region in boundary layer flows, as many as half of the terms in the Navier-Stokes equations can be reduced by using some scaling techniques. To achieve this, he did a theoretical study of boundary layer flow by setting a flat plate to be in the x-direction in the Cartesian plane. This work is becoming the basis of boundary layer flow over a plate. Blasius (1908) extended the work by Prandtl (1904) by introducing a similarity solution for a steady, two-dimensional laminar boundary layer over a semi-infinite plate. This solution is valid if a certain transformation applied to the governed equation where the boundary conditions are invariant. This transformation produced an equation in third-order nonlinear ordinary differential equation (ODE). Later, this is known as Blasius flow. Howarth (1949) generalised the Blasius flow by expanding the solution in series form for the velocity distribution for a particular pressure distribution. He suggested that to arrive at the point of flow separation, more terms of the series expansion are required and it was a quite tedious work. So he used approximation theory to overcome this problem and he successfully determined the point of separation. Utz (1977) proved the existence of the uniqueness of the Blasius flow equation and some special cases such as Falkner-Skan flow and Homann flow. Sakiadis (1961) studied on the boundary layer flow of static fluid with two cases; moving continuous flat plate and moving finite length plate. This is known as Sakiadis flow. Crane (1970) manipulated the work of Sakiadis (1961) by varying the velocity of which the infinite plate moves in the static fluid. He provided the theoretical analysis which becomes the basis work for boundary layer flow over a stretching or shrinking sheet or plate.

Lock (1951) studied the velocity distribution in the laminar boundary layer between two parallel streams. He showed that the solution of the momentum equation depends only on the ratio of the velocities of the two parallel flows. Carragher and Crane (1982) presented a theoretical investigation on a continuous stretching sheet. The temperature gradient of the fluid is observed for moderate and large Prandtl numbers. Magyari and Keller (2000) investigated on the exact solutions for self-similar boundary layer flows induced by permeable stretching walls. Hayat et al. (2008) studied on slip flow and heat transfer of a second-grade fluid past a stretching sheet through a porous space by using homotopy analysis method (HAM). They observed that as the value of the second-grade parameter increases, the velocity of the fluid increases. An exact solution for slip MHD viscous flow over a stretching sheet was found by Fang et al. (2009). They found that as the wall slip velocity parameter increases, the fluid velocity increases under suction.

Hayat et al. (2009) published on a three-dimensional rotating flow induced by a shrinking sheet in the presence of suction by using HAM. They investigated the series solutions of MHD and rotating flow past a porous shrinking sheet. For a fixed value of magnetic field parameter, as suction parameter increases, it is found that the velocity of the fluid increases. Aziz (2009) studied on the similarity solution for laminar thermal boundary layer past a flat plate by using Runge-Kutta-Fehlberg fourth-fifth order method. It can be observed that as Prandtl number increases from 0.1 to 20, the value of $-\theta'(0)$ increases. Rashidi and Mohimanian (2010) reported on the analytic approximation solutions for heat transfer on unsteady boundary layer flow over a stretching sheet. Yao et al. (2011) investigated on the heat transfer of a generalised stretching wall with convective boundary conditions. They found that for Prandtl number from 0.7 to 10, the temperature gradient of the fluid decreases with suction applied to both upper and lower solution branches. Heat transfer over a stretching porous sheet subjected to power law heat flux in presence of heat source is studied by Kumar (2011). It is found that as the permeable parameter increases, the temperature profile of the fluid increases. Mukhopadhyay (2012) investigated on heat transfer of an unsteady flow of Maxwell fluid over a stretching surface in presence of heat source and sink. Mushtaq et al. (2016) obtained the numerical solutions for Sakiadis flow of upper-convected Maxwell (UCM) fluid using Cattaneo-Christov heat flux model by employing Keller-Box and shooting methods. They found that as Prandtl number increases, the temperature of the fluid decreases.

2.2 Boundary Layer Flow over a Horizontal Wedge

Boundary layer flow past a wedge has been studied since the early years when Prandtl (1904) proposed his boundary layer theory. Falkner and Skan (1931, November) analysed the steady laminar flow over two flat plates with one end meets at a point, forming a wedge shape. They showed the extension of the application of boundary layer theory which is suggested by Prandtl (1904). They introduced the velocity gradient over a wedge by considering the free stream velocity in the form of $U_\infty x^m$ in the $x-$direction of the Cartesian plane, where U_∞ and m are constants. The wedge angle parameter, m is defined as $m = \dfrac{\beta_w}{2-\beta_w}$, where β_w is a wedge parameter. Hartree (1937) continued to study Falker and Skan's work by doing some approximate treatments to the problem when $\beta_w < 2$. For the case of $\beta_w > 2$, the problems are unlikely to be used in practice. He found that the limiting value for negative β_w is when $\beta_w \simeq -0.199$, the point in which the laminar flow of the boundary layer breaks away. He also coined the term β_w to be the wedge pressure gradient, which became Hartree pressure gradient for the following works.

Stewartson (1954) did some in-depth investigation on Falkner-Skan flow. He tried to find the solutions for outside the range of β_w found by Hartree (1937). He found that the boundary layer flow separation occurs at $\beta_w = -0.1988$ and that there exists a reversed flow or backflow for the region when $\beta_w < -0.1988$. This reversed flow region has a displacement thickness tends to infinity as β_w approaches to zero from the negative side. Libby and Liu (1967) carried an extensive study on the reversed flow region by not ruling out the solution of the Falkner-Skan equation for $\beta_w < \beta_0$, where β_0 is the fluid separation point. Later, Chen and Libby (1968) presented their work which they consider a boundary layer flow close to Falkner-Skan flow. They found that for $\beta_w > \beta_0$, the upper branch solution for the eigenvalues are all positive, which denotes the flow is stable.

The investigation of boundary layer flow past a wedge has been extensively studied with different conditions and fluids. Rajagopal et al. (1983) studied on the boundary layer flow of laminar incompressible second-grade fluid past a wedge by using perturbation method. They found that as β_w increases, the value of $f''(0)$ for $0.05 < \beta_w < 1.60$ also increases accordingly. Brodie and Banks (1986) obtained the analytical solution of Falkner-Skan equation by using perturbation analysis for $2 < \beta_w < \infty$ and confirmed its spatial stability. Pantokratoras (2006) reported on the Falkner-Skan flow with constant wall temperature and variable viscosity where the wall shear stress and wall heat transfer are tabulated for Prandtl number from 1 to 10000. The exact solution of the Falkner-Skan equation with mass transfer and wall stretching is investigated by Fang and Zhang (2008). They observed that the velocity overshoots and reversal flows occur in the presence of mass transfer and wall stretching at $\beta_w = -1$.

Alizadeh et al. (2009) used Adomian decomposition method in the form of infinite series to solve the Falkner-Skan equation for the case of accelerated flow and decelerated flow with separation with $0 < \beta_w < 1$. Abbasbandy and Hayat (2009) conducted a study about boundary layer flow of an MHD fluid over a wedge. They used three different methods to solve the problem; HAM, Crocco's transformation and Runge-Kutta method. It is shown that as magnetic field parameter increases, the value of $f''(0)$ increases. The study of Falkner-Skan flow for static and moving wedge in nanofluid has been done by Yacob et al. (2011). They used three different types of nanofluid; copper (Cu), alumina (Al_2O_3) and titania (TiO_2) and employed Keller-Box method to solve it numerically. They observed that as the wedge angle parameter increases, the skin friction coefficient of the nanofluid also increases. Hayat et al. (2012) published on mixed convection Falkner-Skan flow of a Maxwell fluid. They analysed the effect of Newtonian heating on the fluid by employing HAM. Khan and Pop (2013) reported on the steady boundary layer flow past a stretching wedge in a nanofluid by using Keller-Box method. They found that the velocity of the fluid increases as the stretching parameter increases and the momentum layer thickness of the fluid decreases with the increasing of wedge angle parameter. Later, convective heat transfer of a nanofluid past a wedge with heat generation/absorption and suction was published by Kasmani et al. (2014). They found that as the wedge angle parameter increases, the fluid velocity, temperature and concentration increase.

2.3 Boundary Layer Flow of Upper-Convected Maxwell Fluid

The power-law model is a general fluid model which describes the thinning and thickening behaviour of fluids. Since it cannot describe the viscoelastic behaviour of the fluid, there are many types of viscoelastic fluid model are studied to take into account different characteristics for a different model. Maxwell (1867) proposed the first and simplest viscoelastic rate type model based on gases. Christensen (1982) documented Maxwell's earliest work regarding this type of viscoelastic fluid, which is known as Maxwell fluid. He described Maxwell fluid as the type of material or fluid which is having dual properties of elasticity and viscosity, two of the most investigated type of characteristics in fluids. Oldroyd later generalised Maxwell material by using upper-convected time derivative. At this time, the viscoelastic fluid model is known as upper-convected Maxwell (UCM) fluid. The details about UCM can be found in Macosco (1994) and Chhabra (2010).

To this day, interest is still growing in the study of UCM fluid flow past different geometries in many situations. Coward and Renardy (1997) studied on the thin film core-annular flow of UCM fluid. Choi et al. (1999) investigated on the UCM fluid suction flow past through a porous surface channel. They solved the governed equations by using fourth order Runge-Kutta method and power series method. Results produced by both methods agreed that for a fixed value of Deborah number, the pressure gradient is dominated when Reynolds number is relatively small. Evans and Hagen (2008) published on UCM sink fluid flow over a wedge. They observed that the local asymptotic structure of the fluid consists of two regions; outside boundary layer region and a thin film boundary layer region near the wedge. This observation is in an excellent agreement as what similarity solution produced from the governed equations. Vieru et al. (2008) reported on the flow of fractional Maxwell fluid between two side walls perpendicular to a plate. They used Fourier and Laplace transformations to find the exact solutions and they investigated special cases of fractional Maxwell fluid. Fetecau et al. (2009) extended the work by Vieru et al. (2008) with a different situation, which is an unsteady flow of generalised Maxwell fluid with fractional derivative due to constantly accelerating plate.

Casanellas and Ortin (2011) reported on the laminar oscillatory flow of UCM fluid inside a tube. It is found that for a large Deborah number, the fluid flow has an increasing number of cylindrical layers inside the annulus with opposite velocity. Shehzad (2012) investigated on the boundary layer flow of UCM fluid with power-law heat flux and heat source by using HAM. It is found that as the Deborah number increases from 0.0 to 1.2, the fluid velocity and the temperature of the fluid decrease. The MHD flow of UCM fluid past a vertical stretching Darcian porous sheet with thermophoresis and chemical reaction was studied by Shateyi (2013). The problem is solved by using spectral relaxation method with Chebyshev pseudo-spectral collocation method. It is observed that for increasing Deborah number, the skin friction coefficient of the fluid increases but both mass and heat flux decrease. Qasim and Noreen (2013) employed HAM to solve the Falkner-Skan flow of UCM fluid with heat transfer and magnetic field. It is found that as the Deborah number increases, the fluid velocity increases. Singh and Agarwal (2013) published on the flow and heat transfer of UCM fluid with variable viscosity and thermal conductivity past through an exponentially stretching sheet by using Keller-Box method. It is found that for the Maxwell parameter increases from 0.0 to 0.8, the fluid velocity decreases but the temperature of the fluid increases. Later, Ramesh and Gireesha (2014) reported on the influence of heat source on UCM nanofluid over a stretching. It is observed that the heat flux for UCM nanofluid is smaller than the Newtonian nanofluid but the mass flux is vice versa.

2.4 Boundary Layer Flow of Carreau Fluid

Other than viscosity and elasticity, other important characteristics of the viscoelastic fluid are the normal and shear stress of the fluid. In his paper, Carreau (1972) mentioned that there are many researchers had studied other rheological models in the past to make a prediction of the normal stress of the fluid such as Spriggs et al. (1966) and Bogue and Doughty (1966), but the models were inadequate. Carreau proposed two rheological models; model A is based on work done by Meister and Biggs (1969) and model B is a compromised Bird-Carreau model. The latter predicts too large stress growth overshoot while the former predicts too small overshoot for stress growth. He deduced that model A is failed to predict the fluid behaviour for suddenly changing flow. However, model B is able to capture simple shear, complex viscosity, stress growth and stress relaxation functions simultaneously. Thus, model B has become the basis for boundary layer flow analysis for fluid which has characteristic of shear stress to be analysed. Boger (1977) extended the work done by Carreau by making an assumption that the infinite shear rate viscosity of the fluid is negligible as compared to the zero shear rate viscosity. This means that the shear rate of the fluid outside the boundary layer region can be cancelled out from the model. This, in turn, simplifies Carreau's rheological model and make it easier to be used and applied to boundary layer problem.

There are many studies done for the investigation of boundary layer flow of Carreau fluid past many geometries. Bush and Phan-Thien (1984) studied on drag force on a sphere in creeping motion through a Carreau model fluid. They used boundary element method to solve the problem numerically and the results are compared with the theoretical prediction. Olajuwon (2011) reported on the heat and mass transfer in hydromagnetic Carreau fluid past a vertical porous plate in the presence of thermal radiation and thermal diffusion by using Runge-Kutta and shooting method. He found that as the power-law index increases, the fluid velocity increases accordingly. Nadeem et al. (2013) investigated the effect of heat and mass transfer on peristaltic flow of Carreau fluid in a vertical annulus by considering a long wavelength. Amoura et al. (2014) published on mixed convection flow of a non-Newtonian Carreau fluid with the effect of viscous dissipation in an annular space between two rotating cylinders coaxially. They observed that for a fixed power-law index, as Eckert number increases from 0.0 to 0.5, the temperature profile of the fluid increases. Boundary layer flow and heat transfer of Carreau fluid over a nonlinearly stretching sheet have been studied by Khan and Hashim (2015). It is shown that as Weissenberg number increases from 1 to 5, the fluid velocity decreases for power-law index less than 1, but increases for power-law index more than 1.

Ali and Masood (2016) investigated on the impact of heat transfer analysis of Carreau fluid flow past a static and moving wedge. By using the fifth order Runge-Kutta Method, the problem was solved numerically and they stated that for a fixed wedge angle parameter, as the velocity ratio parameter increases, the fluid velocity increases but the fluid temperature decreases. Later, Khan et al. (2016) reported on heat transfer of squeezed flow of Carreau fluid over a sensor surface with a variable thermal conductivity by employing Runge-Kutta and shooting methods. As power-law index increases from 1.2 to 5.0, the fluid velocity decreases, and for a fixed value of the power-law index, the fluid velocity decreases as Weissenberg number increases from 0.1 to 5.0. The effect of the power-law index on the stretched flow of Carreau nanofluid with convective boundary condition is presented by Hayat et al. (2016b).

2.5 Boundary Layer Flow with Cattaneo-Christov Heat Flux Model

Fourier law of heat conduction has been used for a long time to describe heat transfer in boundary layer flow problem. Cattaneo (1948) stated that Fourier law, although it was simple to use, it is not enough to describe in a detailed way of the heat transfer phenomenon in fluid flow. He decided to include a thermal relaxation time to the Fourier's law to overcome the drawback of the model which affected the whole system if any initial disturbance is applied to the system. Later, Christov (2009) stated that Maxwell-Cattaneo law was intended to overcome the paradox of heat conduction, but not that successful. Although it was not successful, the law has led the path to the generalisation of Fourier's law. Christov modified the Maxwell-Cattaneo law by obtaining material invariant formulation and frame indifferent by using Oldroyd-B upper convected derivatives. This modification has become the basis for the study of heat transfer in fluid flow.

The investigation on the heat transfer of boundary layer flow by using Cattaneo-Christov heat flux model has been expanding. Han et al. (2014) studied on the coupled flow and heat transfer in a viscoelastic fluid with Cattaneo-Christov heat flux model by using HAM. It is shown that as Deborah number increases, the temperature of the fluid decreases. They also noted that if Deborah number is equal to zero, the heat transfer of the fluid behaves according to Fourier law. Abbasi et al. (2015) reported on the analytical study of Cattaneo-Christov heat flux model for boundary layer of Oldroyd-B fluid. They observed that as Deborah number increases, the fluid temperature decreases. They also noted that the fluid temperature decreases when Prandtl number increases with a fixed Deborah number. The investigation on boundary layer heat and mass transfer with Cattaneo-Christov heat flux model in UCM nanofluid past a stretching sheet was done by Sui et al. (2016). Shehzad et al. (2016) reported on the Cattaneo-Christov heat flux model for third-grade fluid flow towards an exponentially stretching sheet. Later, Hayat et al. (2016a) published on Darcy-Forchheimer flow with variable thermal conductivity and Cattaneo-Christov heat flux model. Waqas et al. (2016) studied on Cattaneo-Christov heat flux model for generalised Burgers' fluid flow of variable thermal conductivity by using HAM. Later, Khan et al. (2017) investigated the UCM fluid flow with Cattaneo-Christov heat flux model and chemical reaction.

2.6 Boundary Layer Flow with Magnetohydrodynamic

Magnetohydrodynamic (MHD) is when the fluid flow is immersed in a magnetic field. Hartmann and Lazarus (1937) were the first person to arise with the idea of combination between electromagnetic and hydrodynamic. Alfvén (1942) expanded the work done by Hartmann and Lazarus (1937). He stated that for a conducting fluid placed in a constant magnetic field, every movement of the fluid produces electric currents. He suggested that the existence of this waves may be important in solar physics field. The word magnetohydrodynamic is the combination of three words; magneto means magnetic field, hydro means water and dynamic means movement or flow. Due to his excellent work on MHD, Alfvén received Nobel Prize in Physics in 1970. Some extensions of Alfvén (1942) were done by Sarpkaya (1961). He found that distribution of the fluid velocity is more uniform when the fluid is placed in a magnetic field between two parallel planes. He investigated two model of fluid; Bingham plastic model and power-law model. The term magnetohydrodynamic and hydromagnetic is interchangeable and having the same meaning.

The work done on MHD have been expanding in the later years. Chakrabarti and Gupta (1979) studied on the hydromagnetic flow and heat transfer over a porous stretching sheet. It is shown that for increasing magnetic field parameter from 1 to 7, the fluid velocity decreases due to the Lorenz force. Chiam (1995) reported on the hydromagnetic flow over a stretching sheet with power-law velocity by using Crocco's transformation along with Runge-Kutta and shooting methods. He found that as the magnetic field parameter increases from 0 to 100, the value of $f''(0)$ increases. Devi and Thiyagarajan (2006) published on steady nonlinear hydromagnetic flow and heat transfer over a stretching surface of variable temperature. It is found that as the magnetic field parameter increases, the fluid velocity decreases.

Muhaimin et al. (2008) investigated the effect of heat and mass transfer on the nonlinear MHD boundary layer flow past a shrinking sheet with suction. Heat transfer analysis for MHD viscous fluid past a nonlinear shrinking sheet was done by Javed et al. (2011). They found that for increasing magnetic field parameter, the fluid velocity for the first solution increases but decreases for the second solution after employing Keller-Box method. Bhattacharyya (2011) reported on the effect of heat source on MHD flow and heat transfer over a shrinking sheet with suction. Later, Waini et al. (2017) studied the aligned magnetic field effect on UCM fluid flow and heat transfer over a stretching and shrinking surface.

2.7 Boundary Layer Flow with Suction/Injection

Based on Schlichting and Gersten (2017), they labelled suction and blowing/injection as ones of the boundary layer flow control. It stated that the position of a boundary layer separation point is dependent on how the velocity of the free stream decelerates. The separation of the boundary layer is not desirable since it wastes a lot of energy from the system. They suggested that there are two ways to apply suction into the system; natural an artificial. Some of the artificial ways of applying suction and injection are the motion of the solid wall, slit suction, tangential blowing and suction, and continuous suction and blowing. Some early experiments on boundary layer flow with slit suction were done by Prandtl (1904) where he tried to confirm his theory about boundary layer. He stated that the slit suction was based on velocity changes of the free stream fluid, resulted in lesser drag force which prevented flow separation.

The applications of boundary layer flow with suction have been studied for different types of fluid and geometry. Yih (1998) studied the effect of uniform suction and blowing on forced convection about a wedge with uniform heat flux. It is found that the fluid velocity increases as the suction and blowing parameter increase. Note that positive value of suction and blowing parameters means suction is present and vice versa. Tsai (1999) reported on a simple approach for evaluating the effect of suction and thermophoresis on aerosol particle deposition of laminar flow over a flat plate. Investigation of heat and mass transfer for boundary layer of stagnation-point flow towards a heated porous stretching sheet with heat absorption and suction was done by Layek et al. (2007) by using the fourth order Runge-Kutta method. It is found that as suction parameter increases, the fluid velocity increases for bigger free stream velocity coefficient.

Shehzad et al. (2013) published on the effect of mass transfer on the MHD flow of Casson fluid with chemical reaction and suction by using HAM. As suction parameter increases, the fluid velocity and the concentration of the fluid decrease. Later, Ganapathirao et al. (2013) studied on the non-uniform single and double slit suctions on an unsteady mixed convection flow past a wedge with heat generation and chemical reaction. It is found that the skin friction coefficient, Nusselt number and Sherwood number for single slit suction are higher than double slit suction. The effects of thermophoresis, thermal conductivity and variable viscosity on free convective heat and mass transfer of non-Darcian MHD dissipative Casson fluid flow with chemical reaction and suction were investigated by Animasaun (2014).

2.8 Boundary Layer Flow with Heat Generation/Absorption

Heat generation and absorption have been known to affect the heat transfer across boundary layer flow in different situations. According to Vajravelu and Nayfeh (1992), the effect of heat generation and absorption on the temperature distribution is apparent in fields which dealing with chemical reaction and dissociating fluids. They also stated that some researchers assumed heat generation and absorption to be constants or some spatial dependent functions, but others treated them as some frictional heatings due to the fluid flow past some surfaces and the expansion effect on the fluid. Based on their work on the boundary layer flow over a wedge, it is shown that as the heat generation and absorption increase, fluid velocity and temperature increase.

Researchers have done many investigations on the boundary layer flow with heat generation and absorption with a different type of fluid, fluid flow and geometry. Chamkha (1997) reported on fully developed hydromagnetic non-Darcian mixed convection in a porous medium channel in the presence of the heat generation. He performed analytical as well as numerical analysis of the problem. It can be found that for a fixed Prandtl number of 0.7, as heat generation increases, the temperature of the fluid increases. The effect of heat generation on free convection boundary layer from a vertical porous plate with thermophoresis is studied by Chamkha et al. (2006) by using iterative finite difference method. Mahmoud and Megahed (2009) investigated the effect of viscous dissipation, heat generation and absorption in a thermal non-Newtonian boundary layer fluid flow past a moving permeable flat plate. They found that as heat generation and absorption parameter increase from -0.3 to 2.0, the temperature profile of the fluid decreases. Kasim et al. (2012) published on the effects of heat generation and absorption on free convection boundary layer flow of a viscoelastic fluid over a horizontal circular cylinder with constant heat flux. It is shown that the temperature gradient of the fluid increases as the heat generation and absorption parameter increase. Awais et al (2015) studied on the heat generation and absorption effects in UCM nanofluid stretched boundary layer fluid flow. Later, Jamaludin et al. (2017) reported on the heat transfer analysis on a viscous boundary layer fluid flow past a stretching sheet in the presence of viscous dissipation, internal heat generation and heat flux.

2.9 Boundary Layer Flow with Heat Radiation

Thermal radiation is an effect which changes the temperature distribution of the fluid by some heat radiation source. According to Krishnaprakas et al. (2000), heat generation plays an important role in many engineering fields such as atmospheric re-entry, metalised solid rocket and shock waves. Meanwhile, Ahmad et al. (2016) stated that heat radiation is important in industrial processes involving high temperatures such as nuclear power plants and gas turbines. Some theoretical work regarding heat radiation was done by Hossain and Takhar (1996). They observed that the presence of radiation effects in the energy equation of any boundary layer flow complicated the system by forming highly nonlinear partial differential equations. By using Rosseland diffusion approximation, the resulting governed equation is solved for three regimes of flow; forced convection, free convection and mixed convection. They concluded that the heat transfer of the fluid decreases as radiation parameter increases.

Many works have been done to investigate the effect of thermal radiation in a boundary layer system due to the useful application of heat radiation in industries. Utreja and Chung (1989) investigated on combined convection-conduction-radiation boundary layer flow by employing optimal control penalty finite elements. It is shown that the inclusion of the radiation parameter to the system thickens the thermal boundary layer of the fluid flow. Ara et al (2014) reported on thermal radiation effect on Eyring-Powell boundary layer fluid flow over an exponentially shrinking sheet. They found that as radiation parameter increases from 0 to 2, the temperature profile of the fluid increases by fixing Prandtl number to 0.5. Krishnamurthy et al. (2016) published on the thermal radiation and chemical reaction effects on nanofluid boundary layer slip flow past a nonlinearly stretching sheet with melting heat transfer by applying the fourth-fifth Runge-Kutta-Fehlberg with shooting method. The effects of thermal radiation and Newtonian heating on boundary layer flow past a flat plate are investigated by Mohamed et al. (2017). They found that the temperature profile of the fluid increases as the radiation parameter increases accordingly.

2.10 Boundary Layer Flow with Chemical Reaction

The study of chemical reaction in boundary layer flow is important in manufacturing industry especially fluid transportation since it is not desirable for the material to react chemically with the fluid that it carried. Chambré and Acrivos (1956) stated that there are two types of the chemical reaction; homogeneous and heterogeneous. A homogeneous chemical reaction occurs in a single phase, while heterogeneous chemical reaction occurs in multiphase at an interphase. There are two cases of heterogeneous chemical reaction. For the first case where the interphase is in a solid state, the surface structure and geometry can be altered by chemical reaction. For the second case, the surface structure and geometry maintained without any changes, which is an important case in chemical engineering field since they often transport reactive chemical and do not want it to react with the surface. According to Muhaimin et al. (2010), some of the examples of chemical reaction application in industries are chemical processing equipment and food processing.

Investigations in the aspect of chemical reaction effect on boundary layer flow was conducted in various system. Kandasamy et al. (2006) studied on the effect of chemical reaction, heat radiation, suction, heat and mass transfer on boundary layer flow past a porous wedge. It is shown that the fluid velocity and temperature decrease when chemical reaction parameter increases but the concentration of the fluid increases. Muhaimin et al. (2010) reported on the heat and mass transfer analysis on boundary layer flow over a permeable shrinking sheet with suction and chemical reaction. They found that the mass concentration of the fluid decreases as the chemical reaction parameter increases. The effect of binary chemical reaction and activation energy on MHD boundary layer flow with dissipation and heat generation was published by Maleque (2013) by using Nachtshein Swigert iteration method. As chemical reaction parameter increases, the fluid concentration decreases with a fixed value of Prandtl number. Khan (2014) studied on MHD boundary layer fluid flow past a shrinking surface with chemical reaction and suction. It is found that as chemical reaction parameter increases from 0.0 to 3.0, the mass concentration profile of the fluid decreases. The effect of chemical reaction parameter on the concentration of the fluid with a fixed value of Schmidt number was reported by Majeed et al. (2017) in his study about UCM boundary layer Ferrofluid flow under magnetic dipole with chemical reaction, suction and Soret effects.

CHAPTER 3: MATHEMATICAL FORMULATION

3.1 Introduction

In this chapter, the governing equations for the boundary layer flow over a horizontal plate and a horizontal wedge are derived. The similarity transformations and local similarity solutions for momentum, thermal and concentration equations are discussed in detail along with the local skin-friction coefficient, local Nusselt number and local Sherwood number. The second and third order finite difference method (FDM) used to compute the numerical solutions of the boundary layer flow are presented later in this chapter.

3.2 The Boundary Layer Flow Model

The boundary layer flow is modelled in the form of partial differential equations. These equations are used to describe the physical characteristics and behaviour of the fluid flow. The model is based on the physics' law of conservations as stated below:

1. The principle of conservation of mass stated that the mass of a fluid is constant across the system. This means there is no mass of fluid created along the surface.

2. The Newton's second law of motion stated that the rate of change of momentum of a fluid in a system is equal to the resultant of all external forces acting on the fluid.

3. The first law of thermodynamics described the principle of conservation of energy which stated that the rate of change of energy in a system is equal to the resultant of all external energy added to the system alongside with the rate of work done by the fluid.

For this research, the following assumptions are employed to describe the behaviour of the fluid in addition to the conservation principles above:

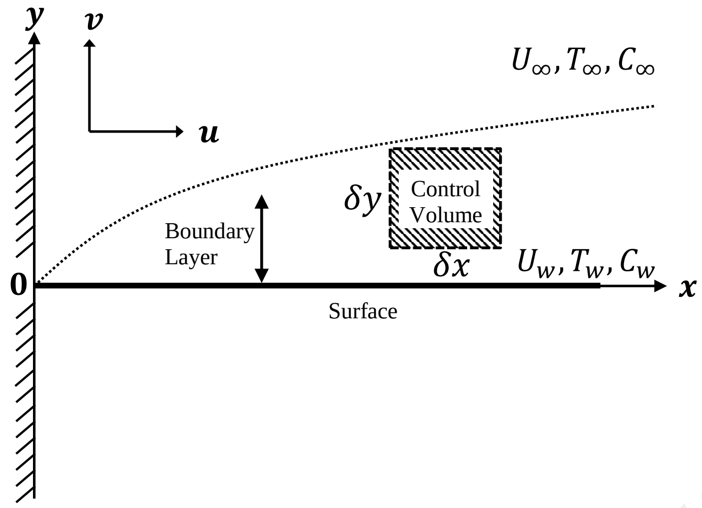

Figure 3.1: The control volume element in the boundary layer region

1. The fluid is incompressible, which means the density of the fluid is constant throughout the system.

2. The fluid is laminar, which means each particle of the fluid is moving by following a smooth path without any interference between each other.

3. There is a no-slip condition, which means at the surface of the wall, the velocity of the fluid is negligible compared to the velocity of the fluid at the boundary.

By above assumptions, the derivation of the governing equations for the boundary layer flow can be done.

3.2.1 The Continuity Equation

Consider a two-dimensional flow in xy-plane. Assume that a part of a control volume is cut from the boundary layer as shown in Figure 3.1. The plane is in the $x-$direction, the normal to the plane is in $y-$direction, u and v are the velocity components in the $x-$ and $y-$ directions respectively, U_w, T_w and C_w are the fluid velocities in the $x-$ direction, temperature and concentration at the surface respectively, and U_∞, T_∞ and C_∞ are the free stream velocity, ambient fluid temperature and ambient fluid concentration respectively.

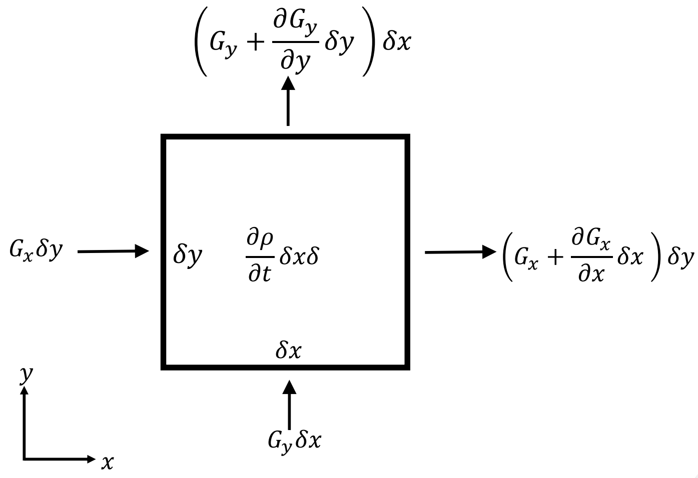

Figure 3.2: The control element in the boundary layer region with the mass flow across the element

Consider the total mass rate of flow across the control element and the rate of change of mass storage within the system. Based on Kays and Crawford (1993), let $\boldsymbol{G}$ be the mass flux of the fluid (mass flow rate per unit of normal area). The mass flux across the control element is as shown in Figure 3.2, where ρ is the density of the fluid and t is the time.

By the principle of conservation of mass, the rate of mass is zero. It means that,

$$\text{Outflow} - \text{Inflow} + \text{Increase of mass} = 0, \tag{3.1}$$

where,

$$\text{Outflow} = \left(G_y + \frac{\partial G_y}{\partial y}\delta y\right)\delta x + \left(G_x + \frac{\partial G_x}{\partial x}\delta x\right)\delta y, \tag{3.2}$$

$$\text{Inflow} = G_x\delta y + G_y\delta x, \tag{3.3}$$

$$\text{Increase of mass} = \frac{\partial \rho}{\partial t}\delta x\delta y, \tag{3.4}$$

such that $G_{x_i} = \rho u_i$ where subscript i indicates the i-th element of the vector. By Eq.(3.1) and doing some simplification,

$$\frac{\partial G_x}{\partial x} + \frac{\partial G_y}{\partial y} + \frac{\partial \rho}{\partial t} = 0. \tag{3.5}$$

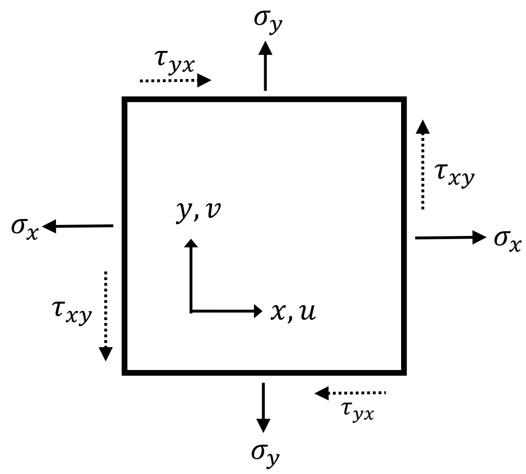

Figure 3.3: The stresses exerted by the control element

Eq.(3.5) can be written in vector notation form and Cartesian tensor form, respectively as,

$$\nabla \cdot \boldsymbol{G} + \frac{\partial \rho}{\partial t} = 0, \tag{3.6}$$

$$\frac{\partial}{\partial x_i}(\rho u_i) + \frac{\partial \rho}{\partial t} = 0. \tag{3.7}$$

For incompressible fluid, $\frac{\partial \rho}{\partial t} = 0$ and $\nabla \cdot \boldsymbol{G} = \boldsymbol{G} \cdot \nabla$. Thus, Eq.(3.7) becomes,

$$\frac{\partial}{\partial x_i}(\rho u_i) = \frac{\partial u}{\partial x} + \frac{\partial v}{\partial y} = 0. \tag{3.8}$$

3.2.2 The Momentum Equation

Consider a part of the same control element from the boundary layer flow cross section in Figure 3.1. Let τ and σ be the shear stress and normal stress of the fluid acting on the control element respectively. Based on Kays and Crawford (1993), the individual component of the stresses acting on the control element is shown in Figure 3.3.

The equation for shear stress and normal stress are as follows,

$$\tau_{xy} = \tau_{yx} = \mu\left(\frac{\partial v}{\partial x} + \frac{\partial u}{\partial y}\right), \tag{3.9}$$

$$\sigma_x = -P - \frac{2}{3}\mu\left(\frac{\partial u}{\partial x} + \frac{\partial v}{\partial y}\right) + 2\mu\frac{\partial u}{\partial x}, \tag{3.10}$$

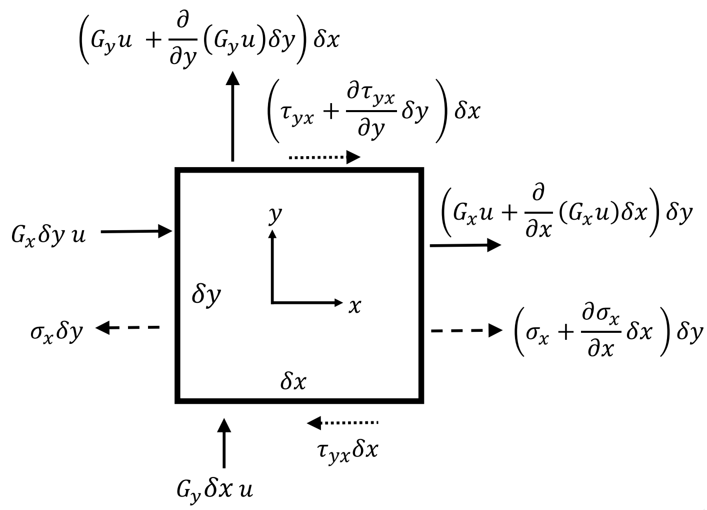

Figure 3.4: The external forces exerting on control element and the momentum fluxes across the control element

$$\sigma_y = -P - \frac{2}{3}\mu\left(\frac{\partial u}{\partial x} + \frac{\partial v}{\partial y}\right) + 2\mu\frac{\partial v}{\partial y}, \tag{3.11}$$

where μ is the viscosity of the fluid and P is the pressure exerted on the fluid. Consider the external forces exerted on the control element and the momentum fluxes across the control element as shown in Figure 3.4.

By Newton's second law of motion,

$$\text{Outflow} - \text{Inflow} + \text{Increase of force} = \text{External forces}, \tag{3.12}$$

where,

$$\text{Outflow} = \left[G_x u + \frac{\partial}{\partial x}(G_x u)\,\delta x\right]\delta y + \left[G_y u + \frac{\partial}{\partial y}\left(G_y u\right)\delta y\right]\delta x, \tag{3.13}$$

$$\text{Inflow} = (G_x \delta y)\,u + \left(G_y \delta x\right)u, \tag{3.14}$$

$$\text{Increase of force} = 0, \tag{3.15}$$

$$\text{External forces} = -\sigma_x \delta y - \tau_{yx} + \left(\sigma_x + \frac{\partial \sigma_x}{\partial x}\delta x\right)\delta y + \left(\tau_{yx} + \frac{\partial \tau_{yx}}{\partial y}\delta y\right)\delta x. \tag{3.16}$$

After simplication, Eq.(3.12) becomes,

$$G_x\frac{\partial u}{\partial x} + u\frac{\partial G_x}{\partial x} + G_y\frac{\partial u}{\partial y} + u\frac{\partial G_y}{\partial y} = \frac{\partial \sigma_x}{\partial x} + \frac{\partial \tau_{yx}}{\partial y}, \tag{3.17}$$

By continuity equation in Eq.(3.8) and for incompressible fluid, $\dfrac{\partial \sigma_x}{\partial x} = 0$, Eq.(3.17) becomes,

$$\rho\left(u\frac{\partial u}{\partial x} + v\frac{\partial u}{\partial y}\right) = \frac{\partial \tau_{yx}}{\partial y}, \tag{3.18}$$

where $\nu = \dfrac{\mu}{\rho}$ is the kinematic viscosity of the fluid.

3.2.3 The Momentum Equation of Upper-Convected Maxwell Fluid

For upper-convected Maxwell (UCM) fluid model, based on work done by Maxwell (1867), the term τ_{yx} is replaced by the Cauchy stress tensor, $\mathbf{T}_s$ where,

$$\mathbf{T}_s = -\lambda_1 \mathbf{T}_s^u + 2\mu D_r, \tag{3.19}$$

with λ_1 is the relaxation time of the fluid, D_r is the deformation rate tensor and $\mathbf{T}_s^u$ is the upper-convected time derivative for the stress tensor. The upper-convected time derivative for the stress tensor is defined as,

$$\mathbf{T}_s^u = \frac{D}{Dt}\mathbf{T}_s - \left[(\nabla \mathbf{v})^T \cdot \mathbf{T}_s + \mathbf{T}_s \cdot (\nabla \mathbf{v})\right], \tag{3.20}$$

where $\dfrac{D}{Dt}$ is the substantive derivative such that,

$$\frac{D}{Dt}\mathbf{T}_s = \frac{\partial}{\partial t}\mathbf{T}_s + \mathbf{v}\cdot(\nabla \mathbf{T}_s), \tag{3.21}$$

For incompressible fluid, $\dfrac{\partial}{\partial t}\mathbf{T}_s = 0$, so Eq.(3.20) becomes,

$$\mathbf{T}_s^u = \mathbf{v}\cdot(\nabla \mathbf{T}_s) - \left[(\nabla \mathbf{v})^T \cdot \mathbf{T}_s + \mathbf{T}_s \cdot (\nabla \mathbf{v})\right]. \tag{3.22}$$

By several calculations and simplifications, Eq.(3.18) together with Eq.(3.19) produce the momentum equation of upper-convected Maxwell fluid in two-dimension fluid flow,

$$u\frac{\partial u}{\partial x} + v\frac{\partial u}{\partial y} + \lambda_1\left(u^2\frac{\partial^2 u}{\partial x^2} + v^2\frac{\partial^2 u}{\partial y^2} + 2uv\frac{\partial^2 u}{\partial x \partial y}\right) = \nu\frac{\partial^2 u}{\partial y^2}. \tag{3.23}$$

3.2.4 The Momentum Equation of Carreau Fluid

For Carreau fluid model based on work done by Carreau (1972), the term τ_{yx} is replaced by the Cauchy stress tensor, $\mathbf{T}_s$ where,

$$\mathbf{T}_s = -P\mathbf{I} + \mu\mathbf{A}_1, \tag{3.24}$$

with P is the pressure, $\mathbf{I}$ is the identity tensor and μ is the material viscosity such that,

$$\mu = \mu_\infty + (\mu_0 - \mu_\infty)\left[1 + (\Gamma\dot{\gamma})^2\right]^{\frac{n-1}{2}}, \tag{3.25}$$

where μ_0 and μ_∞ are the zero and infinite shear rate viscosity of the material respectively, Γ is the material time constant, n is the power-law index, $\mathbf{A}_1$ is the first Rivlin-Ericksen tensor with $\mathbf{A}_1 = (\text{grad } \mathbf{v}) + (\text{grad } \mathbf{v})^T$ and $\dot{\gamma}$ is the shear rate, given that,

$$\dot{\gamma} = \sqrt{\frac{1}{2}\sum_j\sum_j \dot{\gamma}_{ij}\dot{\gamma}_{ji}} = \sqrt{\frac{1}{2}\left(\mathbf{A}_1^2\right)^T}. \tag{3.26}$$

For most practical purposes, μ_0 is relatively negligible to μ_∞, so that μ_0 can be taken to be zero. Thus, for two-dimensional fluid flow,

$$\dot{\gamma} = \sqrt{\left[4\left(\frac{\partial u}{\partial x}\right)^2 + \left(\frac{\partial u}{\partial y} + \frac{\partial v}{\partial x}\right)^2\right]}. \tag{3.27}$$

Therefore Eq.(3.24) becomes,

$$\mathbf{T}_s = -P\mathbf{I} + \mu_0\left[1 + \Gamma^2\left\{4\left(\frac{\partial u}{\partial x}\right) + \left(\frac{\partial u}{\partial y} + \frac{\partial v}{\partial x}\right)^2\right\}\right]^{\frac{n-1}{2}}\mathbf{A}_1, \tag{3.28}$$

where $n \in [0, \infty)$.

The general momentum equation from Eq.(3.18) combined with Eq.(3.28), with some modification and computation, produces,

$$u\frac{\partial u}{\partial x} + v\frac{\partial u}{\partial y} = \nu\frac{\partial^2 u}{\partial y^2}\left[1 + \Gamma^2\left(\frac{\partial u}{\partial y}\right)^2\right]^{\frac{n-1}{2}} + \nu(n-1)\Gamma\frac{\partial^2 u}{\partial y^2}\left(\frac{\partial u}{\partial y}\right)^2\left[1 + \Gamma^2\left(\frac{\partial u}{\partial y}\right)^2\right]^{\frac{n-3}{2}}. \tag{3.29}$$

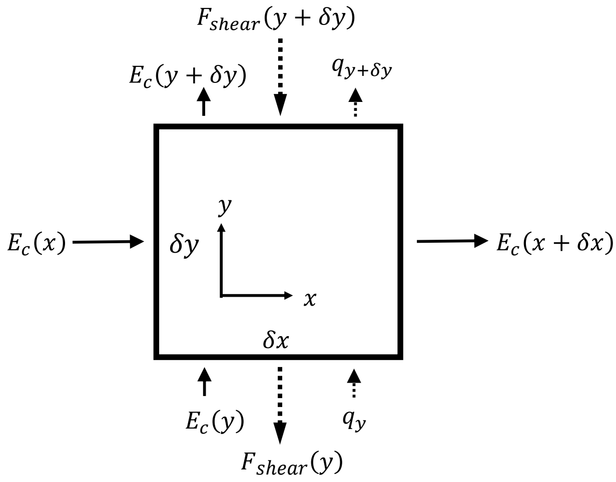

Figure 3.5: The energy-transfer term for a control element

3.2.5 The General Thermal Energy Equation

Consider a part of control element from the boundary layer flow in Figure 3.1. Let E_c be the energy of convection and T be the temperature of the fluid. The flow work done passes through the control element is simply $\frac{P}{\rho}$. The mixture enthalpy is the sum of internal energy E_i and the flow work done of the fluid and is given by the formula $i = E_i + \frac{P}{\rho}$. In addition to the assumptions made in Section 3.2, the following assumptions are also used:

1. The gradient of normal stresses is the gradient of thermodynamic pressure.
2. No internal heat generation and no work done by external fields.
3. The value of v^2 is negligible relative to u^2 .

Based on Kays and Crawford (1993), consider the energy and work done in the control element as shown in Figure 3.5. The component labelled in the figure are formulated as follows, with k is the thermal conductivity,

$$E_c(x) = G_x \delta y \left(i + \frac{1}{2}u^2 \right), \tag{3.30}$$

$$E_c(x+\delta x) = \left[G_x \left(i + \frac{1}{2}u^2 \right) + \frac{\partial}{\partial x} \left\{ G_x \left(i + \frac{1}{2}u^2 \right) \right\} \delta x \right] \delta y, \tag{3.31}$$

$$E_c(y) = G_y \delta x \left(i + \frac{1}{2}u^2 \right) \tag{3.32}$$

$$E_c(y + \delta y) = \left[G_y \left(i + \frac{1}{2}u^2 \right) + \frac{\partial}{\partial y} \left\{ G_y \left(i + \frac{1}{2}u^2 \right) \right\} \delta y \right] \delta x, \tag{3.33}$$

$$q_y = -k \left(\frac{\partial T}{\partial y} \right) \delta x, \tag{3.34}$$

$$q_{y+\delta y} = -\left[k \left(\frac{\partial T}{\partial y} \right) + \frac{\partial}{\partial y} \left\{ k \left(\frac{\partial T}{\partial y} \right) \right\} \delta y \right] \delta x, \tag{3.35}$$

$$F_{shear}(y) = \left(\tau_{yx} u \right) \delta x, \tag{3.36}$$

$$F_{shear}(y + \delta y) = \left[\tau_{yx} u + \frac{\partial}{\partial y} \left(\tau_{yx} u \right) \delta y \right] \delta x. \tag{3.37}$$

By Newton second law of motion and simplify,

$$\frac{\partial}{\partial x} \left[G_x \left(i + \frac{1}{2}u^2 \right) \right] + \frac{\partial}{\partial y} \left[G_y \left(i + \frac{1}{2}u^2 \right) \right] - \frac{\partial}{\partial y} k \left(\frac{\partial T}{\partial y} \right) - \frac{\partial}{\partial y} \left(\tau_{yx} u \right) = 0. \tag{3.38}$$

By Eq.(3.8), Eq.(3.9) and Eq.(3.18), Eq.(3.38) becomes (Kays and Crawford (1993)),

$$\rho u \frac{\partial i}{\partial x} + \rho v \frac{\partial i}{\partial y} - \frac{\partial}{\partial y} \left(k \frac{\partial T}{\partial y} \right) - \mu \left(\frac{\partial u}{\partial y} \right)^2 = 0. \tag{3.39}$$

For incompressible fluid, ρ is constant and $di = c_p\, dT + \frac{1}{\rho} dP$ where c_p is the specific heat capacity of the fluid (Kays and Crawford (1993)). Thus Eq.(3.39) becomes,

$$\rho u c_p \frac{\partial T}{\partial x} + \rho v c_p \frac{\partial T}{\partial y} - \frac{\partial}{\partial y} \left(k \frac{\partial T}{\partial y} \right) - \mu \left(\frac{\partial u}{\partial y} \right)^2 = 0. \tag{3.40}$$

Under the assumption that k is constant and the dissipation term $\left(\frac{\partial u}{\partial y} \right)^2$ can be neglected because it is only significant when the velocity of the fluid approaches the speed of sound, Eq.(3.40) finally becomes,

$$u \frac{\partial T}{\partial x} + v \frac{\partial T}{\partial y} = \alpha \frac{\partial^2 T}{\partial y^2}, \tag{3.41}$$

or in vector form,

$$\rho c_p \mathbf{V} \cdot \nabla \mathbf{T} = -\nabla \cdot \mathbf{q}, \tag{3.42}$$

where $\alpha = \dfrac{k}{\rho c_p}$ is the thermal diffusivity coefficient and $\mathbf{q} = -k\nabla\mathbf{T}$ is the thermal flux vector. Eqs.(3.41) - (3.42) is the Fourier law of heat conduction.

3.2.6 The Thermal Energy Equation of Cattaneo-Christov Heat Flux Model

Consider the Fourier law of heat condution in vector form from Eq.(3.42). Maxwell and Cattaneo (1948) introduced thermal relaxation time for thermal flux, λ_2 so that the thermal flux vector becomes,

$$\left(1 + \lambda_2 \frac{\partial}{\partial t}\right) \mathbf{q} = -k\nabla\mathbf{T}. \tag{3.43}$$

To generalise Fourier law based on Eq.(3.43), Christov (2009) used Oldroyd's upper convected derivative since it is time derivative invariant. To make it frame indifferent, Eq.(3.42) becomes (Christov (2009)),

$$\rho c_p \left(\frac{\partial T}{\partial t} + \mathbf{V} \cdot \nabla\mathbf{T}\right) = -\nabla \cdot \mathbf{q}, \tag{3.44}$$

where,

$$\mathbf{q} + \lambda_2 \left[\frac{\partial q}{\partial t} + \mathbf{V} \cdot \nabla\mathbf{q} - \mathbf{q} \cdot \nabla\mathbf{V} + (\nabla \cdot \mathbf{V})\, \mathbf{q}\right] = -k\nabla\mathbf{T}. \tag{3.45}$$

For incompressible fluid, $(\nabla \cdot \mathbf{V})\, \mathbf{q} = 0$. For two-dimensional fluid flow, after some substitution and calculation (Christov (2009)), Eqs.(3.44) - (3.45) finally become,

$$\begin{aligned} u\frac{\partial T}{\partial x} + v\frac{\partial T}{\partial y} + \lambda_2 \Bigg[u^2\frac{\partial^2 T}{\partial x^2} + v^2\frac{\partial^2 T}{\partial y^2} + 2uv\frac{\partial^2 T}{\partial x \partial y} + \left(u\frac{\partial u}{\partial x} + v\frac{\partial u}{\partial y}\right)\frac{\partial T}{\partial x} \\ + \left(u\frac{\partial v}{\partial x} + v\frac{\partial v}{\partial y}\right)\frac{\partial T}{\partial y}\Bigg] = \alpha\frac{\partial^2 T}{\partial y^2}. \end{aligned} \tag{3.46}$$

Eq.(3.46) is the Cattaneo-Christov heat flux model.

3.2.7 The Concentration Equation

Consider a part of control element from the boundary layer flow in Figure 3.1. Let C be the mass concentration of the fluid, D is the mass diffusion coefficient and $\gamma_c = \rho D$ is the mass diffusion parameter. Based on Kays and Crawford (1993), consider the mass

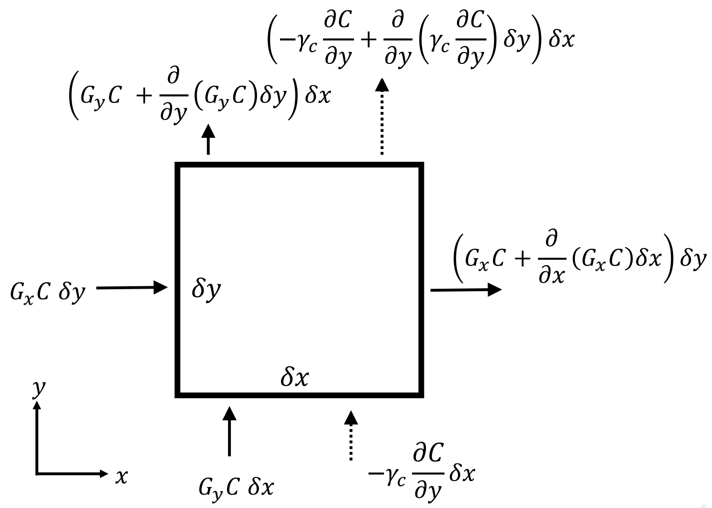

Figure 3.6: The mass transfer term for a control element

transfer passes through the control element as shown in Figure 3.6. By the principle of conservation of mass, and since there is no chemical reaction occurs within the fluid,

$$\text{Outflow} - \text{Inflow} + \text{Increase of mass} = 0, \tag{3.47}$$

where,

$$\text{Inflow} = G_x C\delta y + G_y C\delta x - \gamma \frac{\partial C}{\partial y}\delta x, \tag{3.48}$$

$$\begin{aligned}\text{Outflow} &= \left[G_x C + \frac{\partial}{\partial x}(G_x C)\,\delta x\right]\delta y + \left[G_y C + \frac{\partial}{\partial y}\left(G_y C\right)\delta y\right]\delta x \\ &\quad - \left[\gamma_c \frac{\partial C}{\partial y} + \frac{\partial}{\partial y}\left(\gamma_c \frac{\partial C}{\partial y}\right)\delta y\right]\delta x,\end{aligned} \tag{3.49}$$

$$\text{Increase of storage} = 0. \tag{3.50}$$

By substituting the terms into Eq.(3.47) and some calculations,

$$G_x \frac{\partial C}{\partial x} + G_y \frac{\partial C}{\partial y} + C\frac{\partial G_x}{\partial x} + C\frac{\partial G_y}{\partial y} - \frac{\partial}{\partial y}\left(\gamma_c \frac{\partial C}{\partial y}\right) = 0. \tag{3.51}$$

By continuity equation in Eq.(3.8), and assuming γ_c is constant, Eq.(3.51) becomes,

$$\rho u \frac{\partial C}{\partial x} + \rho v \frac{\partial C}{\partial y} - \gamma_c \frac{\partial^2 C}{\partial y^2} = 0, \tag{3.52}$$

and since $\gamma_c = \rho D$, Eq.(3.52) finally becomes,

$$u\frac{\partial C}{\partial x} + v\frac{\partial C}{\partial y} = D\frac{\partial^2 C}{\partial y^2}. \tag{3.53}$$

The above Eq.(3.53) is the concentration equation for boundary layer problem.

3.2.8 The Boundary Conditions

The boundary conditions are very important to solve the boundary layer problem since they decide the behaviour of the fluid. Different boundary conditions give different outcomes to the fluid pass through some surface. Eqs.(3.8), (3.23), (3.29), (3.46) and (3.53) can be solved by applying the boundary conditions using chosen numerical method. Sakiadis flow describes a moving plate in a calm fluid while Blasius flow constitutes a static plate in a constantly moving fluid. Static Falkner-Skan flow means a static wedge in a flowing fluid with a constant velocity.

The boundary conditions for the momentum equation are,

1. for Sakiadis flow:

$$\begin{gathered} u = U_\infty, \quad v = 0 \quad \text{at} \quad y = 0, \\ u \to 0 \quad \text{as} \quad y \to \infty. \end{gathered} \tag{3.54}$$

2. for Blasius flow and static Falkner-Skan flow:

$$\begin{gathered} u = 0, \quad v = 0 \quad \text{at} \quad y = 0, \\ u \to U_\infty \quad \text{as} \quad y \to \infty, \end{gathered} \tag{3.55}$$

where U_∞ is the free stream velocity and the moving plate velocity.

The boundary conditions for thermal energy equation are,

$$\begin{gathered} T = T_w, \quad \text{at} \quad y = 0, \\ T \to T_\infty \quad \text{as} \quad y \to \infty, \end{gathered} \tag{3.56}$$

where T_w is the temperature of the fluid at the surface and T_∞ is the ambient temperature of the fluid.

The boundary conditions for concentration equation are,

$$C = C_w, \quad \text{at} \quad y = 0, \qquad (3.57)$$
$$C \to C_\infty \quad \text{as} \quad y \to \infty,$$

where C_w is the mass concentration of the fluid at the surface and C_∞ is the ambient mass concentration of the fluid.

3.2.9 The Stream Function

To solve the governing equations in Eqs.(3.8), (3.23), (3.29), (3.46) and (3.53), a stream function is introduced. The single stream function can be replaced by the velocity components u and v. It is chosen so that the continuity equation in Eq.(3.8) is satisfied automatically. The stream function $\psi(x, y)$ is defined as,

$$u = \frac{\partial \psi}{\partial y}, \qquad v = -\frac{\partial \psi}{\partial x}. \qquad (3.58)$$

3.3 Similarity Transformation for the Boundary Layer Equations

The system of governing equation is composed of four fundamental equations. Those are the continuity equation, the momentum equation, the energy equation and the concentration equation. It may be quite difficult to deal with the system directly since it is in the form of partial differential equations. To overcome this problem, the equations are transformed into ordinary differential equations by similarity transformation. The word similarity means the variation of the fluid velocity u is the same for all values of y. By doing this, the reduced governing equations may be described as similar as the original governing equations,

$$u = [y \cdot g(x)]\,. \qquad (3.59)$$

By using stream function as defined in Eq.(3.58), Eq.(3.59) can be written as,

$$\psi = h(x) f(\eta), \qquad (3.60)$$

and the dimensionless distance from the surface is defined as,

$$\eta = y \cdot g(x). \tag{3.61}$$

For thermal energy T and mass concentration C, the similarity transformation must be made so that the similarity transformation for η and ψ is kept true. By that, the dimensionless temperature θ and the dimensionless concentration ϕ are defined as,

$$\theta(\eta) = \frac{T - T_\infty}{T_w - T_\infty}, \qquad \phi(\eta) = \frac{C - C_\infty}{C_w - C_\infty}. \tag{3.62}$$

The continuity, momentum, thermal energy and mass concentration equations derived in Section 3.2 can be written as,

$$\frac{\partial u}{\partial x} + \frac{\partial v}{\partial y} = 0, \tag{3.63}$$

$$u\frac{\partial u}{\partial x} + v\frac{\partial u}{\partial y} + \lambda_1\left(u^2\frac{\partial^2 u}{\partial x^2} + v^2\frac{\partial^2 u}{\partial y^2} + 2uv\frac{\partial^2 u}{\partial x \partial y}\right) = \nu\frac{\partial^2 u}{\partial y^2}, \tag{3.64}$$

$$u\frac{\partial u}{\partial x} + v\frac{\partial u}{\partial y} = \nu\frac{\partial^2 u}{\partial y^2}\left[1 + \Gamma^2\left(\frac{\partial u}{\partial y}\right)^2\right]^{\frac{n-1}{2}} + \nu\,(n-1)\,\Gamma\frac{\partial^2 u}{\partial y^2}\left(\frac{\partial u}{\partial y}\right)^2\left[1 + \Gamma^2\left(\frac{\partial u}{\partial y}\right)^2\right]^{\frac{n-3}{2}}, \tag{3.65}$$

$$\begin{aligned} u\frac{\partial T}{\partial x} + v\frac{\partial T}{\partial y} + \lambda_2\Bigg[u^2\frac{\partial^2 T}{\partial x^2} + v^2\frac{\partial^2 T}{\partial y^2} + 2uv\frac{\partial^2 T}{\partial x \partial y} + \left(u\frac{\partial u}{\partial x} + v\frac{\partial u}{\partial y}\right)\frac{\partial T}{\partial x} \\ + \left(u\frac{\partial v}{\partial x} + v\frac{\partial v}{\partial y}\right)\frac{\partial T}{\partial y}\Bigg] = \alpha\frac{\partial^2 T}{\partial y^2}, \end{aligned} \tag{3.66}$$

$$u\frac{\partial C}{\partial x} + v\frac{\partial C}{\partial y} = D\frac{\partial^2 C}{\partial y^2}. \tag{3.67}$$

3.3.1 Similarity Transformation for a Horizontal Plate

Consider the stream function as defined in Eq.(3.58). By evaluating ψ and its derivative, the stream function becomes,

$$\psi = \sqrt{U_\infty \nu x}\, f(\eta) = h(x) f(\eta), \tag{3.68}$$

and the dimensionless distance becomes,

$$\eta = y\sqrt{\frac{U_\infty}{\nu x}} = y \cdot g(x), \tag{3.69}$$

where U_∞ is constant which is the free stream velocity and $\nu = \dfrac{\mu}{\rho}$ is the kinematic viscosity of the fluid. By the above equations, the followings are derived,

$$h(x)g(x) = \sqrt{U_\infty \nu x}\sqrt{\frac{U_\infty}{\nu x}} = U_\infty, \tag{3.70}$$

$$\frac{dU_\infty}{dx} = 0, \tag{3.71}$$

$$\frac{\partial \eta}{\partial x} = g' y. \tag{3.72}$$

Thus by Eq.(3.58), the velocity components u and v in terms of η and f are,

$$u = U_\infty \frac{\partial f}{\partial \eta}, \qquad v = \left[h' f + h\left(\frac{\partial f}{\partial x} + \frac{\partial f}{\partial \eta} g' y\right)\right]. \tag{3.73}$$

By using the transformation from Eq.(3.73), the momentum equation for upper-convected Maxwell (UCM) fluid in Eq.(3.64), the momentum equation for Carreau fluid in Eq.(3.65), the thermal energy equation in Eq.(3.66) and the mass concentration equation in Eq.(3.67) can be written as below respectively,

$$\frac{\partial^3 f}{\partial \eta^3} + \frac{1}{2} f \frac{\partial^2 f}{\partial \eta^2} - \frac{\beta}{2}\left[\eta\left(\frac{\partial f}{\partial \eta}\right)^2 \frac{\partial^2 f}{\partial \eta^2} + 2f\frac{\partial f}{\partial \eta}\frac{\partial^2 f}{\partial \eta^2} + f^2 \frac{\partial^3 f}{\partial \eta^3}\right] = x\left(\frac{\partial^2 f}{\partial x \partial y}\frac{\partial f}{\partial \eta} - \frac{\partial^2 f}{\partial \eta^2}\frac{\partial f}{\partial x}\right), \tag{3.74}$$

$$\left[1 + n\mathrm{We}^2\left(\frac{\partial^2 f}{\partial \eta^2}\right)^2\right]\left[1 + \mathrm{We}^2\left(\frac{\partial^2 f}{\partial \eta^2}\right)^2\right]^{\frac{n-3}{2}} \frac{\partial^3 f}{\partial \eta^3} + \frac{1}{2} f \frac{\partial^2 f}{\partial \eta^2} = x\left(\frac{\partial^2 f}{\partial x \partial y}\frac{\partial f}{\partial \eta} - \frac{\partial^2 f}{\partial \eta^2}\frac{\partial f}{\partial x}\right), \tag{3.75}$$

$$\frac{\partial^2 \theta}{\partial \eta^2} + \frac{1}{2}\mathrm{Pr} f \frac{\partial \theta}{\partial \eta} - \frac{1}{2}\mathrm{Pr}\gamma\left[3f\frac{\partial f}{\partial \eta}\frac{\partial \theta}{\partial \eta} + f^2\frac{\partial^2 \theta}{\partial \eta^2}\right] = \mathrm{Pr}x\left(\frac{\partial f}{\partial \eta}\frac{\partial \theta}{\partial x} - \frac{\partial f}{\partial x}\frac{\partial \theta}{\partial \eta}\right), \tag{3.76}$$

$$\frac{\partial^2 \phi}{\partial \eta^2} + \frac{1}{2}\mathrm{Sc} f \frac{\partial \phi}{\partial \eta} = \mathrm{Sc}x\left(\frac{\partial f}{\partial \eta}\frac{\partial \phi}{\partial x} - \frac{\partial f}{\partial x}\frac{\partial \phi}{\partial \eta}\right). \tag{3.77}$$

The various dimensionless parameters used in Eqs.(3.74) - (3.77) are defined as follows,

$$\beta = \frac{\lambda_1 U_\infty}{2x} \quad \text{(local Deborah number for momentum)}, \tag{3.78}$$

$$\gamma = \frac{\lambda_2 U_\infty}{2x} \quad \text{(local Deborah number for energy)}, \tag{3.79}$$

$$\mathrm{We} = \sqrt{\frac{\Gamma^2 U_\infty^3 x^3}{\nu}} \quad \text{(Weissenberg number)}, \tag{3.80}$$

$$\mathrm{Pr} = \frac{\nu}{\alpha} \quad \text{(Prandtl number)}, \tag{3.81}$$

$$\mathrm{Sc} = \frac{\nu}{D} \quad \text{(Schmidt number)}. \tag{3.82}$$

3.3.2 Similarity Transformation for a Horizontal Wedge

Consider the stream function as defined in Eq.(3.58). By Falkner and Skan (1931, November), the free stream velocity U_∞ is defined as,

$$U_\infty = ax^m, \tag{3.83}$$

where a is a constant and m is the wedge angle parameter which depends on the Hartree pressure gradient β_w, and is related to,

$$\beta_w = \frac{2m}{m+1}. \tag{3.84}$$

By evaluating ψ and its derivative, the stream function becomes,

$$\psi = \sqrt{\frac{2U_\infty \nu x}{m+1}} f(\eta) = h(x) f(\eta). \tag{3.85}$$

and the dimensionless distance becomes,

$$\eta = y\sqrt{\frac{(m+1)U_\infty}{2\nu x}} = y \cdot g(x). \tag{3.86}$$

where $\nu = \dfrac{\mu}{\rho}$ is the kinematic viscosity of the fluid. By the above equations, the followings are derived,

$$h(x)g(x) = \sqrt{\frac{2U_\infty \nu x}{m+1}}\sqrt{\frac{(m+1)U_\infty}{2\nu x}} = U_\infty = ax^m, \tag{3.87}$$

$$\frac{dU_\infty}{dx} = max^{m-1}, \tag{3.88}$$

$$\frac{\partial \eta}{\partial x} = \frac{h'\eta}{h}. \tag{3.89}$$

Thus by Eq.(3.58), the velocity components u and v in terms of η and f are,

$$u = U_\infty \frac{\partial f}{\partial \eta}, \qquad v = \left[h' f + h\left(\frac{\partial f}{\partial x} + \frac{\partial f}{\partial \eta}\frac{h'\eta}{h}\right)\right]. \tag{3.90}$$

By using the transformation from Eq.(3.90), the momentum equation for upper-convected Maxwell (UCM) fluid in Eq.(3.64), the thermal energy equation in Eq.(3.66) and the mass concentration equation in Eq.(3.67) can be written as below respectively,

$$\begin{aligned}\frac{\partial^3 f}{\partial \eta^3} + f\frac{\partial^2 f}{\partial \eta^2} + \frac{2m}{m+1}\left[1 - \left(\frac{\partial f}{\partial \eta}\right)^2\right] + \beta\Bigg[2m\frac{m-1}{m+1}\left\{1 - \left(\frac{\partial f}{\partial \eta}\right)^2\right\} \\ + \frac{m-1}{2}\eta\left(\frac{\partial f}{\partial \eta}\right)^2\frac{\partial^2 f}{\partial \eta^2} - \frac{m+1}{2}f^2\frac{\partial^3 f}{\partial \eta^3} + (3m-1)f\frac{\partial f}{\partial \eta}\frac{\partial^2 f}{\partial \eta^2}\Bigg] \\ = \frac{2x}{m+1}\left(\frac{\partial^2 f}{\partial x \partial y}\frac{\partial f}{\partial \eta} - \frac{\partial^2 f}{\partial \eta^2}\frac{\partial f}{\partial x}\right),\end{aligned} \tag{3.91}$$

$$\frac{\partial^2 \theta}{\partial \eta^2} + \mathrm{Pr} f\frac{\partial \theta}{\partial \eta} - \mathrm{Pr}\gamma\left[f\frac{\partial f}{\partial \eta}\frac{\partial \theta}{\partial \eta} + \frac{m+1}{2}f^2\frac{\partial^2 \theta}{\partial \eta^2}\right] = \mathrm{Pr}\frac{2x}{m+1}\left(\frac{\partial f}{\partial \eta}\frac{\partial \theta}{\partial x} - \frac{\partial f}{\partial x}\frac{\partial \theta}{\partial \eta}\right), \tag{3.92}$$

$$\frac{\partial^2 \phi}{\partial \eta^2} + \mathrm{Sc} f\frac{\partial \phi}{\partial \eta} = \mathrm{Sc}\frac{2x}{m+1}\left(\frac{\partial f}{\partial \eta}\frac{\partial \phi}{\partial x} - \frac{\partial f}{\partial x}\frac{\partial \phi}{\partial \eta}\right). \tag{3.93}$$

The various dimensionless parameters used in Eqs.(3.91) - (3.93) are defined as follows,

$$\beta = \frac{\lambda_1 U_\infty}{x} \quad \text{(local Deborah number for momentum),} \tag{3.94}$$

$$\gamma = \frac{\lambda_2 U_\infty}{x} \quad \text{(local Deborah number for energy),} \tag{3.95}$$

$$\mathrm{Pr} = \frac{\nu}{\alpha} \quad \text{(Prandtl number),} \tag{3.96}$$

$$\mathrm{Sc} = \frac{\nu}{D} \quad \text{(Schmidt number).} \tag{3.97}$$

3.3.3 The Dimensionless Boundary Conditions

The boundary conditions for the boundary layer flow are transformed using similarity transformation so that they still describe the flow without any changes.

The boundary conditions for the momentum equation that satisfy f are,

1. for Sakiadis flow:

$$\begin{aligned} f = 0, \quad \frac{\partial f}{\partial \eta} &= 1 \quad \text{at} \quad \eta = 0, \\ \frac{\partial f}{\partial \eta} &\to 0 \quad \text{as} \quad \eta \to \infty, \end{aligned} \tag{3.98}$$

2. for Blasius flow and static Falkner-Skan flow:

$$\begin{aligned} f = 0, \quad \frac{\partial f}{\partial \eta} &= 0 \quad \text{at} \quad \eta = 0, \\ \frac{\partial f}{\partial \eta} &\to 1 \quad \text{as} \quad \eta \to \infty. \end{aligned} \tag{3.99}$$

The boundary conditions for thermal energy equation that satisfy θ are,

$$\begin{aligned} \theta &= 1, \quad \text{at} \quad \eta = 0, \\ \theta &\to 0 \quad \text{as} \quad \eta \to \infty. \end{aligned} \tag{3.100}$$

The boundary conditions for concentration equation that satisfy ϕ are,

$$\begin{aligned} \phi &= 1, \quad \text{at} \quad \eta = 0, \\ \phi &\to 0 \quad \text{as} \quad \eta \to \infty, \end{aligned} \tag{3.101}$$

3.3.4 Local Similarity Solution

Consider the transformed governing equations, Eqs.(3.74) - (3.77) and Eqs.(3.91) - (3.93). The variables x, y and their derivatives exist after the similarity transformation. By Kays and Crawford (1993), consider a general transformation of (x, y) to (ξ, η) where ξ is the dimensionless distance in x-direction. If either ξ or the derivative with respect to x remains, there is no similarity solution exists.

To compensate this, local similarity solution is employed. Local similarity solution can be obtained by dropping the derivatives containing ξ from the transformed equations and retaining ξ as a parameter. The resulting solutions are generally valid if ξ or its discarded derivatives are kept small enough.

3.3.5 Local Similarity Solution for Horizontal Plate

From Kays and Crawford (1993), as for a horizontal plate, $m = 0$, ξ and its derivative with respect to x are defined as,

$$\xi = bx^{\frac{1}{2}}, \qquad \frac{\partial \xi}{\partial x} = \frac{1}{2x}\xi. \tag{3.102}$$

By substituting Eq.(3.102) into Eqs.(3.74) - (3.77), the equations become,

$$\frac{\partial^3 f}{\partial \eta^3} + \frac{f}{2}\frac{\partial^2 f}{\partial \eta^2} - \frac{\beta}{2}\left[\eta\left(\frac{\partial f}{\partial \eta}\right)^2\frac{\partial^2 f}{\partial \eta^2} + 2f\frac{\partial f}{\partial \eta}\frac{\partial^2 f}{\partial \eta^2} + f^2\frac{\partial^3 f}{\partial \eta^3}\right] = \frac{1}{2}\xi\left(\frac{\partial^2 f}{\partial \xi \partial \eta}\frac{\partial f}{\partial \eta} - \frac{\partial^2 f}{\partial \eta^2}\frac{\partial f}{\partial \xi}\right), \tag{3.103}$$

$$\left[1 + n\mathrm{We}^2\left(\frac{\partial^2 f}{\partial \eta^2}\right)^2\right]\left[1 + \mathrm{We}^2\left(\frac{\partial^2 f}{\partial \eta^2}\right)^2\right]^{\frac{n-3}{2}}\frac{\partial^3 f}{\partial \eta^3} + \frac{1}{2}f\frac{\partial^2 f}{\partial \eta^2} = \frac{1}{2}\xi\left(\frac{\partial^2 f}{\partial \xi \partial \eta}\frac{\partial f}{\partial \eta} - \frac{\partial^2 f}{\partial \eta^2}\frac{\partial f}{\partial \xi}\right), \tag{3.104}$$

$$\frac{\partial^2 \theta}{\partial \eta^2} + \frac{1}{2}\mathrm{Pr}f\frac{\partial \theta}{\partial \eta} - \frac{1}{2}\mathrm{Pr}\gamma\left[3f\frac{\partial f}{\partial \eta}\frac{\partial \theta}{\partial \eta} + f^2\frac{\partial^2 \theta}{\partial \eta^2}\right] = \frac{1}{2}\mathrm{Pr}\xi\left(\frac{\partial f}{\partial \eta}\frac{\partial \theta}{\partial \xi} - \frac{\partial f}{\partial \xi}\frac{\partial \theta}{\partial \eta}\right), \tag{3.105}$$

$$\frac{\partial^2 \phi}{\partial \eta^2} + \frac{1}{2}\mathrm{Sc}f\frac{\partial \phi}{\partial \eta} = \frac{1}{2}\mathrm{Sc}\xi\left(\frac{\partial f}{\partial \eta}\frac{\partial \phi}{\partial \xi} - \frac{\partial f}{\partial \xi}\frac{\partial \phi}{\partial \eta}\right). \tag{3.106}$$

Since there exists ξ and its derivative in the equations, the similarity solution does not exist. By employing the assumption made in Section 3.3.4, the governing equations from Eqs.(3.103) - (3.106) can be reduced to,

$$f''' + \frac{1}{2}ff'' - \frac{\beta}{2}\left[\eta(f')^2 + 2ff'f'' + f^2f'''\right] = 0, \tag{3.107}$$

$$\left[1 + n\mathrm{We}^2(f'')^2\right]\left[1 + \mathrm{We}^2(f'')^2\right]^{\frac{n-3}{2}}f''' + \frac{1}{2}ff'' = 0, \tag{3.108}$$

$$\theta'' + \frac{1}{2}\mathrm{Pr}f\theta' - \frac{1}{2}\mathrm{Pr}\gamma\left[3ff'\theta' + f^2\theta''\right] = 0, \tag{3.109}$$

$$\phi'' + \frac{1}{2}\mathrm{Sc}f\phi' = 0, \tag{3.110}$$

where primes denote the differentiation with respect to η.

3.3.6 Local Similarity Solution for Horizontal Wedge

From Kays and Crawford (1993), ξ and its derivative with respect to x are defined as,

$$\xi = bx^{\frac{1-m}{2}}, \qquad \frac{\partial \xi}{\partial x} = \frac{1-m}{2x}\xi. \tag{3.111}$$

By substituting Eq.(3.111) into Eqs.(3.91) - (3.93),

$$\begin{aligned}\frac{\partial^3 f}{\partial \eta^3} + f\frac{\partial^2 f}{\partial \eta^2} + \frac{2m}{m+1}\left[1-\left(\frac{\partial f}{\partial \eta}\right)^2\right] + \beta\left[2m\frac{m-1}{m+1}\left\{1-\left(\frac{\partial f}{\partial \eta}\right)^2\right\}\right.\\ \left. + \frac{m-1}{2}\eta\left(\frac{\partial f}{\partial \eta}\right)^2\frac{\partial^2 f}{\partial \eta^2} - \frac{m+1}{2}f^2\frac{\partial^3 f}{\partial \eta^3} + (3m-1)f\frac{\partial f}{\partial \eta}\frac{\partial^2 f}{\partial \eta^2}\right]\\ = \frac{1-m}{m+1}\xi\left(\frac{\partial^2 f}{\partial \xi \partial \eta}\frac{\partial f}{\partial \eta} - \frac{\partial^2 f}{\partial \eta^2}\frac{\partial f}{\partial \xi}\right),\end{aligned} \tag{3.112}$$

$$\frac{\partial^2 \theta}{\partial \eta^2} + \mathrm{Pr} f\frac{\partial \theta}{\partial \eta} - \mathrm{Pr}\gamma\left[f\frac{\partial f}{\partial \eta}\frac{\partial \theta}{\partial \eta} + \frac{m+1}{2}f^2\frac{\partial^2 \theta}{\partial \eta^2}\right] = \frac{1-m}{m+1}\mathrm{Pr}\xi\left(\frac{\partial f}{\partial \eta}\frac{\partial \theta}{\partial \xi} - \frac{\partial f}{\partial \xi}\frac{\partial \theta}{\partial \eta}\right), \tag{3.113}$$

$$\frac{\partial^2 \phi}{\partial \eta^2} + \mathrm{Sc} f\frac{\partial \phi}{\partial \eta} = \mathrm{Sc}\frac{1-m}{m+1}\left(\frac{\partial f}{\partial \eta}\frac{\partial \phi}{\partial \xi} - \frac{\partial f}{\partial \xi}\frac{\partial \phi}{\partial \eta}\right). \tag{3.114}$$

Since there exists ξ and its derivative in the equations, the similarity solution does not exist. By employing the assumption made in Section 3.3.4, the governing equations (3.112) - (3.114) can be reduced to,

$$\begin{aligned}f''' + \frac{2m}{m+1}\left(1-(f')^2\right) + ff'' + \beta\left[2m\frac{m-1}{m+1}\left(1-(f')^3\right)\right.\\ \left. + \frac{m-1}{2}\eta(f')^2 f'' - \frac{m+1}{2}f^2 f''' + (3m-1)ff'f''\right] = 0,\end{aligned} \tag{3.115}$$

$$\theta'' + \mathrm{Pr} f\theta' - \mathrm{Pr}\gamma\left[\frac{m+1}{2}f^2\theta'' + ff'\theta'\right] = 0, \tag{3.116}$$

$$\phi'' + \mathrm{Sc} f\phi' = 0, \tag{3.117}$$

where primes denotes the differentiation with respect to η.

3.4 The Local Skin Friction Coefficient, Local Nusselt Number and Local Sherwood Number

The local skin-friction coefficient for upper-convected Maxwell fluid, local skin-friction coefficient for Carreau fluid, local Nusselt number and local Sherwood number respectively, are defined as,

$$C_f = \frac{\mu}{\rho U_\infty^2}\left(\frac{\partial u}{\partial y}\right)_{y=0}, \tag{3.118}$$

$$C_f = \frac{\mu}{\rho U_\infty^2}\left(\frac{\partial u}{\partial y}\right)_{y=0}\left[1+\Gamma^2\left\{\left(\frac{\partial u}{\partial y}\right)^2\right\}_{y=0}\right]^{\frac{n-1}{2}}, \tag{3.119}$$

$$\mathrm{Nu} = -\frac{x}{(T_w - T_\infty)}\left(\frac{\partial T}{\partial y}\right)_{y=0}, \tag{3.120}$$

$$\mathrm{Sh} = -\frac{x}{(C_w - C_\infty)}\left(\frac{\partial C}{\partial y}\right)_{y=0}. \tag{3.121}$$

By some substitutions and calculations, the following are the local skin-friction coefficient for UCM fluid, local skin-friction coefficient for Carreau fluid, local Nusselt number and local Sherwood number for a horizontal plate respectively,

$$C_f(\mathrm{Re}_x)^{1/2} = f''(0), \tag{3.122}$$

$$C_f(\mathrm{Re}_x)^{1/2} = f''(0)\left[1+\mathrm{We}^2\left\{f''(0)\right\}^2\right]^{\frac{n-1}{2}}, \tag{3.123}$$

$$\mathrm{Nu}(\mathrm{Re}_x)^{-1/2} = \theta'(0), \tag{3.124}$$

$$\mathrm{Sh}(\mathrm{Re}_x)^{-1/2} = \phi'(0). \tag{3.125}$$

By the same substitutions and calculations, the following are the local skin-friction coefficient, local Nusselt number and local Sherwood number for a horizontal wedge respectively,

$$C_f(\mathrm{Re}_x)^{1/2} = \sqrt{\frac{m+1}{2}}f''(0), \tag{3.126}$$

$$\mathrm{Nu}(\mathrm{Re}_x)^{-1/2} = -\sqrt{\frac{m+1}{2}}\theta'(0), \tag{3.127}$$

$$\mathrm{Sh}(\mathrm{Re}_x)^{-1/2} = -\sqrt{\frac{m+1}{2}}\phi'(0), \tag{3.128}$$

where $\mathrm{Re}_x = \dfrac{U_\infty x}{\nu}$ is the local Reynolds number.

3.5 Numerical Method

The nonlinear ordinary differential equations, Eqs. (3.107) - (3.110) and Eqs. (3.115) - (3.117) are the third order in f and second order in θ and ϕ. These equations are numerically solved and computed by using two different algorithms. The third order finite difference method (FDM) proposed by Pandey (2017) is used to solve Eqs. (3.107), (3.108) and (3.115), meanwhile for Eqs. (3.109), (3.110), (3.116) and (3.117), the standard second-order FDM (Burden & Faires, 2011) is used to solve the equation. The third order ordinary differential equation is solved first and then followed by the second-order ordinary differential equation by treating the function f as a constant in which the value used is retrieved from the results calculated in the first method.

The third order FDM proposed by Pandey (2017) has many advantages such as simplicity and at least of second-order accuracy. In addition, the calculations of the partial derivatives to find the Jacobian of the equations involved are not needed. Since other variation of third-order FDMs are needed to find the partial derivatives of the equations such as the continuous fourth derivative FDM proposed by Sahi et al. (2013) and the fourth-order FDM to solve a third order boundary value problem as proposed by Salama (2005), the present proposed method is chosen.

3.5.1 Second-Order Ordinary Differential Equation

Based on Burden and Faires (2011), the domain is set as $[a_1, a_2] \in \mathbb{N}$ where a_1 and a_2 are some finite values that approximate η as $\eta \to \infty$. The domain is divided into $(N + 1)$ subdomains, where the endpoints are at $\eta_i = a_1 + ih$, for $i = 0, 1, 2, ..., N + 1$ and $h = \dfrac{a_2 - a_1}{N}$ is the stepsize. Suppose the theoretical solution is $\Theta(\eta, \theta, \theta') = \theta''$ at points $\eta = \eta_i, i = 0, 1, 2, ..., N + 1$. The central divided difference formula of second-order accuracy is considered,

$$\begin{aligned} y_i' &= \frac{1}{2h}\left[y_{i+1} - y_{i-1}\right], \\ y_i'' &= \frac{1}{h^2}\left[y_{i+1} - 2y_i + y_{i-1}\right]. \end{aligned} \tag{3.129}$$

Thus, it can be written as,

$$\frac{-\theta_{i+1} - 2\theta_i + \theta_{i-1}}{h^2} + \Theta_i = 0, \tag{3.130}$$

where the function of Θ_i is in the form of,

$$\theta_i'' = \Theta_i(\eta_i, \theta_i, \theta_i'), \quad i = 1, 2, ..., N + 1, \tag{3.131}$$

subject to the following boundary condition,

$$\theta_0 = \beta_1, \quad \theta_{N+1} = \beta_2. \tag{3.132}$$

Newton-Raphson iterative method is used to solve Eq.(3.130) as proposed in Burden and Faires (2011, Chapter 11.4) by finding the value of $\theta_i^{[k]}$ such that k^{th} iteration gives the tolerance level of 10^{-5} and the initial guess for $\theta_i^{[0]}$ is written as,

$$\theta_i^{[0]} = 1 - e^{\eta_i}, i = 0, 1, 2, ..., N. \tag{3.133}$$

The summary of the algorithm explained above are presented in a flowchart in Figure 3.7.

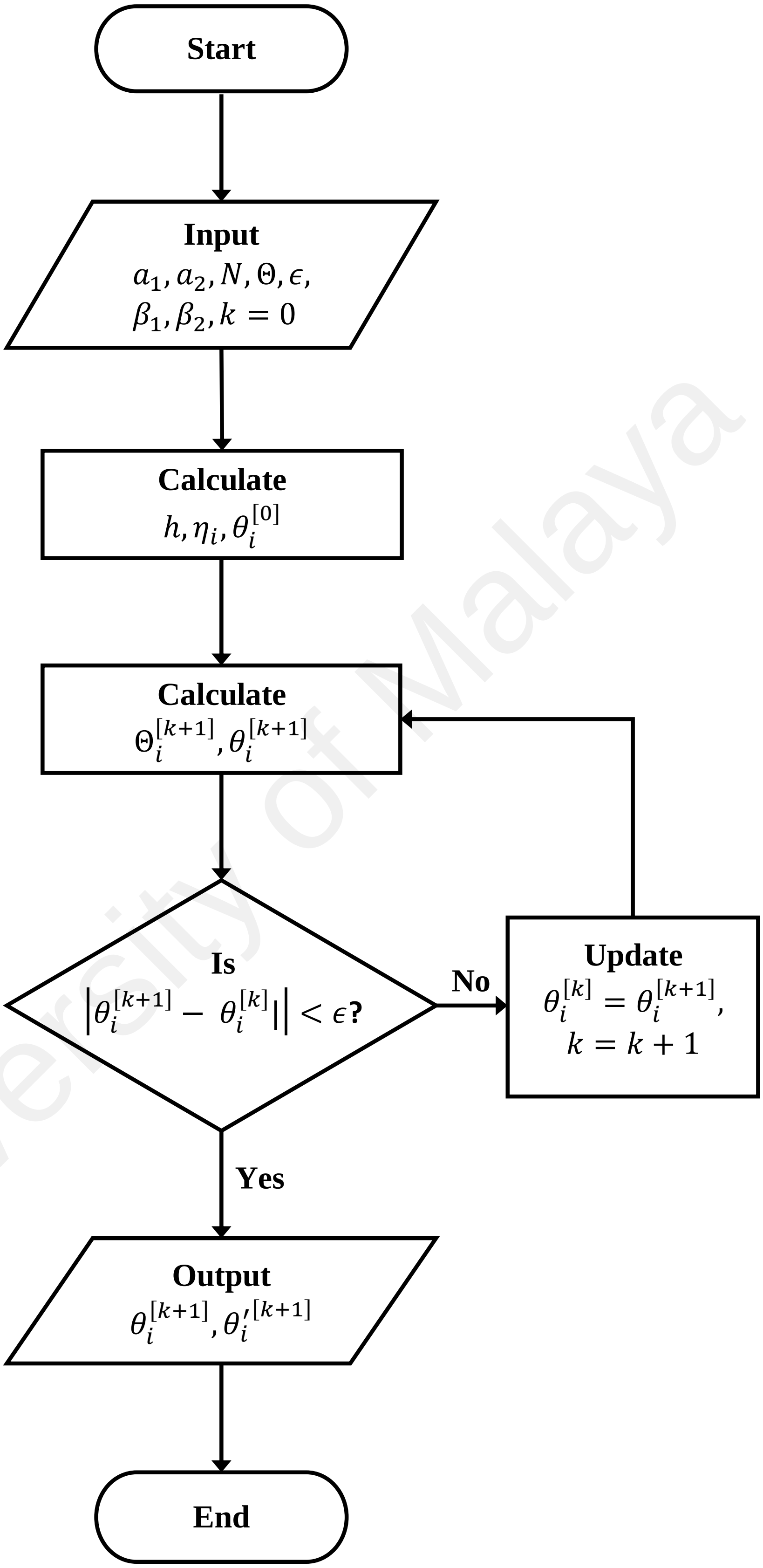

Figure 3.7: The flowchart of the algorithm for second-order finite difference method (FDM) to solve second-order ordinary differential equation (ODE)

3.5.2 Third-Order Ordinary Differential Equation

Based on Pandey (2017), the domain is set as $[a_1, a_2] \in \mathbb{N}$ where a_1 and a_2 are some finite values and it approximates η as $\eta \to \infty$ are defined. The domain are divided into N subdomains, so that $a_1 = \eta_0 < \eta_1 < \eta_2 < ... < \eta_N = a_2$ with uniform step size h such that $\eta_i = a_1 + ih, i = 0, 1, 2, ..., N$. Suppose the exact solution is $F(\eta)$ at nodal point $\eta_i, i = 1, 2, 3, ..., N$. The numerical approximations of $f(\eta)$ at node η_i are denoted as f_i, and the source functions are denoted as $F_i(\eta_i)$, at node $\eta = \eta_i, i = 0, 1, 2, ..., N$. Thus the momentum equations (3.107), (3.108) and (3.115) can be written as,

$$F_i(\eta, f_i, f_i', f_i'') = f_i''', \text{ at } \eta = \eta_i, \quad a_1 < \eta_i < a_1, \tag{3.134}$$

subject to the following boundary condition

$$f_0 = \alpha_1, \quad f_0' = \alpha_2, \quad f_N' = \alpha_3. \tag{3.135}$$

For the next step, nodes $\eta_{i+\frac{1}{2}} = \eta_i + \frac{h}{2}$, $i = 0, 1, 2, ..., N - 1$ are defined and $f_{i+\frac{1}{2}}$, $i = 0, 1, 2, ..., N - 1$ denotes the approximate solution of Eq.(3.134) at those nodes. The following approximations are defined,

$$\bar{f}'_{i-\frac{1}{2}} = \begin{cases} \frac{1}{h}\left[4\left(f_{i-\frac{1}{2}} - f_{i-1}\right) - hf'_{i-1}\right], & \text{if } i = 1, \\ \frac{1}{2h}\left[f_{i+\frac{1}{2}} - f_{i-\frac{3}{2}}\right], & \text{if } i = 2, \ 4 \leqslant i \leqslant N-1, \\ \frac{1}{2h}\left[3f_{i-\frac{1}{2}} - 4f_{i-\frac{3}{2}} + f_{i-\frac{5}{2}}\right], & \text{if } i = 3, \\ \frac{1}{2h}\left[f_{i-\frac{1}{2}} - f_{i-\frac{3}{2}} + 2hf_i'\right], & \text{if } i = N, \end{cases} \tag{3.136}$$

$$\bar{f}''_{i-\frac{1}{2}} = \begin{cases} \frac{1}{h^2}\left[h\left(f_{i+\frac{1}{2}} - f_{i-\frac{1}{2}}\right) - f'_{i-1}\right], & \text{if } i = 1, \\ \frac{1}{h^2}\left[f_{i+\frac{1}{2}} - 2f_{i-\frac{1}{2}} + f_{i-\frac{3}{2}}\right], & \text{if } i = 2, \ 4 \leqslant i \leqslant N-1, \\ \frac{1}{35h^2}\left[-88f_{i-3} + 200f_{i-\frac{5}{2}} - 180f_{i-\frac{3}{2}} + 68f_{i-\frac{1}{2}}\right], & \text{if } i = 3, \\ \frac{1}{23h^2}\left[26f_{i-\frac{3}{2}} - 25f_{i-\frac{1}{2}}f_{i-\frac{5}{2}} + 24hf_i'\right], & \text{if } i = N. \end{cases} \tag{3.137}$$

By using Eq.(3.134), the following approximations are produced,

$$f''' = \bar{F}_{i+\frac{1}{2}}(\eta_{i+\frac{1}{2}}, f_{i+\frac{1}{2}}, \bar{f}'_{i+\frac{1}{2}}, \bar{f}''_{i+\frac{1}{2}}), \quad i = 1, 2, ..., N-1. \tag{3.138}$$

The above $N \times N$ nonlinear system of equations with unknowns $f_{i-\frac{1}{2}}, \;\; i = 1, 2, ..., N$ can be written into a system of matrix,

$$D\mathbf{f} = \mathbf{a(f)}, \tag{3.139}$$

where

$$D = \begin{bmatrix} 9 & -1 & 0 & 0 & 0 & 0 & 0 \\ -15 & 10 & -3 & 0 & 0 & 0 & 0 \\ 1 & -3 & 3 & -1 & 0 & 0 & 0 \\ 0 & 1 & -3 & 3 & -1 & 0 & 0 \\ \vdots & \vdots & \ddots & \ddots & \ddots & \ddots & \vdots \\ 0 & 0 & 0 & 1 & -3 & 3 & -1 \\ 0 & 0 & 0 & 0 & 1 & -3 & 2 \end{bmatrix}, \quad \mathbf{f} = \begin{bmatrix} f_{\frac{1}{2}} \\ f_{\frac{3}{2}} \\ f_{\frac{5}{2}} \\ f_{\frac{7}{2}} \\ \vdots \\ f_{N-\frac{3}{2}} \\ f_{N-\frac{1}{2}} \end{bmatrix}, \quad \mathbf{a} = \begin{bmatrix} a_{\frac{1}{2}} \\ a_{\frac{3}{2}} \\ a_{\frac{5}{2}} \\ a_{\frac{7}{2}} \\ \vdots \\ a_{N-\frac{3}{2}} \\ a_{N-\frac{1}{2}} \end{bmatrix}, \tag{3.140}$$

$$a_i = \begin{cases} 8f_0 + 3hf'_0 - \dfrac{3h^3}{8}\bar{F}_{\frac{1}{2}}, & \text{if } i = 1, \\ -8f_0 - \dfrac{5h^3}{16}\left(11\bar{F}_{\frac{3}{2}} - 3\bar{F}_{\frac{5}{2}}\right), & \text{if } i = 2, \\ -\dfrac{h^3}{8}\left(\bar{F}_{i-\frac{3}{2}} + \bar{F}_{i-\frac{1}{2}}\right), & \text{if } 3 \leqslant i \leqslant N-1, \\ hf'_N + \dfrac{h^3}{48}\left(-25\bar{F}_{N-\frac{3}{2}} + 21\bar{F}_{N-\frac{1}{2}}\right), & \text{if } i = N. \end{cases} \tag{3.141}$$

Newton-Raphson iterative method is used to solve Eq.(3.139) by finding the value of $f_i^{[k]}$ such that k^{th} iteration is the approximate solution with tolerance level of 10^{-5}. The initial guess for $f_i^{[0]}$ is defined by,

$$f_i^{[0]} = 1 - e^{\eta_i}, \quad i = 0, 1, 2, ..., N. \tag{3.142}$$

Then the value of $f_i^{[m]}, \;\; m \leq k$ are calculated by using the following second order central divided difference approximations,

$$f_i^{[m]} = \begin{cases} \dfrac{1}{2}\left(f_{i-\frac{1}{2}}^{[m]} + f_{i+\frac{1}{2}}^{[m]}\right), & i = 1, 2, \ldots, N-1, \\ f_{i-\frac{1}{2}}^{[m]} + \dfrac{1}{2}hf_i', & i = N. \end{cases} \tag{3.143}$$

The summary of the algorithm explained above is presented in a flowchart in Figure 3.8.

3.6 Code Validation

The algorithm for the numerical method from Section 3.5 is written in MATLAB for numerical computation. The present results of $f''(0)$ for various values of m when $\beta = 0$ from Eq.(3.115) are compared with the data published by Yih (1998), Khan et al. (2013), Ganapathirao et al. (2013) and Khan et al. (2014) in order to verify the accuracy and to ensure the algorithm is written correctly. The data comparisons along with the method used are shown in Table 3.1. The present results are in a very good agreement with previous results. It can be concluded that the algorithm for the numerical method chosen in this study is acceptably accurate and the programming code is written correctly.

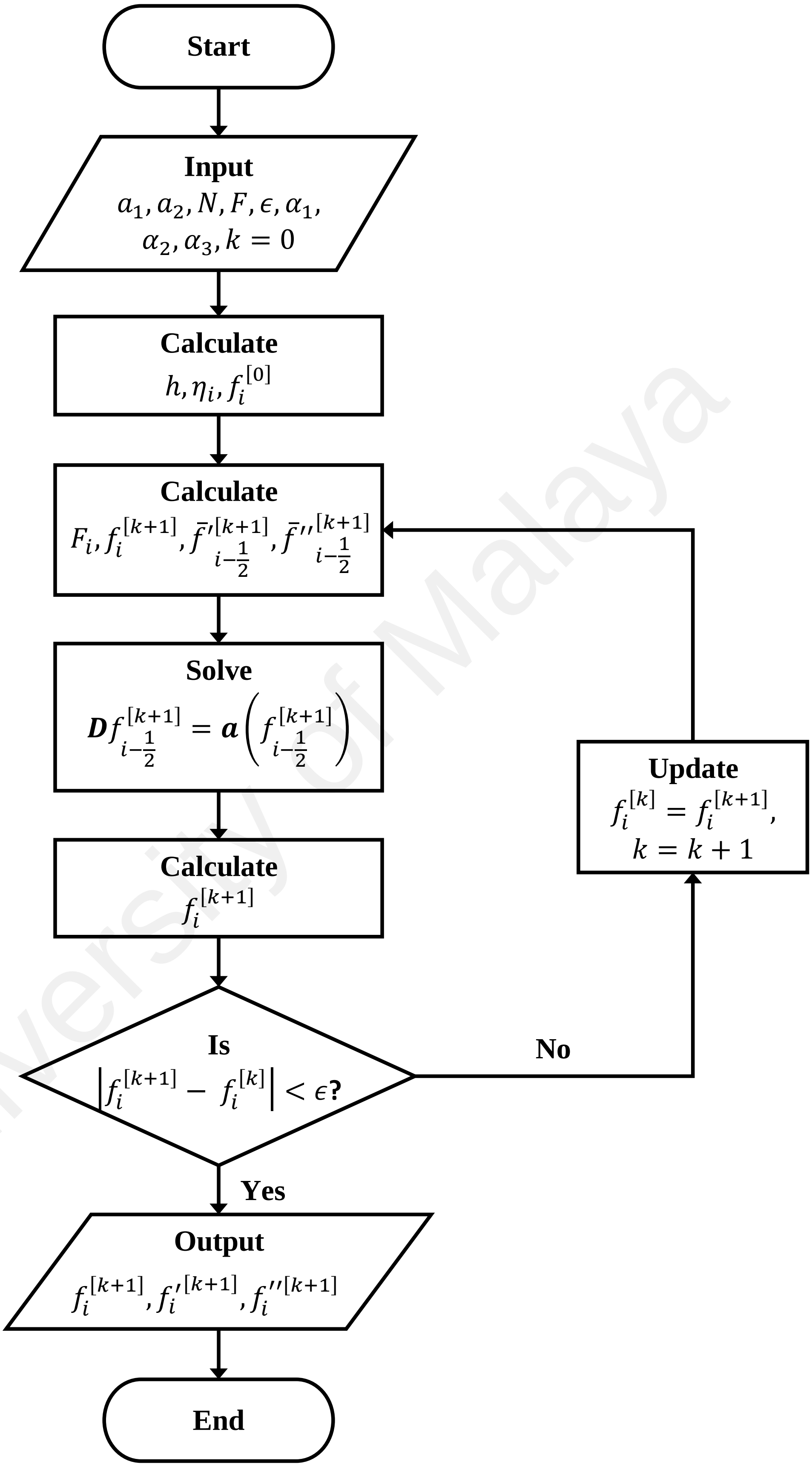

Figure 3.8: The flowchart of the algorithm for third-order finite difference method (FDM) to solve third-order ordinary differential equation (ODE)

Table 3.1: Comparison of the value of $f''(0)$ with different values of m from Yih (1998), Khan et al. (2013), Ganapathirao (2013) and Khan et al. (2014) with the present results where $\beta = 0$

	Yih (1998)	Khan et al. (2013)	Ganapathirao et al. (2013)	Khan et al. (2014)	Present
Method used	Keller-Box	Keller-Box	Implicit FDM	Runge-Kutta with Shooting	FDM
m					
0.0000	0.469600	0.469600	0.469720	0.469900	0.469443
0.0141	0.504614	-	0.504810	-	0.506152
0.0909	0.654979	0.655000	0.654930	0.657400	0.655053
0.1429	0.731998	-	0.731960	-	0.729816
0.2000	0.802125	0.802100	0.802150	0.804500	0.802897
0.3333	0.927653	0.927700	0.927670	0.929800	0.928139
0.5000	-	1.038900	1.038930	1.039400	1.038879

CHAPTER 4: NUMERICAL ANALYSIS OF MASS AND HEAT TRANSFER FOR SAKIADIS AND BLASIUS FLOWS OF UPPER-CONVECTED MAXWELL FLUID WITH CATTANEO-CHRISTOV HEAT FLUX MODEL OVER A HORIZONTAL PLATE

This chapter discussed the heat and mass transfer of upper-convected Maxwell (UCM) Sakiadis and Blasius boundary layer fluid flows past a horizontal plate using Cattaneo-Christov heat flux model. The effect of Deborah number, Prandtl number and Schmidt number on the velocity profile, temperature profile and concentration profile are also discussed in this chapter.

4.1 Mathematical Formulation

The two-dimensional laminar flow of (UCM) fluid over a semi-infinite plate at $y = 0$ is considered. An assumption is made that the plate has a constant temperature T_w and constant concentration C_w, and the ambient fluid temperature and ambient concentration are T_∞ and C_∞ respectively. The governed equations for the steady incompressible laminar Sakiadis and Blasius flows of UCM fluid with heat and mass transfer are expressed as,

$$\frac{\partial u}{\partial x} + \frac{\partial v}{\partial y} = 0, \tag{4.1}$$

$$u\frac{\partial u}{\partial x} + v\frac{\partial u}{\partial y} + \lambda_1\left(u^2\frac{\partial^2 u}{\partial x^2} + v^2\frac{\partial^2 u}{\partial y^2} + 2uv\frac{\partial^2 u}{\partial x \partial y}\right) = \nu\frac{\partial^2 u}{\partial y^2}, \tag{4.2}$$

$$\begin{aligned} u\frac{\partial T}{\partial x} + v\frac{\partial T}{\partial y} + \lambda_2\Bigg[u^2\frac{\partial^2 T}{\partial x^2} + v^2\frac{\partial^2 T}{\partial y^2} + 2uv\frac{\partial^2 T}{\partial x \partial y} + \left(u\frac{\partial u}{\partial x} + v\frac{\partial u}{\partial y}\right)\frac{\partial T}{\partial x} \\ + \left(u\frac{\partial v}{\partial x} + v\frac{\partial v}{\partial y}\right)\frac{\partial T}{\partial y}\Bigg] = \alpha\frac{\partial^2 T}{\partial y^2}, \end{aligned} \tag{4.3}$$

$$u\frac{\partial C}{\partial x} + v\frac{\partial C}{\partial y} = D\frac{\partial^2 C}{\partial y^2}, \tag{4.4}$$

with x and y are the coordinates along and normal to the heated plate respectively, u and v are the velocity components along the x and y axis respectively, λ_1 is the relaxation time of the UCM fluid, ν is the kinematic viscosity of the fluid, $\alpha = \dfrac{k}{\rho C_p}$ is the thermal diffusivity, k is the thermal conductivity, ρ is the density of the fluid, C_p is the specific heat capacity of the fluid, λ_2 is the relaxation time for heat flux, T is the local fluid temperature, C is the local fluid concentration and D is the mass diffusion coefficient.

The boundary conditions for the system are,

1. Sakiadis flow

$$\begin{aligned} u = U_\infty, \quad v = v_0, \quad T = T_w, \quad C = C_w, \quad \text{at} \quad y = 0, \\ u \to 0, \quad T \to T_\infty, \quad C \to C_\infty, \quad \text{as} \quad y \to \infty, \end{aligned} \tag{4.5}$$

2. Blasius flow

$$\begin{aligned} u = 0, \quad v = v_0, \quad T = T_w, \quad C = C_w, \quad \text{at} \quad y = 0, \\ u \to U_\infty, \quad T \to T_\infty, \quad C \to C_\infty, \quad \text{as} \quad y \to \infty, \end{aligned} \tag{4.6}$$

where U_∞ is the constant free stream velocity. The following dimensionless variables are introduced to obtain similarity solution for the problem,

$$\eta = y\sqrt{\frac{U_\infty}{\nu x}}, \quad \psi = f(\eta)\sqrt{U_\infty \nu x}, \quad \theta(\eta) = \frac{T - T_\infty}{T_w - T_\infty}, \quad \phi(\eta) = \frac{C - C_\infty}{C_w - C_\infty}, \tag{4.7}$$

where η is the dimensionless similarity variable, ψ is the stream function defined as $u = \dfrac{\partial \psi}{\partial y}$ and $v = -\dfrac{\partial \psi}{\partial x}$. By substituting Eq.(4.7) into Eqs.(4.2) - (4.4), the following set of nonlinear ordinary differential equation are obtained,

$$f''' + \frac{1}{2} f f'' - \frac{\beta}{2}\left(\eta\,(f')^2 f'' + 2 f f' f'' + f^2 f'''\right) = 0, \tag{4.8}$$

$$\frac{1}{\mathrm{Pr}}\theta'' + \frac{1}{2} f \theta' - \frac{\gamma}{2}\left(3 f f' \theta' + f^2 \theta''\right) = 0, \tag{4.9}$$

$$\phi'' + \frac{\mathrm{Sc}}{2} f \phi' = 0, \tag{4.10}$$

where prime denotes the normal differentiation with respect to η, $\beta = \dfrac{\lambda_1 U_\infty}{2x}$ is the local Deborah number for fluid velocity, $\gamma = \dfrac{\lambda_2 U_\infty}{2x}$ is the local Deborah number for fluid temperature, $\mathrm{Pr} = \dfrac{\nu}{\alpha}$ is the Prandtl number and $\mathrm{Sc} = \dfrac{\nu}{D}$ is the Schmidt number. The local similarity solutions are used for β and γ since it contains the function of x, and the solution found is used to analyse the fluid behaviour.

The transformed boundary conditions are,

1. Sakiadis flow

$$\begin{aligned} f = 0, \quad f' = 1, \quad \theta = 1, \quad \phi = 1, \quad &\text{at} \quad \eta = 0, \\ f' \to 0, \quad \theta \to 0, \quad \phi \to 0, \quad &\text{as} \quad \eta \to \infty, \end{aligned} \tag{4.11}$$

2. Blasius flow

$$\begin{aligned} f = 0, \quad f' = 0, \quad \theta = 1, \quad \phi = 1, \quad &\text{at} \quad \eta = 0, \\ f' \to 1, \quad \theta \to 0, \quad \phi \to 0, \quad &\text{as} \quad \eta \to \infty, \end{aligned} \tag{4.12}$$

The important physical quantities of the flow are the local skin-friction coefficient C_f, local Nusselt number Nu and local Sherwood number Sh, which are related to the value of $f''(0)$, $-\theta'(0)$ and $\phi'(0)$ respectively. These parameter are defined as $C_f = \dfrac{\mu}{\rho U_\infty^2}\left(\dfrac{\partial u}{\partial y}\right)_{y=0}$, $\mathrm{Nu} = -\dfrac{x}{(T_w - T_\infty)}\left(\dfrac{\partial T}{\partial y}\right)_{y=0}$ and $\mathrm{Sh} = -\dfrac{x}{(C_w - C_\infty)}\left(\dfrac{\partial C}{\partial y}\right)_{y=0}$ respectively. By substituting Eq.(4.7), the local skin-friction coefficient, local Nusselt number and local Sherwood number are,

$$C_f\,(\mathrm{Re}_x)^{1/2} = f''(0), \tag{4.13}$$

$$\mathrm{Nu}\,(\mathrm{Re}_x)^{-1/2} = -\theta'(0), \tag{4.14}$$

$$\mathrm{Sh}\,(\mathrm{Re}_x)^{-1/2} = -\phi'(0), \tag{4.15}$$

where $\mathrm{Re}_x = \dfrac{U_\infty x}{\nu}$ is the local Reynolds number.

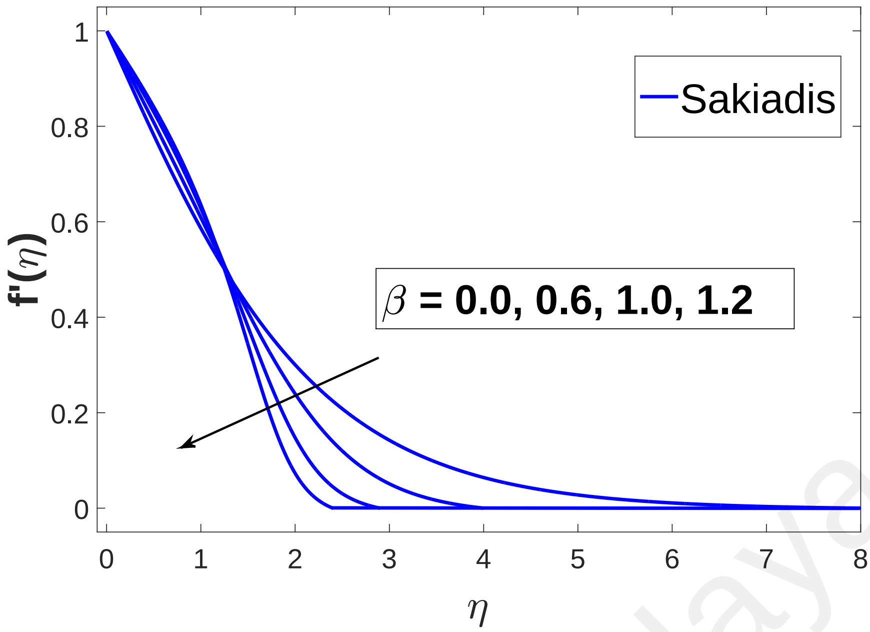

Figure 4.1: The velocity profile for different values of β with Pr = Sc = 1 and γ = 0.25

4.2 Results and Discussion

Table 4.1 presents the values of $f''(0)$, $-\theta'(0)$ and $-\phi'(0)$ for various values of parameters. From Table 4.1, the value of $f''(0)$ decreases as the Deborah number β increases for Sakiadis flow but decreases for Blasius flow. Noted that the value of $f''(0)$ remains unchanged when the values of Pr, γ and Sc increase. This is because the aforementioned parameters do not present in the momentum equation, and thus, they do not disturb the fluid velocity of the system. It is also can be seen that the values of $-\theta'(0)$ and $-\phi'(0)$ are increasing when the Deborah number β increases for both Sakiadis and Blasius flows, although the value of $-\theta'(0)$ and $-\phi'(0)$ for Blasius flow are higher than of Sakiadis flow.

In Figure 4.1, the effects of the Deborah number β to the fluid velocity profile f' for Sakiadis flow are graphed. For velocity profile of Blasius flow, the value of β is fixed to be zero. It is shown that for increasing value of β, the fluid velocity seems to be increased slightly within the domain $0 < \eta < 1.2$ approximately, but for the region $\eta > 1.2$ the fluid velocity decreases with the increase of β. For information, β is defined as the ratio of fluid relaxation time to its deformation rate, thus as β increases, the deformation time of the

Table 4.1: The values of $f''(0)$, $-\theta'(0)$ and $-\phi'(0)$ for various values of β, Pr, γ and Sc

β	Pr	γ	Sc	$f''(0)$		$-\theta'(0)$		$-\phi'(0)$	
				Sakiadis	Blasius	Sakiadis	Blasius	Sakiadis	Blasius
0.0000	1.0	0.25	1.0	0.44367	-0.33246	0.40669	0.25287	0.44464	0.32083
0.6000				0.37877	-0.23245	0.42757	0.31265	0.47654	0.34970
1.2000				0.30376	-0.27800	0.52017	0.39847	0.52995	0.39086
0.5000	1.0	0.30	1.0	0.38916	-0.22737	0.40867	0.29198	0.46347	0.33267
	2.0					0.59465	0.34143		
	3.0					0.73692	0.39535		

Continued on next page

Table 4.1, continued

β	Pr	γ	Sc	$f''(0)$		$-\theta'(0)$		$-\phi'(0)$	
				Sakiadis	Blasius	Sakiadis	Blasius	Sakiadis	Blasius
0.5000	1.0	0.00	1.0	0.38916	-0.22737	0.44247	0.32083	0.46347	0.33267
		0.30				0.40867	0.29198		
		0.50				0.36890	0.26163		
		0.70				0.33662	0.23655		
0.5000	1.0	0.30	1.0	0.38916	-0.22737	0.40867	0.29198	0.46347	0.32083
			2.0					0.68924	0.38112
			3.0					0.87328	0.43131
			4.0					1.02822	0.47356

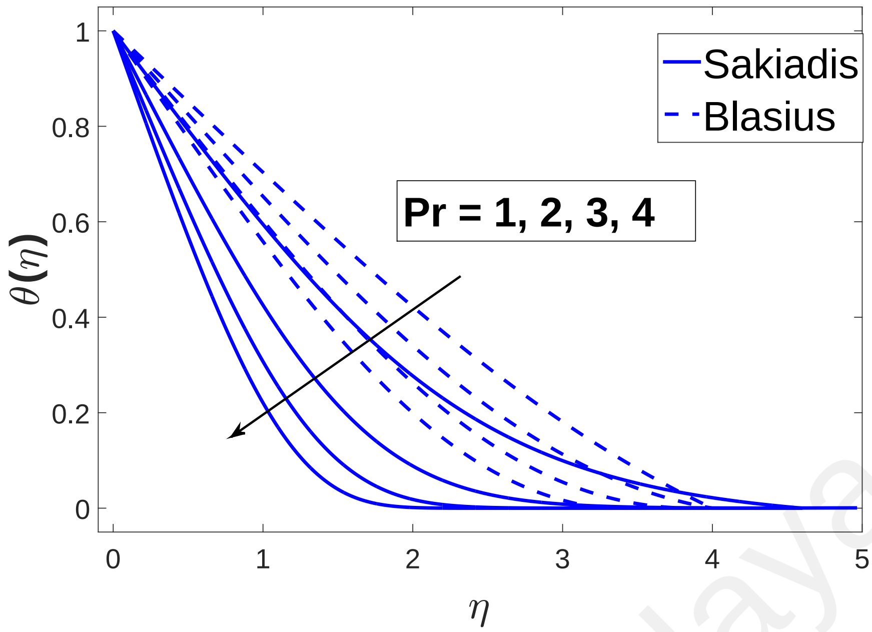

(a)

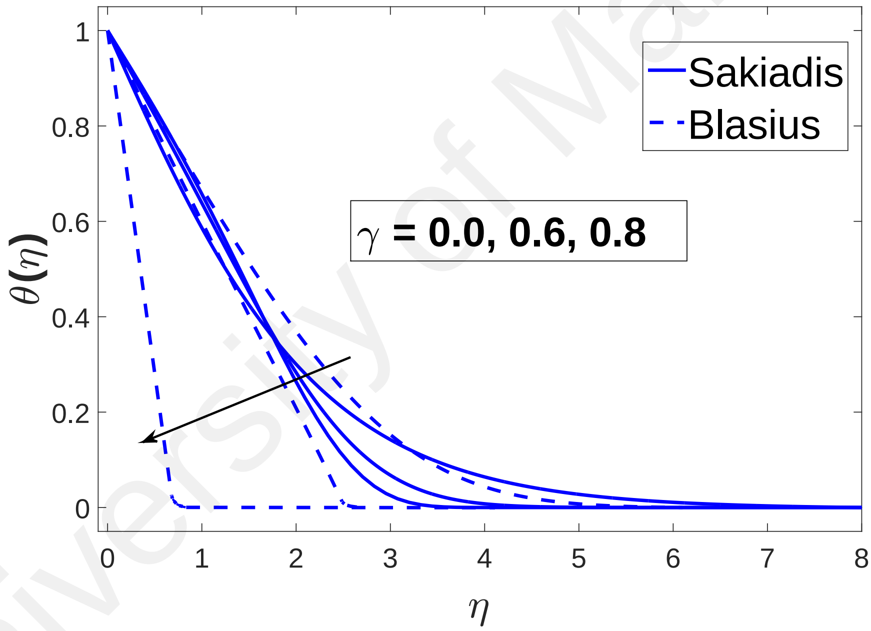

(b)

Figure 4.2: The temperature profile for different values of: (a) Pr when $\gamma = 0.3$; (b) γ when Pr $= 1$; with $\beta = 0.5$ and Sc $= 1$

fluid decreases and the relaxation time increases. The relaxation causes the thickness of the momentum boundary layer to increase.

Figure 4.2(a) describes the effect of the Prandtl number Pr on the fluid temperature profile θ for both Sakiadis and Blasius flows. It can be seen Figure 4.2(a) that as Pr increases, the temperature profile for both types of flow decreases. Prandtl number is

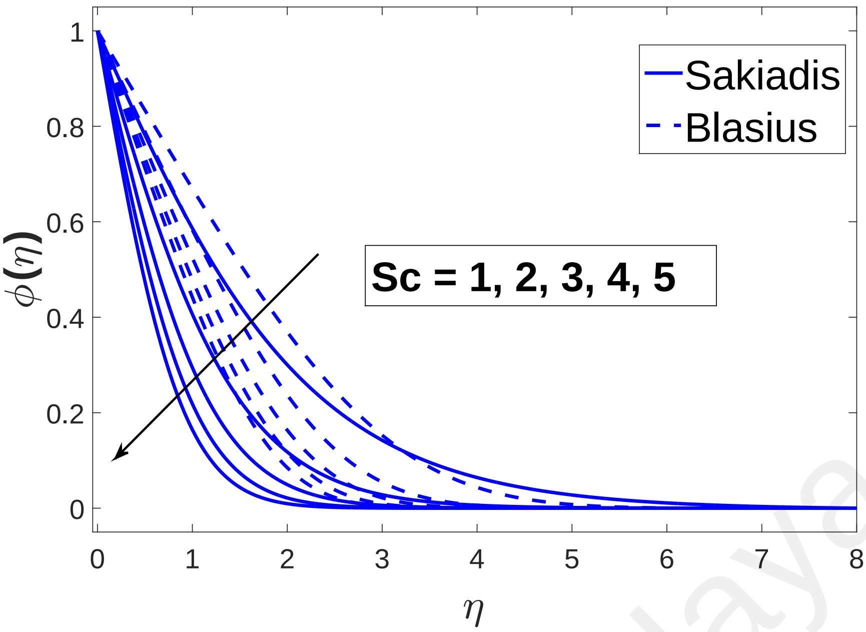

Figure 4.3: The concentration profile for different values of Sc with $\beta = 0.5$**, Pr** $= 1$ **and** $\gamma = 0.3$

defined as the ratio of the momentum diffusivity and the thermal diffusivity. For lower Pr value, i.e. Pr < 1, the thermal diffusivity dominates. This means the velocity of the fluid does not interfere with the thermal boundary layer thickness, which makes heat distribution slower. For Pr > 1, momentum diffusivity dominates. At this stage, the fluid velocity largely affects the thermal diffusivity and helps the heat diffusion in the fluid, thus makes the heat diffusion quicker. From Figure 4.2(a) it can be also seen that the fluid temperature profile for Blasius flow is greater than Sakiadis flow as Pr increases. The relationship between the Deborah number γ and the fluid temperature distribution for both types of flow is shown in Figure 4.2(b). Based on Figure 4.2(b), the temperature profile θ decreases with the increasing value of γ. This means that as the fluid takes longer time for it to experience heat conduction, the thermal boundary layer thickness becomes smaller, thus makes the heat dissipates quickly for both Sakiadis and Blasius flows.

The effect of Schmidt number Sc on the fluid concentration distribution ϕ for Sakiadis and Blasius flows is presented in Figure 4.3. It can be shown from Figure 4.3 that as η tends to infinity, the mass concentration profile tends to zero, and as Sc increases, the

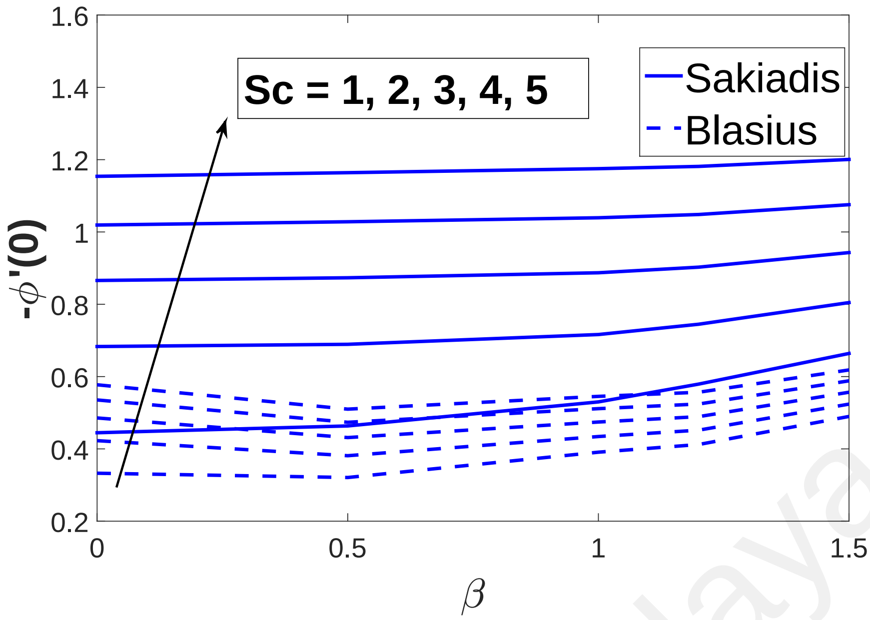

Figure 4.4: The effect of β on $-\phi'(0)$ for different values of Sc

concentration of the fluid decreases for both flows. Since Schmidt number is defined as the ratio momentum diffusivity and mass diffusivity, it means that an increase of the ratio of momentum diffusivity and mass diffusivity results in a thinner boundary layer of mass transfer. This causes the response time of concentration transport of the fluid becomes longer.

Figure 4.4 presents the effect of β on $-\phi'(0)$ with different values of Sc. We notice that the value of $-\phi'(0)$ increases as β and Sc increase. For a fixed value of Sc, a larger magnitude of the velocity of the fluid results in a lower pressure of the fluid inside the boundary layer. This situation causes the particle concentration at the wall decreases, which increases the value of $-\phi'(0)$.

To gain a better understanding on the heat transfer within the system, the dimensional form for several different systems are investigated. Table 4.2 shows the physical properties of fluid used in the demonstration.

Figure 4.5(a) presents the heat map of Sakiadis flow of air, while Figure 4.5(b) shows the heat map of Blasius flow of air, both at constant T_∞, T_w, U_∞, β, γ and Sc. Based

Table 4.2: The physical properties for selected fluid

Fluid	Pr	T_∞(°C)	ν (cm^2/s)
Air	0.7-1	20	0.1506

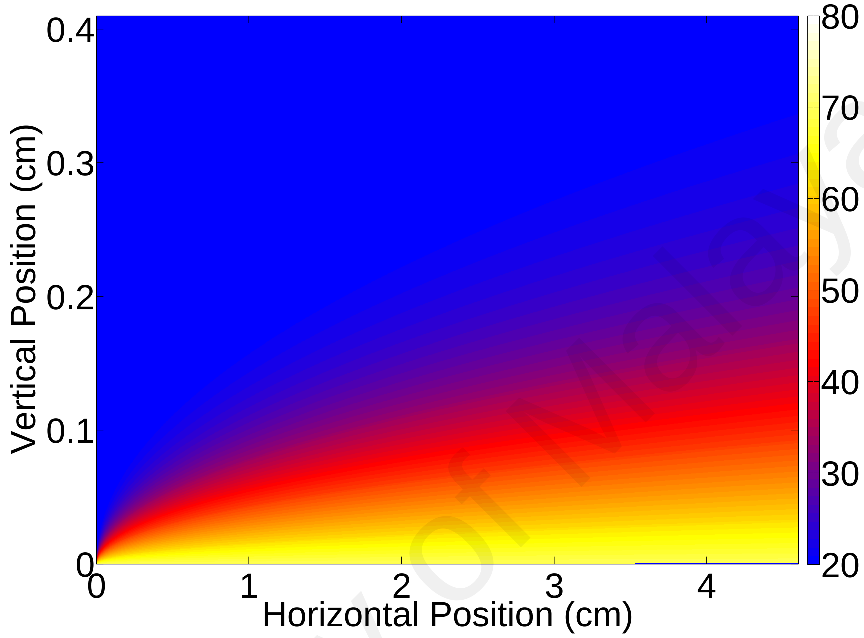

(a)

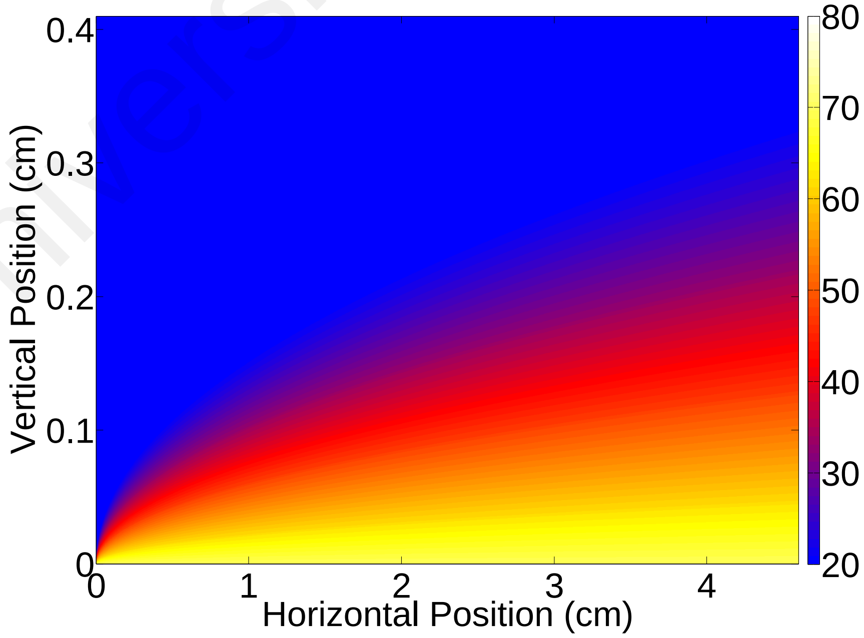

(b)

Figure 4.5: The heat map of: (a) Sakiadis flow; (b) Blasius flow; for air at $T_\infty = 20°$C with $U_\infty = 100$ cm/s, $T_w = 70°$C, $\beta = 0.5$, $\gamma = 0.3$ and Sc = 1

on these two figures, the thermal boundary layer can be seen clearly. It is shown that the thermal boundary layer for Sakiadis flow is thinner than Blasius flow. The thinner the thermal boundary layer, the heat dissipation from the wall in the fluid becomes more efficient. This means that based on the Figure 4.5, the heat dissipation for Sakiadis flow is more efficient and quicker than Blasius flow. This fact supported the result shown in Figure 4.2(a).

Figure 4.6 presents the heat map of Sakiadis flow for air at constant T_∞, T_w, U_∞, β and Sc, with $\gamma = 0$ for Figure 4.6(a) and $\gamma = 0.5$ for Figure 4.6(b). It is noted that $\gamma = 0$ corresponds to the classical Fourier law heat transfer model. Based on the heat map shown in Figure 4.6, it can be seen that the thermal boundary layer for $\gamma = 0$ is thicker than $\gamma = 0.5$. This means that when the fluid behaves like Fourier law model, the heat dissipation is not as efficient as Cattaneo-Christov heat flux model. It can be concluded that Cattaneo-Christov heat flux model increase the efficiency of heat dissipation in the fluid. These results are in good match with the results from Figure 4.2(b).

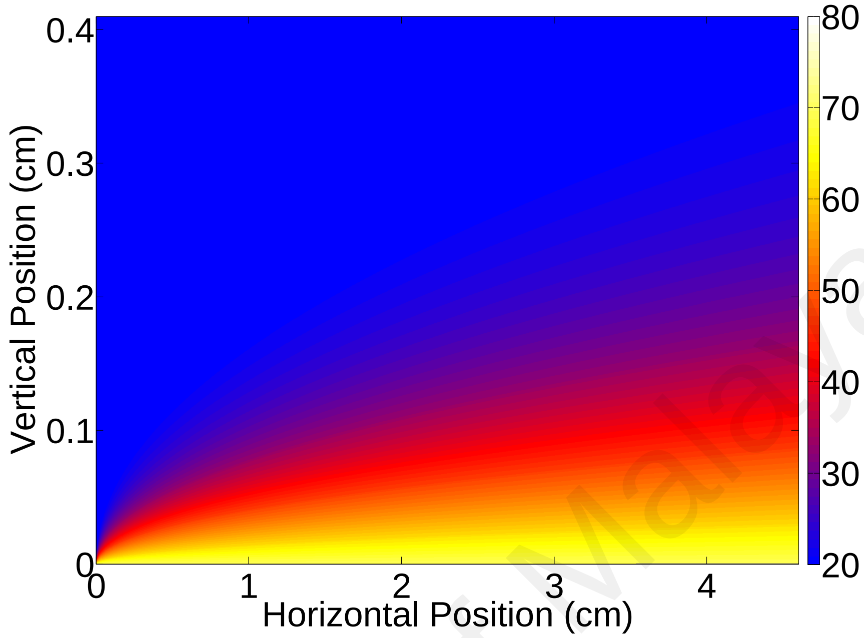

(a)

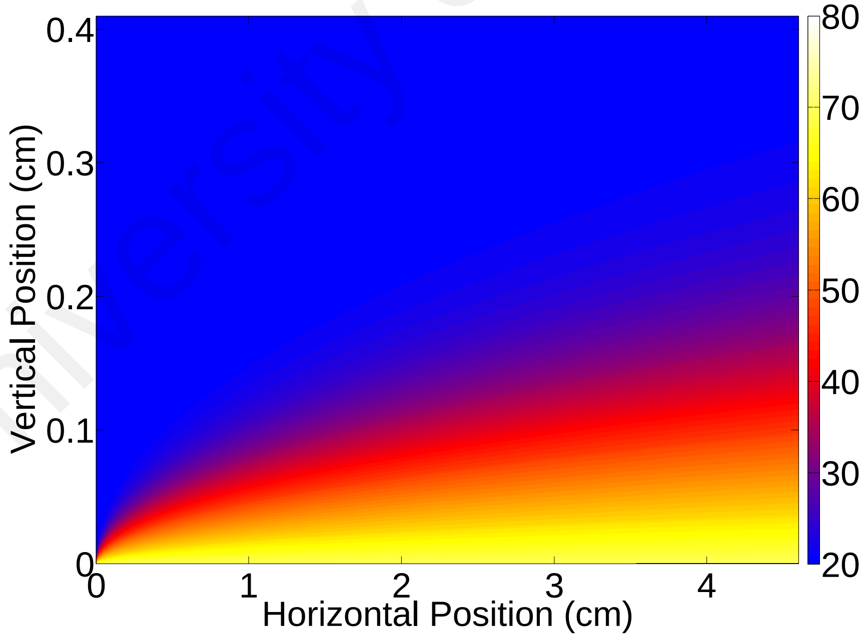

(b)

Figure 4.6: The heat map of Sakiadis flow with (a) $\gamma = 0$, (b) $\gamma = 0.5$; for air at $T_\infty = 20°$C with $U_\infty = 100$ cm/s, $T_w = 70°$C, $\beta = 0.5$ and Sc $= 1$

CHAPTER 5: NUMERICAL STUDY OF MASS AND HEAT TRANSFER FOR SAKIADIS FLOW OF MAGNETOHYDRODYNAMIC CARREAU FLUID OVER A HORIZONTAL PLATE USING CATTANEO-CHRISTOV HEAT FLUX MODEL

The numerical investigation of mass and heat transfer for magnetohydrodynamic (MHD) Carreau fluid over a horizontal plate for Sakiadis flow with Cattaneo-Christov heat flux model is presented in this chapter. The results are tabulated and graphed and the analysis of the results are also discussed later.

5.1 Mathematical Formulation

The two-dimensional laminar flow of an incompressible and electrically conducting Carreau fluid over a semi-infinite plate at $y = 0$ is considered . An assumption is made that the plate has a constant temperature T_w and constant concentration C_w, and the ambient fluid temperature and ambient concentration are T_∞ and C_∞ respectively. The governed equations for steady incompressible laminar MHD Carreau boundary layer Sakiadis fluid flow with mass and heat transfer using Cattaneo-Christov heat flux model are as follow,

$$\frac{\partial u}{\partial x} + \frac{\partial v}{\partial y} = 0, \tag{5.1}$$

$$\begin{aligned} u\frac{\partial u}{\partial x} + v\frac{\partial u}{\partial y} = \nu(n-1)\Gamma^2 \frac{\partial^2 u}{\partial y^2}\left(\frac{\partial u}{\partial y}\right)^2 \left[1 + \Gamma^2\left(\frac{\partial u}{\partial y}\right)^2\right]^{\frac{n-3}{2}} \\ + \nu\frac{\partial^2 u}{\partial y^2}\left[1 + \Gamma^2\left(\frac{\partial u}{\partial y}\right)^2\right]^{\frac{n-1}{2}} - \frac{\sigma_c B_0^2}{\rho}u \end{aligned} \tag{5.2}$$

$$\begin{aligned} u\frac{\partial T}{\partial x} + v\frac{\partial T}{\partial y} + \lambda_2\left[u^2\frac{\partial^2 T}{\partial x^2} + v^2\frac{\partial^2 T}{\partial y^2} + 2uv\frac{\partial^2 T}{\partial x \partial y} + \left(u\frac{\partial u}{\partial x} + v\frac{\partial u}{\partial y}\right)\frac{\partial T}{\partial x} \right. \\ \left. + \left(u\frac{\partial v}{\partial x} + v\frac{\partial v}{\partial y}\right)\frac{\partial T}{\partial y}\right] = \alpha\frac{\partial^2 T}{\partial y^2}, \end{aligned} \tag{5.3}$$

$$u\frac{\partial C}{\partial x} + v\frac{\partial C}{\partial y} = D\frac{\partial^2 C}{\partial y^2}, \tag{5.4}$$

where x and y are the coordinates along and normal to the plate respectively, u and v are the velocity components along the x and y axis respectively, ν is the kinematic viscosity of the fluid, Γ is the Carreau fluid parameter, n is the power-law index, $\alpha = \dfrac{k}{\rho C_p}$ is the thermal diffusivity, k is the thermal conductivity, ρ is the density of the fluid, σ_c is the electrical conductivity, B_0 is the magnetic field normal to the plate, C_p is the specific heat capacity of the fluid, T is the local fluid temperature, D is the mass diffusion coefficient and C is the local mass concentration.

The boundary conditions are,

$$\begin{aligned} u = U_\infty, \quad v = v_0, \quad T = T_w, \quad C = C_w, \quad \text{at} \quad y = 0, \\ u \to 0, \quad T \to T_\infty, \quad C \to C_\infty, \quad \text{as} \quad y \to \infty, \end{aligned} \tag{5.5}$$

where U_∞ is the constant free stream velocity. To find the similarity solution, the following dimensionless variables are introduced,

$$\eta = y\sqrt{\frac{U_\infty}{\nu x}}, \quad \psi = f(\eta)\sqrt{U_\infty \nu x}, \quad \theta(\eta) = \frac{T - T_\infty}{T_w - T_\infty}, \quad \phi(\eta) = \frac{C - C_\infty}{C_w - C_\infty}, \tag{5.6}$$

where η is the dimensionless similarity variable, ψ is the stream function defined as $u = \dfrac{\partial \psi}{\partial y}$ and $v = -\dfrac{\partial \psi}{\partial x}$. By substituting Eq.(5.6) into Eqs.(5.2) - (5.4), the following set of nonlinear ordinary differential equation are obtained,

$$\left[1 + n\mathrm{We}^2 (f'')^2\right] \left[1 + \mathrm{We}^2 (f'')^2\right]^{\frac{n-3}{2}} f''' + \frac{1}{2} f f'' - \mathrm{M} f' = 0, \tag{5.7}$$

$$\frac{1}{\mathrm{Pr}}\theta'' + \frac{1}{2} f\theta' - \frac{\gamma}{2}\left(3 f f'\theta' + f^2\theta''\right) = 0, \tag{5.8}$$

$$\phi'' + \frac{\mathrm{Sc}}{2} f\phi' = 0, \tag{5.9}$$

where prime denotes the differentiation with respect to η, $\mathrm{We} = \sqrt{\dfrac{\Gamma^2 U_\infty^3 x^3}{\nu}}$ is the local Weissenberg number, $\mathrm{M} = \dfrac{\sigma_c \mathrm{B}_0^2 x}{U_\infty \rho}$ is the local magnetic field parameter, $\mathrm{Pr} = \dfrac{\nu}{\alpha}$ is the Prandtl number, $\gamma = \dfrac{\lambda_2 U_\infty}{2x}$ is the local Deborah number for the energy and $\mathrm{Sc} = \dfrac{\nu}{D}$ is the Schmidt number.

Since the parameters M, We and γ contains the function of x, the availability of the local similarity solutions are used instead, and the local solution found can be used to see the effect of parameters to the system.

The transformed boundary conditions are, with boundary condition

$$
\begin{aligned}
f = 0, \quad f' = 1, \quad \theta = 1, \quad \phi = 1, \quad \text{at} \quad \eta = 0, \\
f' \to 0, \quad \theta \to 0, \quad \phi \to 0, \quad \text{as} \quad \eta \to \infty,
\end{aligned}
\tag{5.10}
$$

It is useful to take into consideration the physical quantities that have practical interest for this problem. The dimensionless quantities that are related to the problem are the local skin-friction coefficient C_f, local Nusselt number Nu and local Sherwood number Sh, which are defined as $C_f = \frac{\mu}{\rho U_\infty^2}\left(\frac{\partial u}{\partial y}\right)_{y=0}\left[1 + \Gamma^2\left\{\left(\frac{\partial u}{\partial y}\right)^2\right\}_{y=0}\right]^{\frac{n-1}{2}}$, $\mathrm{Nu} = -\frac{x}{(T_w - T_\infty)}\left(\frac{\partial T}{\partial y}\right)_{y=0}$ and $\mathrm{Sh} = -\frac{x}{(C_w - C_\infty)}\left(\frac{\partial C}{\partial y}\right)_{y=0}$ respectively. By substituting Eq.(5.6), the local skin-friction coefficient, local Nusselt number and local Sherwood number are,

$$
C_f(\mathrm{Re}_x)^{1/2} = f''(0)\left[1 + \mathrm{We}^2\left\{f''(0)\right\}^2\right]^{\frac{n-1}{2}}, \tag{5.11}
$$

$$
\mathrm{Nu}\,(\mathrm{Re}_x)^{-1/2} = -\theta'(0), \tag{5.12}
$$

$$
\mathrm{Sh}\,(\mathrm{Re}_x)^{-1/2} = -\phi'(0), \tag{5.13}
$$

where $\mathrm{Re}_x = \frac{U_\infty x}{\nu}$ is the local Reynolds number.

5.2 Results and Discussion

Table 5.1 presents the values of $f''(0)$, $-\theta'(0)$ and $-\phi'(0)$ for different values of parameters. It can be seen from Table 5.1 that as the value of power-law index increases from 1 to 15, the values of $f''(0)$ increases but the values of $\theta'(0)$ and $\phi'(0)$ decrease. The value of $-\phi'(0)$ are unchanged for different values of Pr and γ since these two parameters absent from the concentration equation, thus varying these parameter does not affect the concentration profile of the fluid.

For the purpose of the study in this chapter, the value of local magnetic field parameter M is fixed at 0.5. The effect of local Weissenberg number on velocity, temperature and concentration profile are shown in Figure 5.1(a). Based on Figure 5.1(a), as We increases, the fluid velocity decreases while the temperature and concentration gradient of the fluid increase. As We increases, the elastic forces dominate and cause the fluid to flow at a low velocity, thus the relaxation times for temperature and concentration gradient also increase. This causes the fluid at the region gains up thermal energy and mass concentration. Figure 5.2(b) shows the effect of power-law index parameter on velocity profile, temperature profile and concentration profile. There is an increase in fluid velocity for increasing value of n, but there is a decrease in temperature and concentration gradient for increasing value of n. By increasing the value of n, the fluid is behaving more like a Newtonian fluid. This makes the momentum boundary layer increases as the fluid becomes more viscous. Since the changes of the fluid velocity profile, temperature profile and concentration profile are small as shown in Figure 5.1(b), it can be concluded that there is a slight effect of n on the fluid flow.

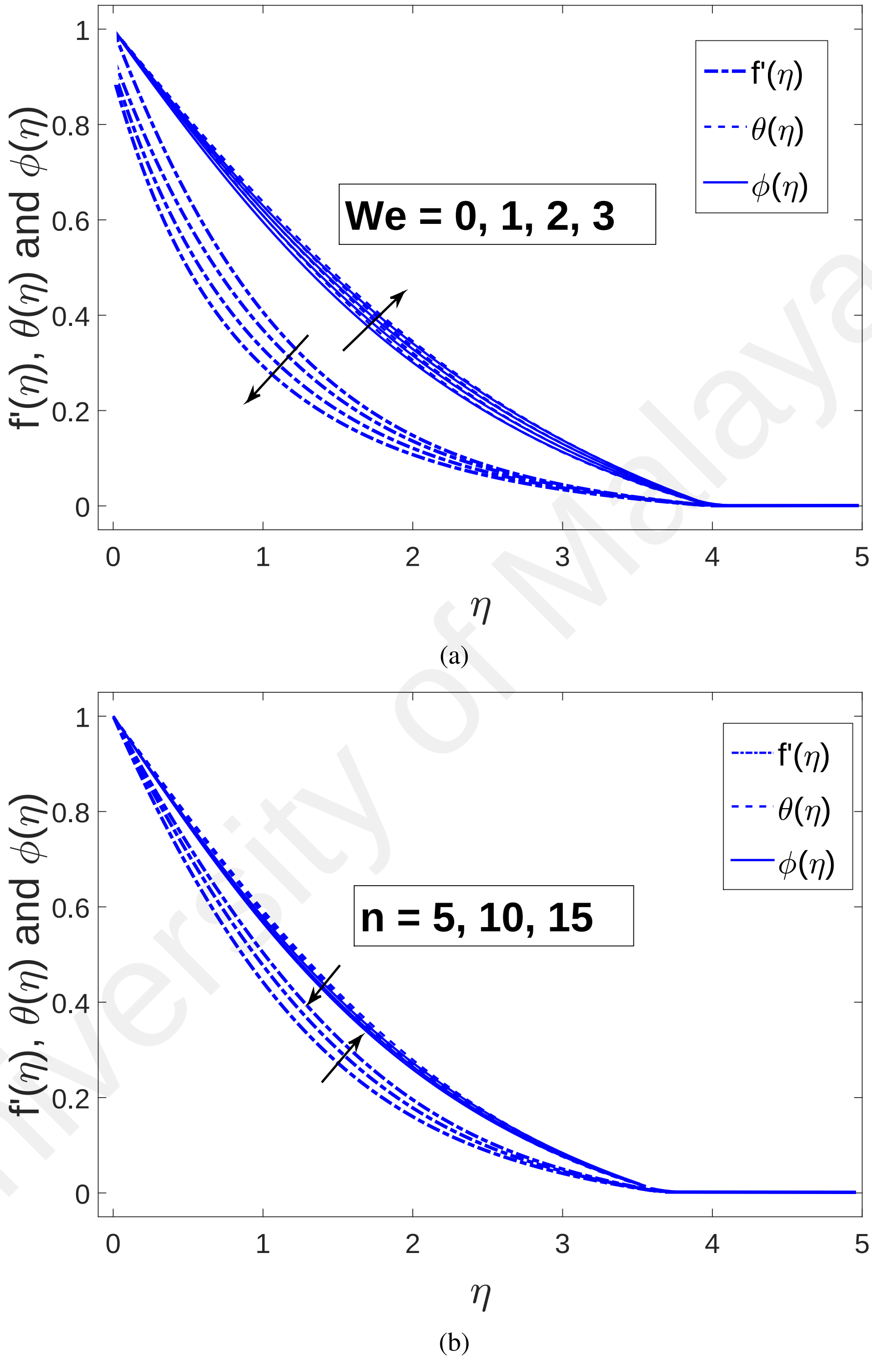

Figure 5.1: The velocity profile, temperature profile and concentration profile for different values of: (a) We when $n = 0.5$; (b) n when We $= 0.5$; with Pr = Sc $= 1$ and $\gamma = 0.2$

Table 5.1: The values of $f''(0)$, $-\theta'(0)$ and $-\phi'(0)$ for various values of We, n, Pr, γ and Sc

We	n	Pr	γ	Sc	$f''(0)$	$-\theta'(0)$	$-\phi'(0)$
0.0	0.5	1	0.2	1	-0.82161	0.42571	0.45104
1.0					-0.84372	0.39489	0.41618
2.0					-0.9826	0.38491	0.40308
0.5	1.0	1	0.2	1	-0.82356	0.41742	0.44308
	5.0				-0.70335	0.42344	0.45189
	10.0				-0.62488	0.42842	0.45948
	15.0				-0.57486	0.43203	0.4652
0.5	1.0	1	0.2	1	-0.82356	0.41742	0.44308
		2				0.57808	
		4				0.86096	
		6				1.08221	

Continued on next page

Table 5.1, continued

We	n	Pr	γ	Sc	$f''(0)$	$-\theta'(0)$	$-\gamma'(0)$
0.5	1.0	1	0.0	1	-0.82356	0.44308	0.44308
			0.4			0.39157	
			1.0			0.31349	
			1.8			0.21596	
0.5	1.0	1	0.2	1	-0.82356	0.41742	0.44308
				2			0.62256
				4			0.93824
				8			1.40867
				11			1.68585

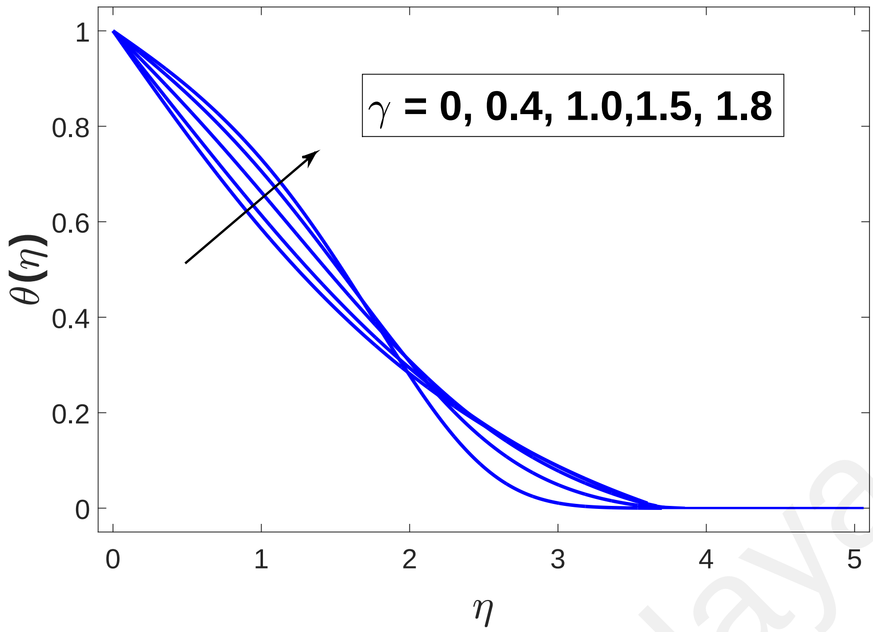

(a)

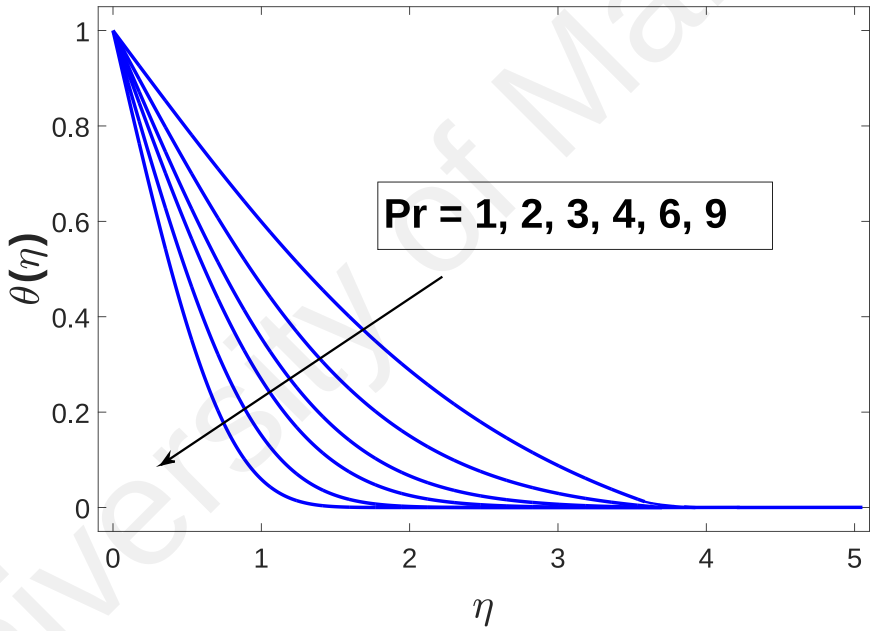

(b)

Figure 5.2: The temperature profile for different values of: (a) γ **when Pr**$= 1$**; (b) Pr when** $\gamma = 0.5$**; with We** $= n = 1$ **and Sc** $= 0.2$

In Figure 5.2(a), the effect of local Deborah number γ on the temperature profile is shown. It can be seen from Figure 5.2(a) that at initial flow within the region $0 < \eta < 2$, the fluid temperature gradient increases as the value of γ increases, but for the region $\eta > 2$, the fluid temperature distribution slightly decreases. It means the time taken for the fluid to experience heat conduction is longer and this causes the thermal boundary

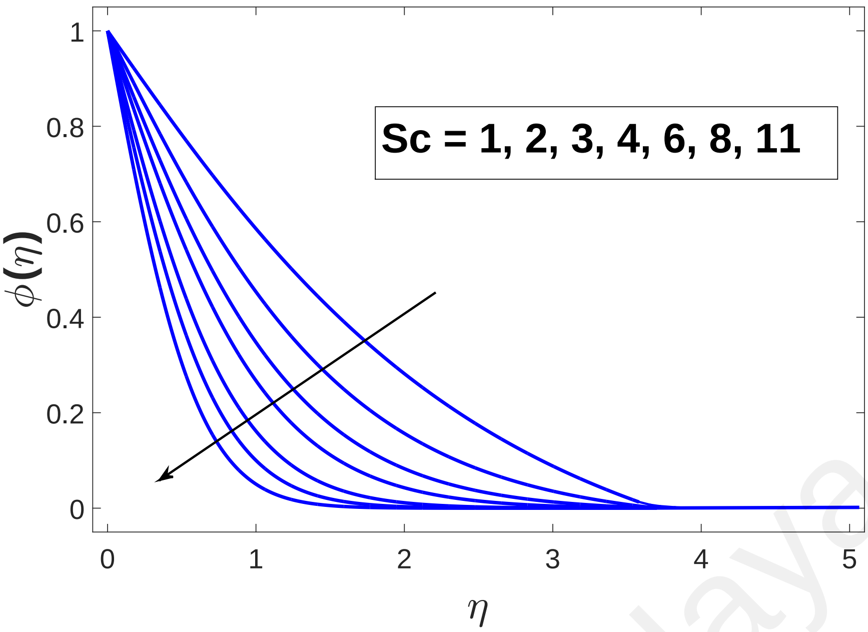

Figure 5.3: The concentration profile for different values of Sc with We $= n = 0.5$**, Pr** $= 1$ **and** $\gamma = 0.2$

layer to become thinner which can be interpreted as the dissipation of heat occurs at a high speed. The effect of the Prandtl number Pr on the temperature profile is presented in Figure 5.2(b). From Figure 5.2(b), as Pr increases, the temperature gradient decreases. Prandtl number is defined as the ratio of momentum diffusivity and thermal diffusivity. For higher Pr number, the momentum diffusivity terms dominate the thermal diffusivity, and the fluid velocity is high enough to help the heat transfer in the region and is causing the heat dissipation to occur in a shorter time.

The effect of Schmidt number Sc on the concentration profile is shown in Figure 5.3. An increase in Sc causes the concentration gradient to decrease based on Figure 5.3. Schmidt number is defined as the ratio momentum diffusivity and mass diffusivity, which is analogous to Prandtl number for temperature gradient. As Sc increases, momentum diffusivity dominates and the velocity of the fluid is high enough to facilitate the mass distribution, thus causes the concentration gradient to decrease faster.

For a better visualisation on the results above, the dimensional form for several different types of system are presented. Table 5.2 shows the physical properties of fluids used in

Table 5.2: The physical properties for selected fluids

Fluid	Pr	T_∞(°C)	ν (cm^2/s)
Air	0.7-1	5	0.1372
		20	0.1506
		25	0.1552
Pure water	6-7	20	0.01

the visualisation. Figure 5.4(a) shows the heat map of air, while Figure 5.4(b) shows the heat map of pure water, both at constant T_∞, T_w, U_∞, We, n, γ and Sc. It can be seen that the thermal boundary layer for pure water is much thinner than the thermal boundary layer for air. This means that the heat transfer in pure water is more efficient and quicker than in air. Since air has a lower Prandtl number, Pr than pure water based on Table 5.2, it can be concluded that the higher the Pr, the thinner the thermal boundary layer, which corresponds to the higher efficiency of heat dissipation from wall in the fluid. This conclusion is supported with the results from Figure 5.2(b).

Figure 5.5(a) presents the heat map of air at 5°C, and Figure 5.5(b) presents the heat map of air at 25°C and at constant T_w, U_∞, We, n, γ and Sc. It can be seen from Figure 5.5 that the thermal boundary layer for air at 5°C is thinner than for air at 25°C. At lower T_∞, the colder fluid further from the wall is able to interact with the hot fluid which gained its heat from the heated wall at a shorter vertical distance from the wall. This causes the heat transfer from the hot region to the cold fluid region happens in that smaller area, thus causes the heat dissipates quickly. It can be concluded that for lower T_∞ of the fluid used, the heat dissipation is more efficient than the higher T_∞.

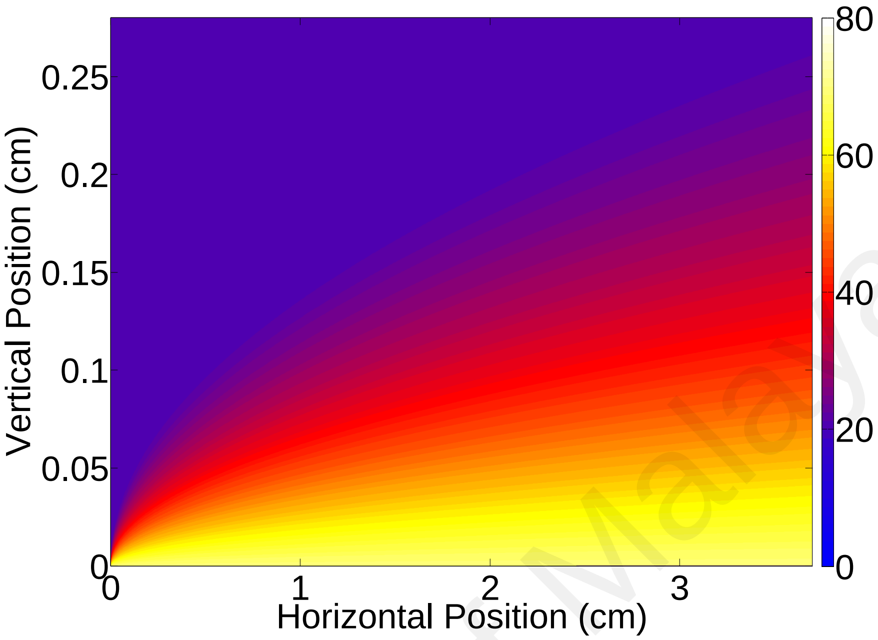

(a)

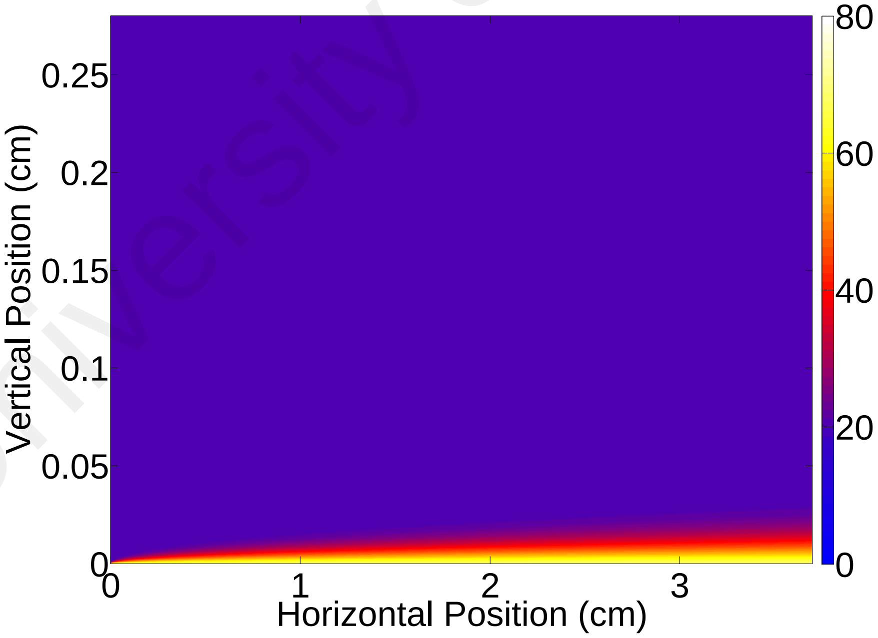

(b)

Figure 5.4: The heat map of: (a) Air; (b) Pure water; at $T_\infty = 20°$C with $U_\infty = 100$ cm/s, $T_w = 70°$C, We $= 0.5$, $n = 1$, $\gamma = 0.2$ and Sc $= 1$

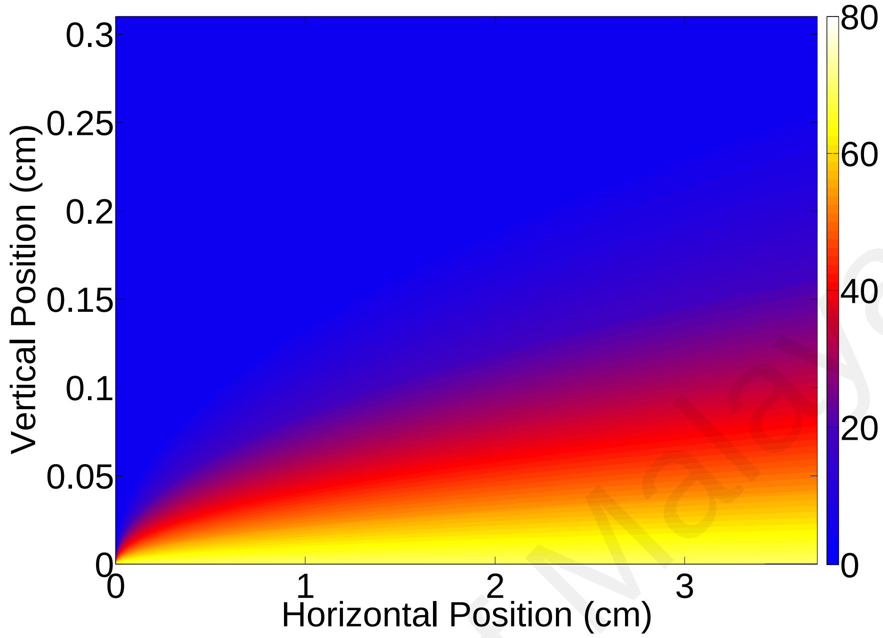

(a)

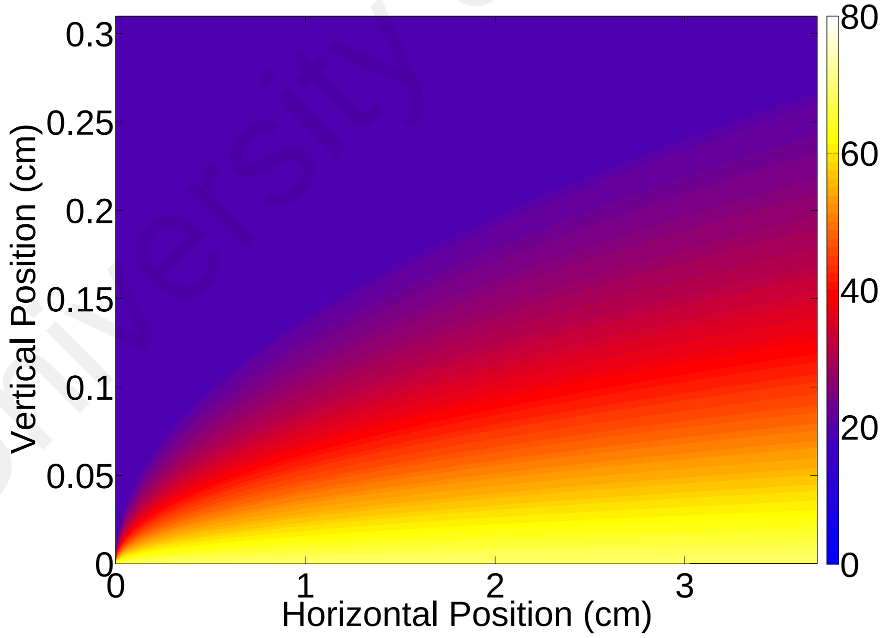

(b)

Figure 5.5: The heat map of air at: (a) $T_\infty = 5°C$**; (b)** $T_\infty = 25°C$**; with** $T_w = 70°C$**,** $U_\infty = 100$ **cm/s, We** $= 0.5$**,** $n = 1$ **and Sc** $= 1$

CHAPTER 6: CONVECTIVE BOUNDARY LAYER OF UPPER-CONVECTED MAXWELL FLUID OVER A HORIZONTAL WEDGE WITH SUCTION AND HEAT GENERATION/ABSORPTION USING CATTANEO-CHRISTOV HEAT FLUX MODEL

The study of boundary layer flow over a wedge with suction or injection has been widely recognised due to its importance in the industrial processes. This includes the reduction of the drag force in a fluid and the entrance region of a pipe flow. The velocity profile, temperature profile and concentration profile of a boundary layer flow are significantly affected by suction or injection. This chapter deals with the effect of the heat generation/absorption on convective heat transfer of upper-convected Maxwell (UCM) fluid over a horizontal wedge using Cattaneo-Christov heat flux model with suction/injection.

6.1 Mathematical Formulation

The two-dimensional laminar flow of UCM fluid over a horizontal wedge with the wedge angle $\Omega = \beta_w \pi$ is considered. The Hartree pressure gradient β_w is defined as $\beta_w = \dfrac{2m}{m+1}$ where m is the wedge angle parameter. An assumption is made that the surface of the wedge has a constant temperature T_w, and the ambient fluid temperature is T_∞. The governed equations for the steady incompressible laminar flow of Maxwell fluid over a horizontal wedge with heat transfer, suction, and heat generation/absorption are expressed as,

$$\frac{\partial u}{\partial x} + \frac{\partial v}{\partial y} = 0, \tag{6.1}$$

$$u\frac{\partial u}{\partial x} + v\frac{\partial u}{\partial y} + \lambda_1\left(u^2\frac{\partial^2 u}{\partial x^2} + v^2\frac{\partial^2 u}{\partial y^2} + 2uv\frac{\partial^2 u}{\partial x \partial y}\right) = \nu\frac{\partial^2 u}{\partial y^2} + U_\infty\frac{\partial U_\infty}{\partial x} + \lambda_1 U_\infty^2\frac{\partial^2 U_\infty}{\partial x^2}, \tag{6.2}$$

$$\begin{aligned} u\frac{\partial T}{\partial x} + v\frac{\partial T}{\partial y} + \lambda_2\Bigg[u^2\frac{\partial^2 T}{\partial x^2} + v^2\frac{\partial^2 T}{\partial y^2} + 2uv\frac{\partial^2 T}{\partial x \partial y} + \left(u\frac{\partial u}{\partial x} + v\frac{\partial u}{\partial y}\right)\frac{\partial T}{\partial x} \\ + \left(u\frac{\partial v}{\partial x} + v\frac{\partial v}{\partial y}\right)\frac{\partial T}{\partial y}\Bigg] = \alpha\frac{\partial^2 T}{\partial y^2} + Q(T - T_\infty), \end{aligned} \tag{6.3}$$

with x and y are the coordinates along and normal to the heated plate respectively, u and v are the velocity components along the x and y axis respectively, λ_1 is the relaxation time of the UCM fluid, ν is the kinematic viscosity of the fluid, $\alpha = \dfrac{k}{\rho C_p}$ is the thermal diffusivity, k is the thermal conductivity, ρ is the density of the fluid, C_p is the specific heat capacity of the fluid, λ_2 is the relaxation time for heat flux, T is the local fluid temperature and Q is the heat generation/absorption coefficient.

The boundary conditions are,

$$\begin{aligned} u = 0, \quad v = v_0, \quad T = T_w \quad \text{at} \quad y = 0, \\ u \to U_\infty, \quad T \to T_\infty, \quad \text{as} \quad y \to \infty, \end{aligned} \tag{6.4}$$

where v_0 is suction, $U_\infty = ax^m$ is free stream velocity and a is a constant. The following dimensionless variables are introduced to obtain similarity solution for the problem,

$$\eta = y\sqrt{\frac{(m+1)U_\infty}{2\nu x}}, \quad \psi = f(\eta)\sqrt{\frac{2U_\infty \nu x}{m+1}}, \quad \theta(\eta) = \frac{T - T_\infty}{T_w - T_\infty} \tag{6.5}$$

where η is the dimensionless similarity variable, ψ is the stream function defined as $u = \dfrac{\partial\psi}{\partial y}$ and $v = -\dfrac{\partial\psi}{\partial x}$. By substituting Eq.(6.5) into Eqs.(6.2) - (6.3), the following set of nonlinear ordinary differential equation are obtained,

$$\begin{aligned} f''' + \frac{2m}{m+1}\left(1 - (f')^2\right) + ff'' + \beta\Bigg[2m\frac{m-1}{m+1}\left(1 - (f')^3\right) \\ + \frac{m-1}{2}\eta\,(f')^2 f'' - \frac{m+1}{2}f^2 f''' + (3m-1)\,ff'f''\Bigg] = 0, \end{aligned} \tag{6.6}$$

$$\theta'' + \Pr f\theta' + \frac{2}{m+1}\Pr\delta\theta - \Pr\gamma\left[\frac{m+1}{2}f^2\theta'' - \frac{6}{m+1}\eta\,(f')^2\theta' + ff'\theta'\right] = 0, \tag{6.7}$$

where prime denotes the differentiation with respect to η, $\beta = \dfrac{\lambda_1 U_\infty}{2x}$ is the local Deborah number for momentum, $\gamma = \dfrac{\lambda_2 U_\infty}{2x}$ is the local Deborah number for energy, $\Pr = \dfrac{\nu}{\alpha}$ is the Prandtl number, $\delta = \dfrac{Q}{ab^2}$ is the heat generation/absorption parameter and b is a constant. Since the value β and γ contain the function of x, the availability of the local similarity solutions is used, and the solution found can be used to see the effect of parameters at a fixed location above the wall.

The transformed boundary conditions are,

$$f = \frac{2}{m+1}s, \qquad f' = 0, \qquad \theta = 1, \qquad \phi = 1, \qquad \text{at} \qquad \eta = 0,$$
$$f' \to 1, \qquad \theta \to 0, \qquad \text{as} \qquad \eta \to \infty, \tag{6.8}$$

where $s = -v_0\sqrt{\frac{(m+1)x}{2U\nu}}$ is the suction parameter.

The expression for local skin-friction coefficient C_f and local Nusselt number Nu are,

$$C_f\,(\mathrm{Re}_x)^{1/2} = \sqrt{\frac{m+1}{2}}f''(0), \tag{6.9}$$

$$\mathrm{Nu}\,(\mathrm{Re}_x)^{-1/2} = \sqrt{\frac{m+1}{2}}\theta'(0), \tag{6.10}$$

where $\mathrm{Re}_x = \frac{U_\infty x}{\nu}$ is the local Reynolds number.

6.2 Results and Discussion

Table 6.1 presented the values of $f''(0)$ and $-\theta'(0)$ for various values of parameters involved in the governed equations. From Table 6.1, the value of $f''(0)$ increases as the wedge angle parameter m increases but the value of $\theta'(0)$ decreases for the same value of wedge angle parameter. Noted that the value of $f''(0)$ remains constant for the increasing values of Pr, γ and δ for a fixed β. This is due to the parameters listed before are absent from the momentum equation, and thus nothing happened when these parameters are set to different values. It is also worth noted that from Table 6.1 the value of $\theta'(0)$ increases when the heat generation parameter increases.

For the purpose of the study in this subchapter, the value of suction parameter s is fixed to be 0.1. The effect of wedge angle parameter m on velocity profile f' and temperature profile θ is presented in Figure 6.1(a). Based on Figure 6.1(a), as the wedge angle parameter m increases, the velocity profile f' increases while the temperature profile θ decreases.

Table 6.1: The values of $f''(0)$ and $-\theta'(0)$ for various values of m, β, Pr, γ and δ

m	β	Pr	γ	δ	$f''(0)$	$-\theta'(0)$
0.0000	0.2	2.0	0.2	0.2	0.292146	0.29231
0.0141					0.305273	0.31305
0.0909					0.365763	0.4057
0.2000					0.430613	0.49054
0.0141	0.0	2.0	0.2	0.2	0.328606	0.34354
	0.1				0.317237	0.32914
	0.2				0.305273	-0.31305
0.0141	0.2	0.5	0.2	0.2	0.305273	0.25687
		1.0				0.25922
		1.5				0.2833
		2.0				0.31305

Continued on next page

Table 6.1, continued

m	β	Pr	γ	δ	$f''(0)$	$-\theta'(0)$
0.0141	0.2	2.0	0.0	0.2	0.305273	0.32805
			0.1			0.31979
			0.2			0.31305
0.0141	0.2	2.0	0.2	-0.2	0.305273	1.24848
				-0.1		1.07252
				0.0		0.86886
				0.1		0.62415
				0.2		0.31305

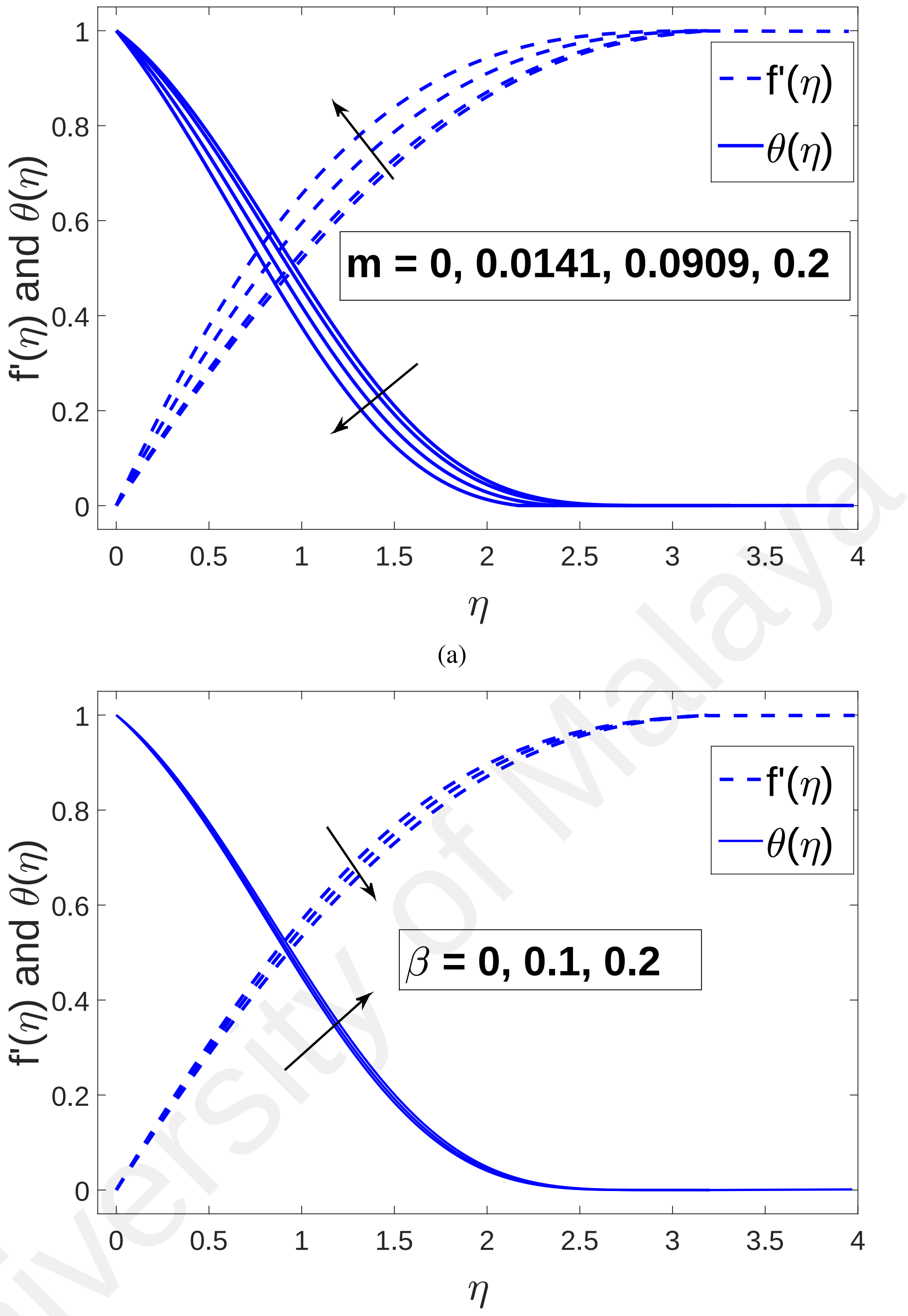

Figure 6.1: The velocity profile and temperature profile for different values of: (a) m **when** $\beta = 0.2$**; (b)** β **when** $m = 0.0141$**; with** $\gamma = \delta = 0.2$ **and Pr**$= 2$

This means as the wedge becomes steeper, the thickness of momentum and thermal boundary layer decreases. In Figure 6.1(b), the effect of the local Deborah number β onto the velocity and temperature profiles are shown. Based on Figure 6.1(b), the velocity profile decreases slightly while β increases in a tiny amount. On the other hand, the temperature profile increases for the increasing value of β. The local Deborah number for

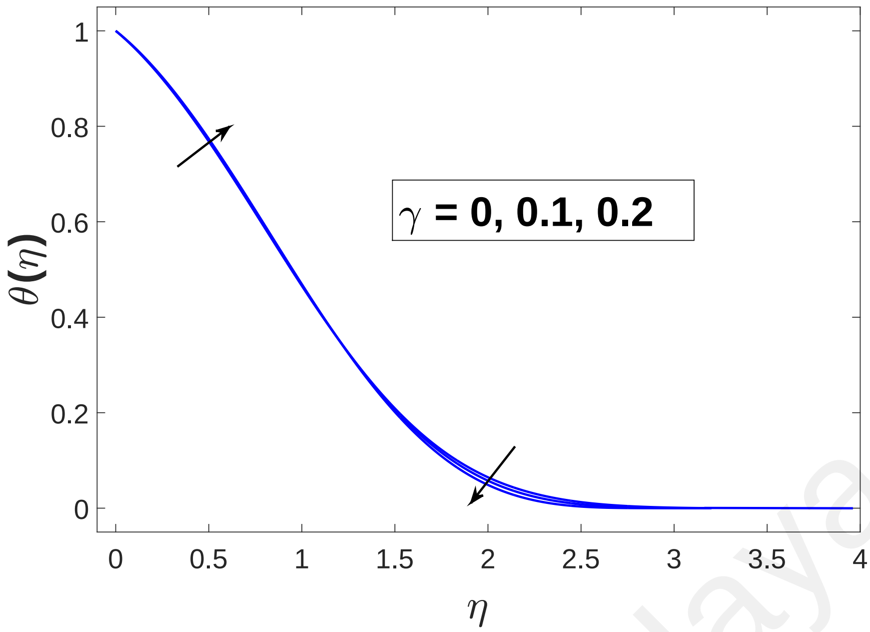

Figure 6.2: The temperature profile for different values of γ with $m = 0.0141$, $\beta = \delta = 0.2$ and Pr = 2

fluid momentum is defined as the ratio of fluid relaxation time to its deformation time. As β increases, the relaxation time of the fluid increases. As a result, it causes the thickness of momentum and thermal boundary layer become thicker. Based on Figure 6.1(b), it can be concluded that the changes in the value of β do affect the velocity and temperature profiles slightly.

The variation of the fluid temperature distribution θ against the different values of the local Deborah number is plotted in Figure 6.2. In Figure 6.2, for increasing γ, the temperature profile decreases slightly. With the same argument as β, as γ increases, the relaxation time of the heat transfer of the fluid increases and delays the time for the fluid to experience heat conduction. This causes the thermal boundary layer becomes thinner and results in faster heat dissipation. Since the effect is not significant, it can be concluded that the changes in the value of γ do not affect the thermal boundary layer in a greater magnitude.

The effect of Prandtl Number Pr on temperature profile θ is shown in Figure 6.3(a). Based on Figure 6.3(a), as Pr increases, the temperature profile decreases. Prandtl number

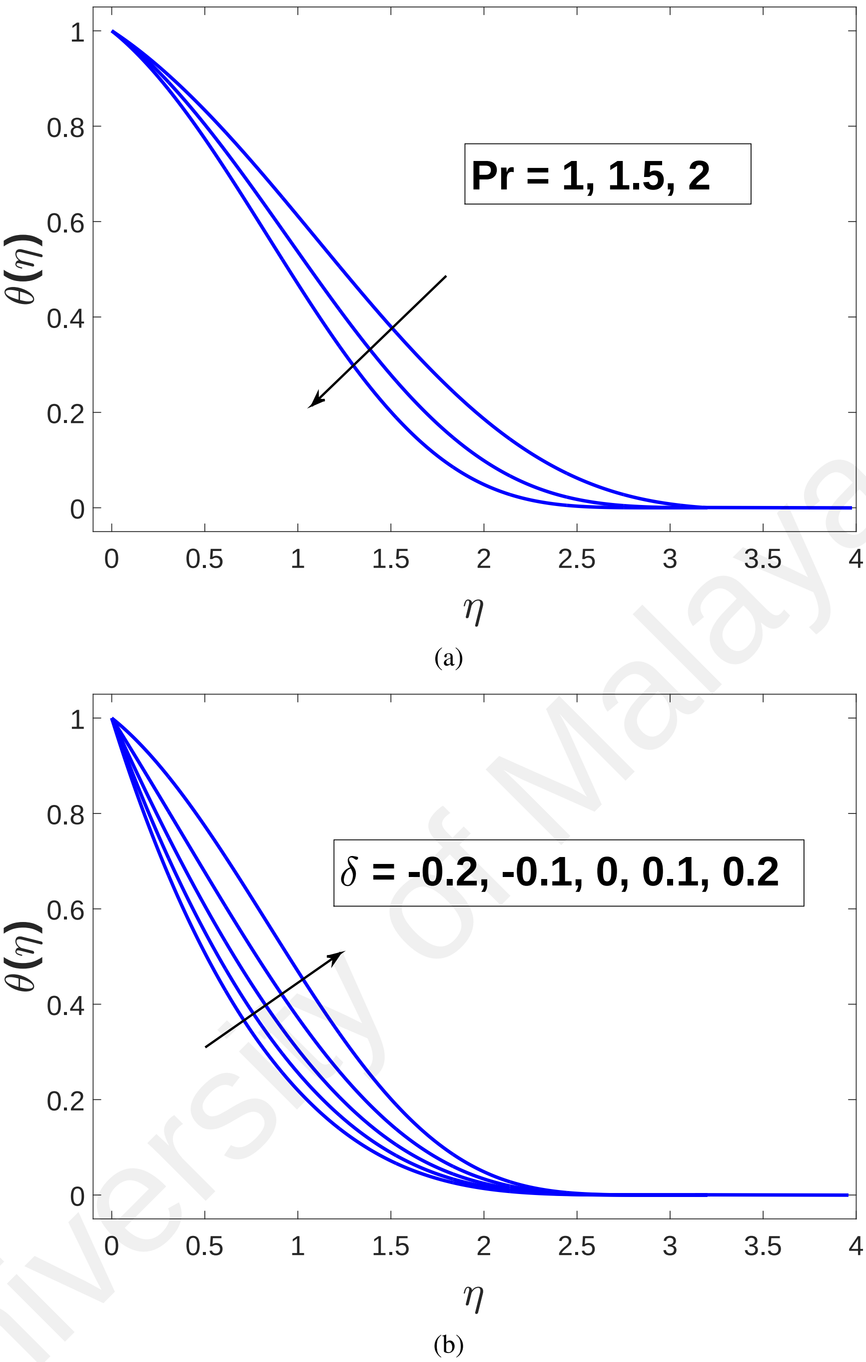

Figure 6.3: The temperature profile for different values of: (a) Pr when $\delta = 0.2$**; (b)** δ **when Pr** $= 2$**; with** $m = 0.0141$ **and** $\beta = \gamma = 0.2$

is defined as the ratio of the momentum diffusivity and thermal diffusivity. As Pr increases, the momentum diffusivity increases and dominates the thermal diffusivity. This means that the fluid velocity is high enough to interfere and helps the heat transfer of the fluid. In turns, the disturbance from the fluid velocity makes the heat dissipation occurs at a faster rate, making the thermal boundary layer thinner. Figure 6.3(b) showed the effect

Table 6.2: The physical properties for selected fluid

Fluid	Pr	T_∞(°C)	ν (cm^2/s)
Gaseous ammonia	1.5-2	25	0.145

of heat generation/absorption parameter δ to the fluid temperature profile θ. In Figure 6.3(b) it can be seen that the temperature profile of the fluid increases with the increasing δ. For $\delta < 0$, it denotes the heat absorption and $\delta > 0$ indicates the heat generation. For $\delta > 0$, since it generates more heat, the temperature profile increases as it takes account the extra heat generated from the fluid. As a contrary, for $\delta < 0$, it absorbs heat energy, thus the temperature profile decreases. This means, as δ increases, the temperature profile increases, makes the heat transfer rate decreases and causes the thickness of the boundary layer increases, i.e becomes thicker.

For a better understanding on the results produced, the dimensional form for several different types of system are presented. Table 6.2 showed the physical properties of fluid used as an example of several system. Figure 6.4(a) presented the heat map of gaseous ammonia with wedge angle parameter $m = 0$, while Figure 6.4(b) presented the heat map of gaseous ammonia with wedge angle parameter $m = 0.2$, both at constant T_∞, T_w, U_∞, β, γ and δ. Here $m = 0$ corresponds to a flat horizontal plate. Based on Figure 6.4, it can be seen that the thermal boundary layer for $m = 0$ is thicker than $m = 0.2$. This means the heat dissipation in a fluid past a horizontal wedge is more efficient than the heat dissipation in a fluid past a horizontal plate. This result corresponds to the results shown in Figure 6.1(a) where as m increases, the heat transfer rate of the fluid increases, thus produces a thinner thermal boundary layer.

Figure 6.5(a) presented the heat map of gaseous ammonia with heat generation/absorption parameter $\delta = -0.2$, while Figure 6.5(b) presented the heat map of gaseous ammonia with heat generation/absorption parameter $\delta = 0.2$, both at constant T_∞, T_w, U_∞, m, β

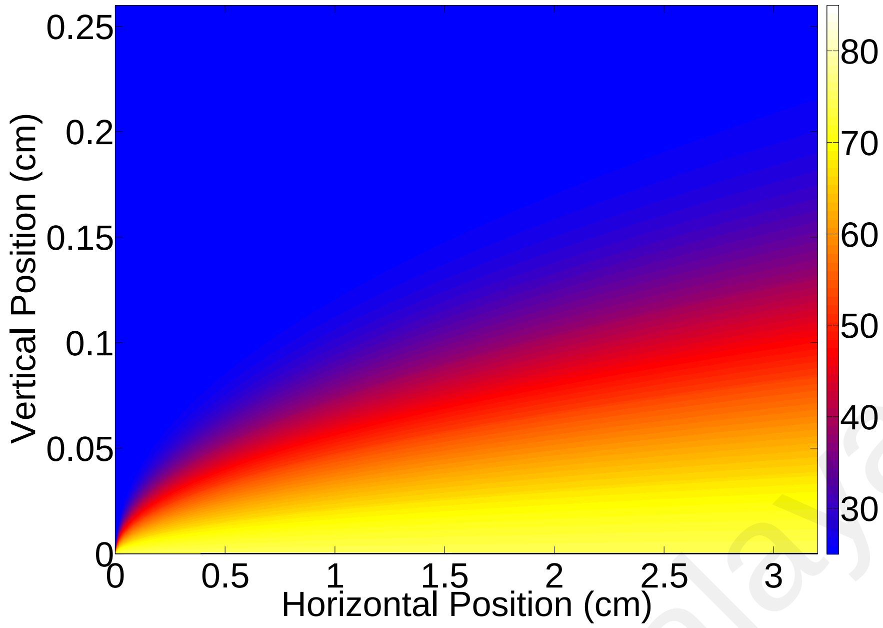

(a)

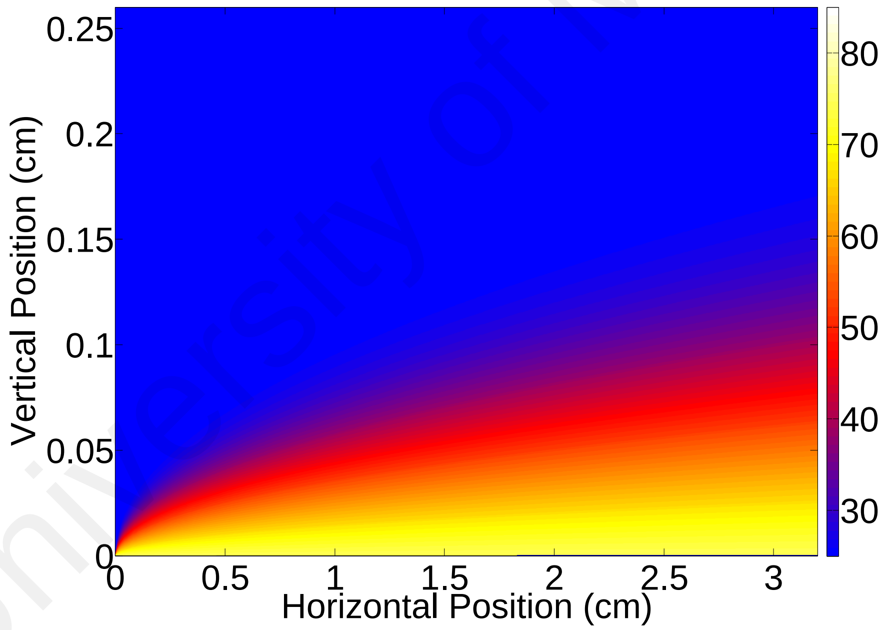

(b)

Figure 6.4: The heat map of gaseous ammonia with: (a) $m = 0$**; (b)** $m = 0.2$**; at** $T_\infty = 25°$**C with** $T_w = 75°$**C,** $U_\infty = 100$ **cm/s, and** $\beta = \gamma = \delta = 0.2$

and γ. It is shown from Figure 6.5 that the thermal boundary layer for $\delta = -0.2$ is much thinner than the thermal boundary layer for $\delta = 0.2$. This means that as δ increases, the thermal boundary layer thickens. For $\delta < 0$, it denotes the heat absorption and $\delta > 0$ indicates the heat generation. Thus, based on Figure 6.5, it can be said that the presence of

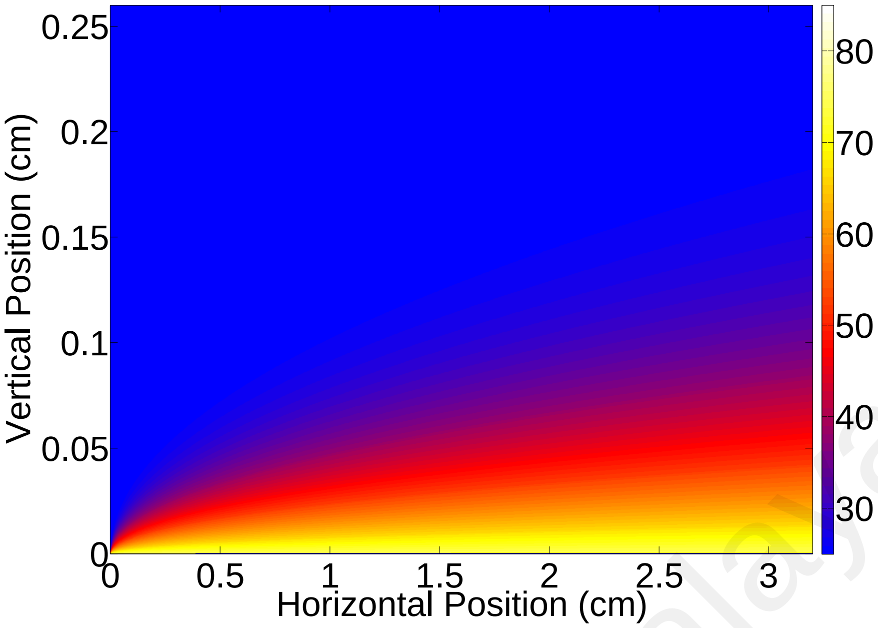

(a)

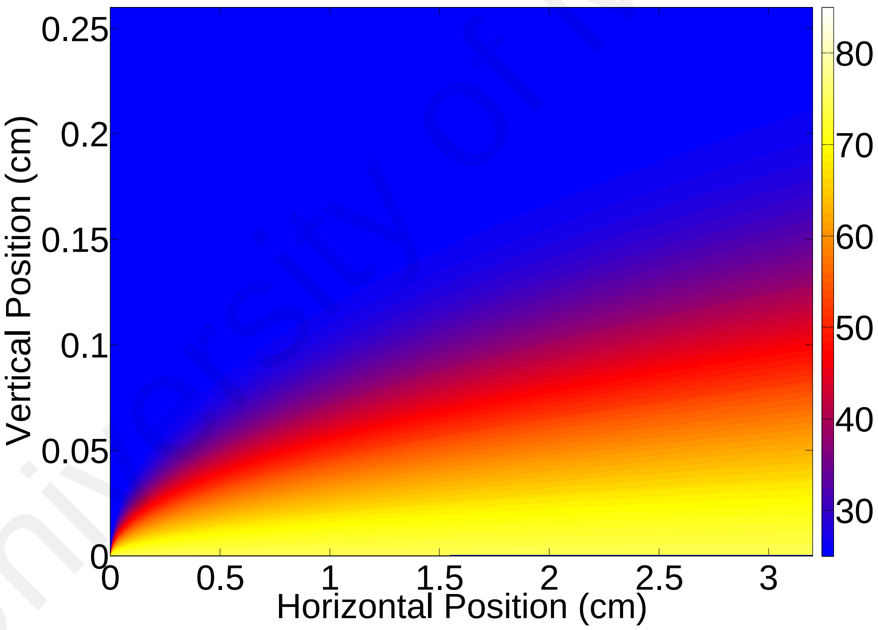

(b)

Figure 6.5: The heat map of gaseous ammonia with: (a) $\delta = -0.2$**; (b)** $\delta = 0.2$**; at** $T_\infty = 25°$**C with** $U_\infty = 100$ **cm/s,** $T_w = 75°$**C,** $m = 0.0141$ **and** $\beta = \gamma = 0.2$

heat absorption helps the heat to dissipate quicker from the system, while the presence of heat generation retards the heat transfer. As a conclusion, as δ increases, the efficiency of heat dissipation from the wall in the fluid flow decreases, which supported by the results presented in Figure 6.3(b).

CHAPTER 7: HEAT TRANSFER ANALYSIS OF UPPER-CONVECTED MAXWELL FLUID OVER A HORIZONTAL WEDGE IN THE PRESENCE OF HEAT GENERATION/ABSORPTION, CHEMICAL REACTION, SUCTION AND HEAT RADIATION USING CATTANEO-CHRISTOV HEAT FLUX MODEL

In this chapter, the problem discussed in Chapter 6 is extended by the inclusion of mass transfer, chemical reaction and heat radiation.

7.1 Mathematical Formulation

The two-dimensional laminar flow of UCM fluid over a horizontal wedge with the wedge angle $\Omega = \beta_w \pi$ is considered. The Hartree pressure gradient β_w is defined as $\beta_w = \dfrac{2m}{m+1}$ where m is the wedge angle parameter. An assumption is made that the surface of the wedge has a constant temperature T_w and constant concentration C_w respectively, and the ambient fluid temperature and ambient concentration are T_∞ and C_∞ respectively. The governed equation for the heat and mass transfer for steady incompressible laminar flow of Maxwell fluid over a horizontal wedge with heat transfer, suction, chemical reaction, heat radiation and heat generation/absorption is expressed as,

$$\frac{\partial u}{\partial x} + \frac{\partial v}{\partial y} = 0, \tag{7.1}$$

$$u\frac{\partial u}{\partial x} + v\frac{\partial u}{\partial y} + \lambda_1\left(u^2\frac{\partial^2 u}{\partial x^2} + v^2\frac{\partial^2 u}{\partial y^2} + 2uv\frac{\partial^2 u}{\partial x \partial y}\right) = \nu\frac{\partial^2 u}{\partial y^2} + U_\infty\frac{\partial U_\infty}{\partial x} + \lambda_1 U_\infty^2\frac{\partial^2 U_\infty}{\partial x^2}, \tag{7.2}$$

$$\begin{aligned} u\frac{\partial T}{\partial x} + v\frac{\partial T}{\partial y} + \lambda_2\Bigg[u^2\frac{\partial^2 T}{\partial x^2} + v^2\frac{\partial^2 T}{\partial y^2} + 2uv\frac{\partial^2 T}{\partial x\partial y} + \left(u\frac{\partial u}{\partial x} + v\frac{\partial u}{\partial y}\right)\frac{\partial T}{\partial x} \\ + \left(u\frac{\partial v}{\partial x} + v\frac{\partial v}{\partial y}\right)\frac{\partial T}{\partial y}\Bigg] = \alpha\frac{\partial^2 T}{\partial y^2} + Q(T - T_\infty) - \frac{1}{\rho c}\frac{\partial q_r}{\partial y}, \end{aligned} \tag{7.3}$$

$$u\frac{\partial C}{\partial x} + v\frac{\partial C}{\partial y} = D\frac{\partial^2 C}{\partial y^2} + K_0(C - C_\infty), \tag{7.4}$$

with x and y are the coordinates along and normal to the heated plate respectively, u and v are the velocity components along the x and y axis respectively, λ_1 is the relaxation time of the UCM fluid, ν is the kinematic viscosity of the fluid, $\alpha = \frac{k}{\rho C_p}$ is the thermal diffusivity, k is the thermal conductivity, ρ is the density of the fluid, C_p is the specific heat capacity of the fluid, λ_2 is the relaxation time for heat flux, T is the local fluid temperature, C is the local fluid concentration, D is the mass diffusion coefficient, Q is the heat generation/absorption coefficient, K_0 is the chemical reaction coefficient, and $q_r = -\left(\frac{4\sigma}{3k_1}\right)\left(\frac{\partial T^4}{\partial y}\right)$ is the radiative heat flux where σ is the Stefan-Boltzmann constant and k_1 is the mean absorption coefficient. By employing Rosseland approximation on the q_r, T^4 can be expressed as a linear function of temperature by using Taylor's series expansion about the ambient fluid temperature T_∞ since the fluid-phase temperature differences within the flow is assumed to be negligible. The Taylor's series expansion of T^4 are truncated to $T^4 \cong 4T_\infty^3 T - 3T_\infty^4$. The radiative heat flux term in Eq.(7.3) becomes $q_r = -\left(\frac{16\sigma T_\infty^3}{3k_1}\right)\left(\frac{\partial T}{\partial y}\right)$.

The boundary conditions are,

$$\begin{aligned} &u = 0, \quad v = v_0, \quad T = T_w, \quad C = C_w, \quad \text{at} \quad y = 0, \\ &u \to U_\infty, \quad T \to T_\infty, \quad C \to C_\infty, \quad \text{as} \quad y \to \infty, \end{aligned} \tag{7.5}$$

where v_0 is suction, $U_\infty = ax^m$ and a is a constant. The following dimensionless variables are introduced to obtain similarity solution for the problem,

$$\eta = y\sqrt{\frac{(m+1)U_\infty}{2\nu x}}, \quad \psi = f(\eta)\sqrt{\frac{2U_\infty \nu x}{m+1}}, \quad \theta(\eta) = \frac{T - T_\infty}{T_w - T_\infty}, \quad \phi(\eta) = \frac{C - C_\infty}{C_w - C_\infty}, \tag{7.6}$$

where η is the dimensionless similarity variable, ψ is the stream function defined as $u = \frac{\partial \psi}{\partial y}$ and $v = -\frac{\partial \psi}{\partial x}$. By substituting Eq.(7.6) into Eqs.(7.2) - (7.4), the following set of nonlinear ordinary differential equations are obtained,

$$f''' + \frac{2m}{m+1}\left(1-(f')^2\right) + ff'' + \beta\left[2m\frac{m-1}{m+1}\left(1-(f')^3\right)\right.$$
$$\left. + \frac{m-1}{2}\eta\,(f')^2\,f'' - \frac{m+1}{2}f^2f''' + (3m-1)\,ff'f''\right] = 0, \quad (7.7)$$

$$\left(1+\frac{4}{3R}\right)\theta'' + \mathrm{Pr}f\theta' + \frac{2}{m+1}\mathrm{Pr}\delta\theta - \mathrm{Pr}\gamma\left[\frac{m+1}{2}f^2\theta''\right.$$
$$\left. - \frac{6}{m+1}\eta\,(f')^2\,\theta' + ff'\theta'\right] = 0, \quad (7.8)$$

$$\phi'' + \mathrm{Sc}f\phi' + \frac{2}{m+1}\mathrm{Sc}K\phi = 0, \quad (7.9)$$

where prime denotes the differentiation with respect to η, $\beta = \dfrac{\lambda_1 U_\infty}{2x}$ is the local Deborah number for fluid momentum, $\gamma = \dfrac{\lambda_2 U_\infty}{2x}$ is the local Deborah number for energy term, $\mathrm{Pr} = \dfrac{\nu}{\alpha}$ is the Prandtl number, $R = \dfrac{k_1\alpha\rho C_p}{4\sigma T_\infty^3}$ is the heat radiation parameter, $\mathrm{Sc} = \dfrac{\nu}{D}$ is the Schmidt number, $K = \dfrac{K_0}{ab^2}$ is the chemical reaction parameter, $\delta = \dfrac{Q}{ab^2}$ is the heat generation/absorption parameter and b is a constant. Since the value β and γ contain the function of x, the availability of the local similarity solution is used, and the solution found can be used to see the effect of parameters at a fixed location above the wall.

The transformed boundary conditions are,

$$\begin{aligned} &f = \frac{2}{m+1}s, \quad f' = 0, \quad \theta = 1, \quad \phi = 1, \quad \text{at} \quad \eta = 0, \\ &f' \to 1, \quad \theta \to 0, \quad \phi \to 0, \quad \text{as} \quad \eta \to \infty, \end{aligned} \quad (7.10)$$

where $s = -v_0\sqrt{\dfrac{(m+1)x}{2U_\infty\nu}}$ is the suction parameter.

The important physical quantities of the flow are the local skin-friction coefficient C_f, local Nusselt number Nu and local Sherwood number Sh, which are related to the value of $f''(0)$, $-\theta'(0)$ and $\phi'(0)$ respectively. These parameter are defined as $C_f = \dfrac{\mu}{\rho U_\infty^2}\left(\dfrac{\partial u}{\partial y}\right)_{y=0}$, $\mathrm{Nu} = -\dfrac{x}{(T_w - T_\infty)}\left(\dfrac{\partial T}{\partial y}\right)_{y=0} - \dfrac{4\sigma x}{3kk_1(T_w - T_\infty)}\left(\dfrac{\partial T^4}{\partial y}\right)_{y=0}$ and $\mathrm{Sh} = -\dfrac{x}{(C_w - C_\infty)}\left(\dfrac{\partial C}{\partial y}\right)_{y=0}$ respectively. By substituting Eq.(7.6), the local skin-friction coefficient, local Nusselt

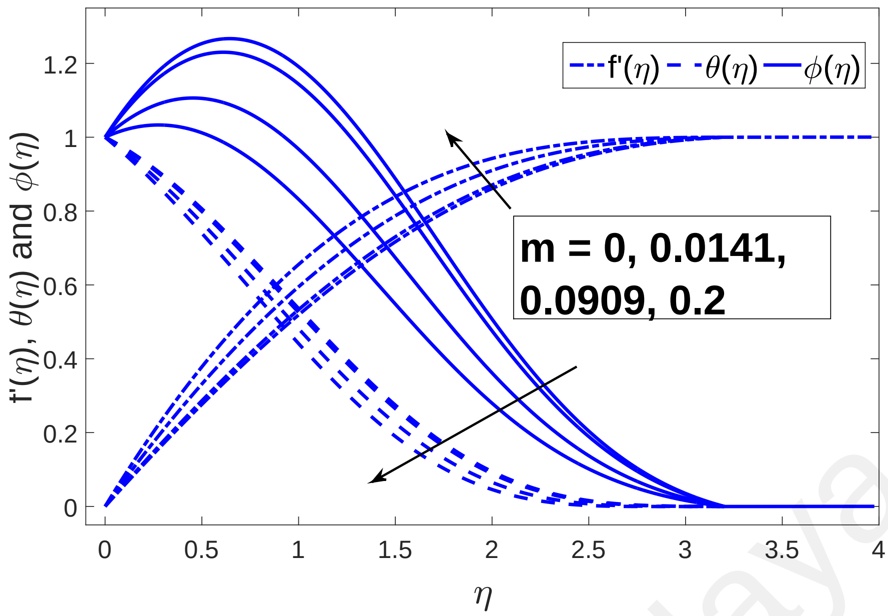

Figure 7.1: The velocity profile, temperature profile and concentration profile for different values of m with $\beta = \gamma = \delta = 0.2$, $s = 0.1$, Pr $= 2$, $K = 0.5$, $R = 5$ and Sc $= 1$

number and local Sherwood number are,

$$C_f\,(\mathrm{Re}_x)^{1/2} = \sqrt{\frac{m+1}{2}}\,f''(0), \tag{7.11}$$

$$\mathrm{Nu}\,(\mathrm{Re}_x)^{-1/2} = \left(1 + \frac{4}{3R}\right)\sqrt{\frac{m+1}{2}}\,\theta'(0), \tag{7.12}$$

$$\mathrm{Sh}\,(\mathrm{Re}_x)^{-1/2} = \sqrt{\frac{m+1}{2}}\,\phi'(0), \tag{7.13}$$

7.2 Results and Discussion

Table 7.1 presented the values of $f''(0)$, $-\theta'(0)$ and $-\phi'(0)$ for various values of parameters. From Table 7.1, the value of $f''(0)$ increases as the suction parameter s increases but the value of $\theta'(0)$ and $\phi'(0)$ decrease. Noted that the value of $-\phi'(0)$ remains constant for the increasing values of Pr, γ, δ and R and this is due to the fact that the parameters listed are only affecting the fluid temperature profile since they do not appear in the concentration equation. The same situation happens for the value of $f''(0)$. The constant value of $f''(0)$ for different values of Sc and K are because of these parameters are absent in the momentum equation. It is also found that from Table 7.1 the value of

Table 7.1: The values of $f''(0)$, $-\theta'(0)$ and $-\phi'(0)$ for various values of m, β, s, Pr, γ, δ, R, Sc and K

m	β	s	Pr	γ	δ	R	Sc	K	$f''(0)$	$-\theta'(0)$	$-\phi'(0)$
0.0000									0.292146	-0.27006	0.809933
0.0141	0.2	0.1	2.0	0.2	0.2	5.0	1.0	0.50	0.305273	-0.28801	0.737449
0.0909									0.365763	-0.36407	0.460332
0.2000									0.430613	-0.43641	0.325276
	0.0								0.328606	-0.31421	0.666493
0.0141	0.1	0.1	2.0	0.2	0.2	5.0	1.0	0.50	0.317237	-0.30182	0.699504
	0.2								0.305273	-0.28801	0.737449
		0.0							0.237142	0.019794	1.236621
0.0141	0.2	0.1	2.0	0.2	0.2	5.0	1.0	0.50	0.305273	-0.28801	0.737449
		0.2							0.383107	-0.61316	0.32545

Continued on next page

Table 7.1, continued

m	β	s	Pr	γ	δ	R	Sc	K	$f''(0)$	$-\theta'(0)$	$-\phi'(0)$
0.0141	0.2	0.1	1.0	0.2	0.2	5.0	1.0	0.50	0.305273	-0.25221	0.737449
			1.5							-0.26521	
			2.0							-0.28801	
			3.0							-0.33425	
0.0141	0.2	0.1	2.0	0.0	0.2	5.0	1.0	0.50	0.305273	-0.30534	0.737449
				0.1						-0.29544	
				0.2						-0.28801	
0.0141	0.2	0.1	2.0	0.2	-0.2	5.0	1.0	0.50	0.305273	-1.09654	0.737449
					-0.1					-0.94222	
					0.0					-0.76462	
					0.1					-0.55307	
					0.2					-0.28801	

Continued on next page

Table 7.1, continued

m	β	s	Pr	γ	δ	R	Sc	K	$f''(0)$	$-\theta'(0)$	$-\phi'(0)$
0.0141	0.2	0.1	2.0	0.2	0.2	1.5	1.0	0.50	0.305273	-0.25921	0.737449
						3.0				-0.27646	
						5.0				-0.28801	
						7.0				-0.29403	
						10.0				-0.29906	
0.0141	0.2	0.1	2.0	0.2	0.2	5.0	0.2	0.50	0.305273	-0.28801	-0.15491
							0.4				0.027124
							0.7				0.350857
							1.0				0.737449
0.0141	0.2	0.1	2.0	0.2	0.2	5.0	1.0	0.00	0.305273	-0.28801	-0.6187
								0.20			-0.28185
								0.35			0.092247
								0.50			0.737449

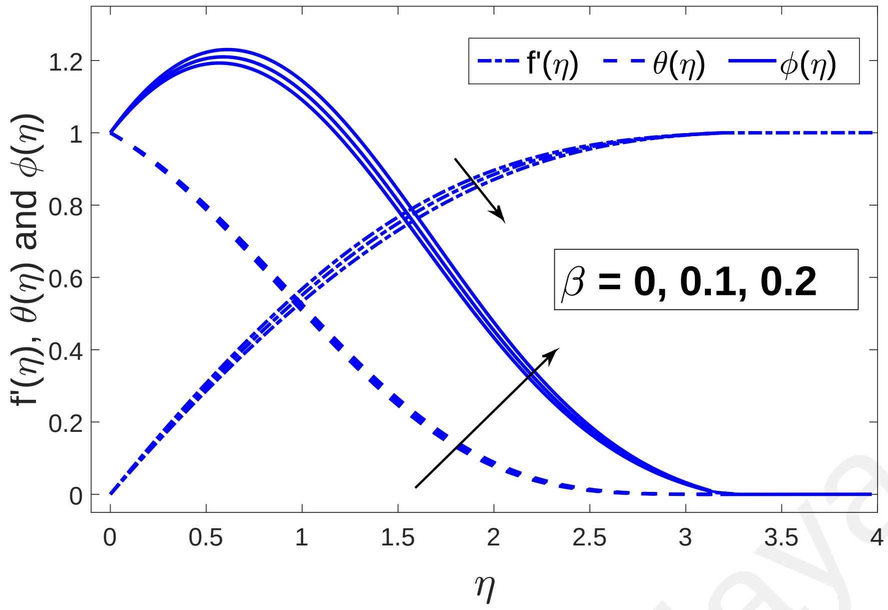

(a)

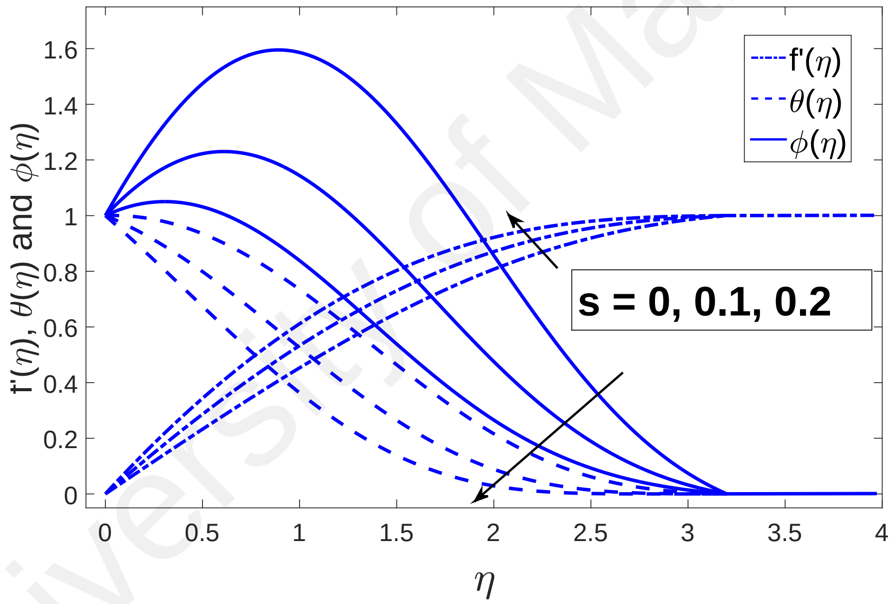

(b)

Figure 7.2: The velocity profile, temperature profile and concentration profile for different values of: (a) β **when** $s = 0.1$**; (b)** s **when** $\beta = 0.2$**; with** $m = 0.0141$**,** $\gamma = \delta = 0.2$**, Pr** $= 2$**,** $K = 0.5$**,** $R = 5$ **and Sc** $= 1$

$\theta'(0)$ decreases as the radiation parameter R increases.

Figure 7.1 shows the effect of wedge angle parameter m on velocity profile f', temperature profile θ and concentration profile ϕ. It can be seen that for increasing value of the wedge angle parameter, the velocity profile increases while the temperature and concentration profile decrease. Note that, $m = 0$ corresponds to a horizontal plate while $m = 1$

corresponds to a stagnation point of a vertical plate. By Figure 7.1, as the wedge becomes steeper, the thickness of momentum, thermal and concentration boundary layer decrease.

The effect of local Deborah number β on f', θ and ϕ is shown in Figure 7.2(a). The velocity profile decreases insignificantly but the temperature and concentration profile increase as the local Deborah number, β increases as presented in Figure 7.2(a). β is defined as the ratio of fluid relaxation time to its deformation rate, thus as β increases, the deformation time of the fluid decreases and the relaxation time increases. The relaxation causes the thickness of the momentum, thermal and concentration boundary layer to decrease. Since the velocity, temperature and mass profiles are affected insignificantly, it is concluded that the change of the value of β does not affect much for both of the profiles. Figure 7.2(b) illustrates the effect of the suction parameter, s on velocity, temperature and concentration profiles. Based on Figure 7.2(b), the velocity profile increases with the increase of the suction parameter while the temperature and concentration profile decrease. As s increases, the shear wall stress of the fluid decreases, causing the thickness of momentum, thermal and concentraton boundary layer decrease.

Figure 7.3(a) shows the effect of Prandtl number, Pr on the temperature profile. From Figure 7.3(a), as the value of Pr increases, the temperature profile decreases. Prandtl number is defined as the ratio of momentum diffusivity and thermal diffusivity. As Pr increases, the momentum diffusivity increases and dominates the thermal diffusivity. The fluid velocity is high enough to facilitate the heat transfer of the fluid. This, in turn, makes the heat dissipation rate occurs faster and makes the thermal boundary layer becomes thinner. Figure 7.3(b) shows the effect of the local Deborah number, γ on the temperature profile. In Figure 7.3(b), the value of temperature profile decreases insignificantly when the value of Deborah number increases. It is noted that the relaxation time of the heat transfer of the fluid increases, which helps the increase in heat transfer, and makes the thermal boundary layer becomes thinner. This illustrates that the dissipation of heat occurs

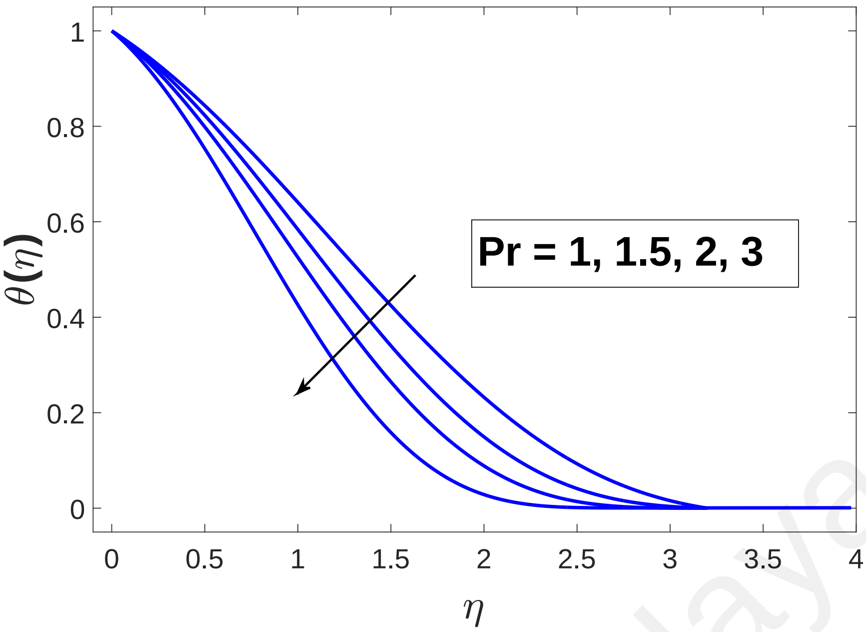

(a)

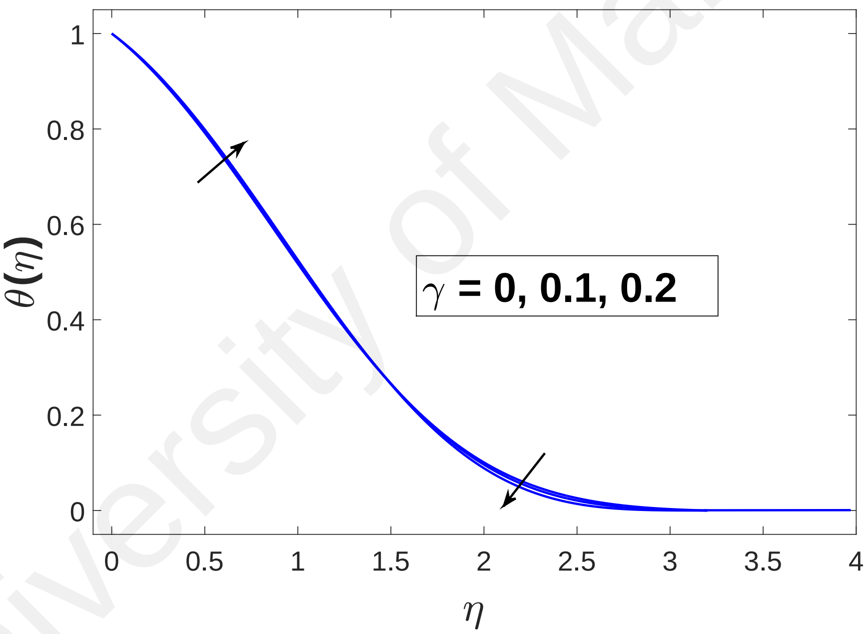

(b)

Figure 7.3: The temperature profile for different values of: (a) Pr when $\gamma = 0.2$**; (b)** γ **when Pr**$= 2$**; with** $m = 0.0141$**,** $\beta = \delta = 0.2$**,** $s = 0.1$**,** $K = 0.5$**,** $R = 5$ **and Sc** $= 1$

at a faster rate.

The effect of heat generation/absorption parameter, δ on the temperature profile is shown in Figure 7.4(a). The temperature profile increases as δ increases. For $\delta < 0$, it corresponds to the heat absorption while $\delta > 0$ means there is presence of heat generation. For $\delta > 0$, it generates more heat and the temperature profile increases as it takes into

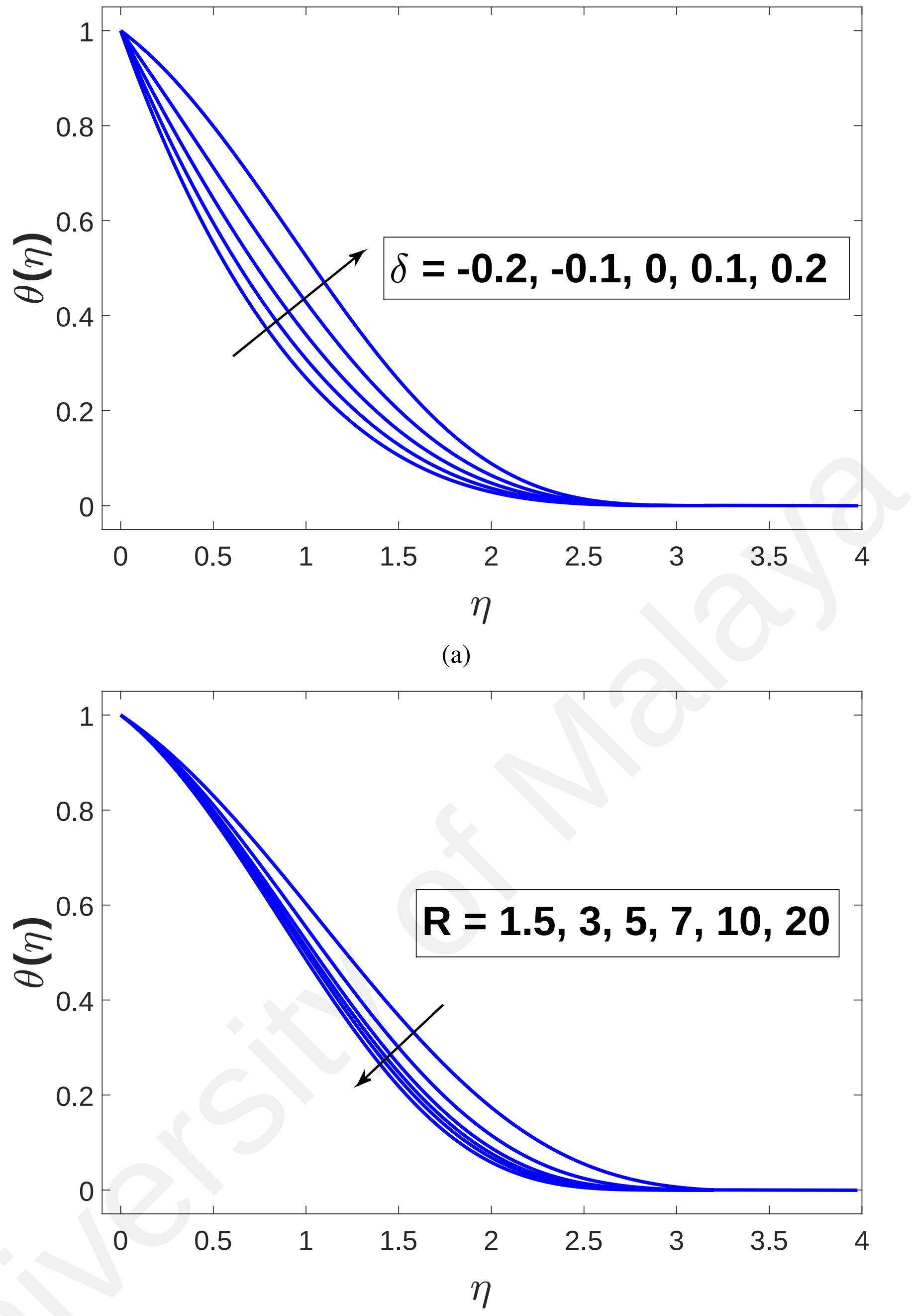

(a)

(b)

Figure 7.4: The temperature profile for different values of: (a) δ when $R = 5$; (b) R when and $\delta = 0.2$; with $m = 0.0141$, $\beta = \gamma = 0.2$, $s = 0.1$, Pr$= 2$, $K = 0.5$ and Sc $= 1$

account the heat generation from the fluid. As a contrary, for $\delta < 0$, the fluid absorbs heat energy, thus the temperature profile decreases. This means that as δ increases, the temperature profile increases. It makes the heat transfer rate decreases and causes the thickness of the thermal boundary layer increases. The effect of radiation parameter R on the temperature profile θ is presented in Figure 7.4(b). It is shown that the temperature

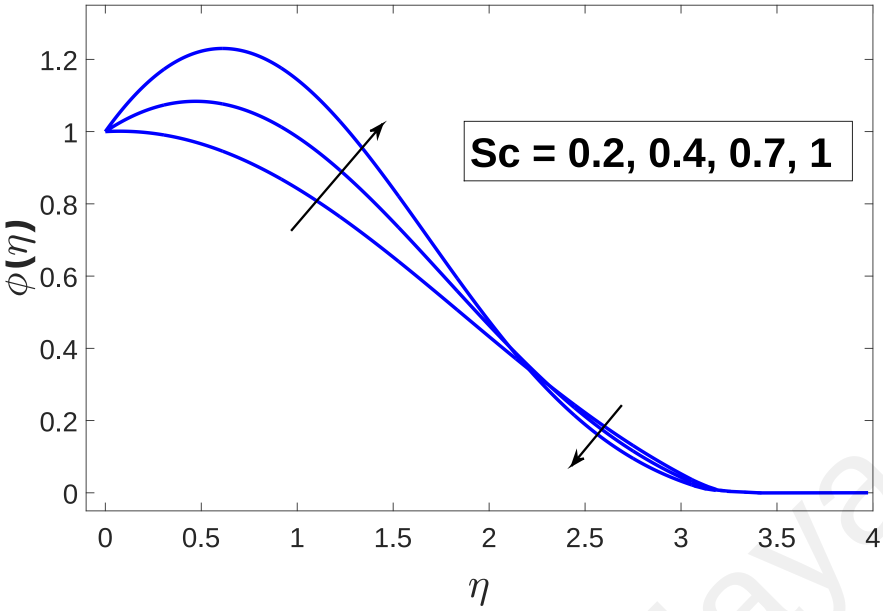

(a)

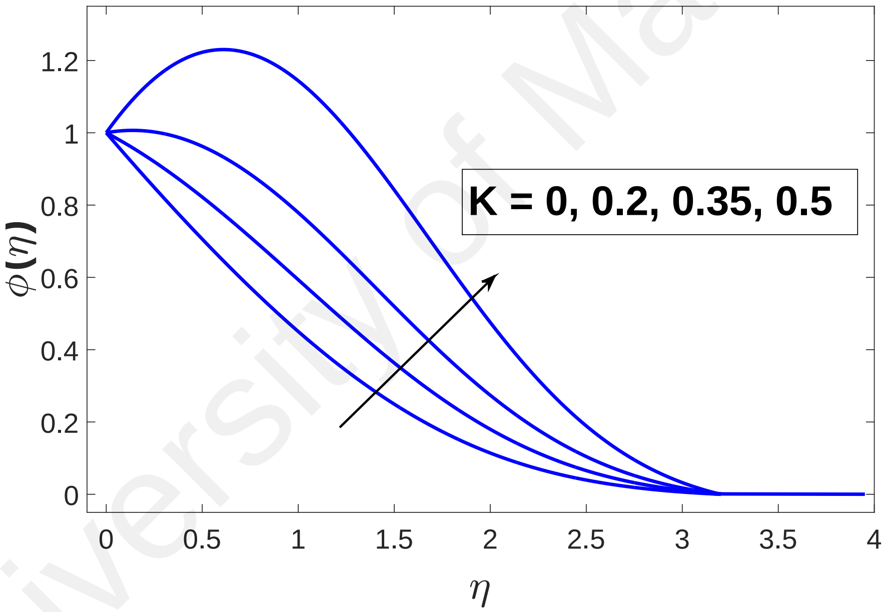

(b)

Figure 7.5: The concentration profile for different values of: (a) Sc when K $= 0.5$**; (b) K when Sc**$= 1$**; with** $m = 0.0141$**,** $\beta = \gamma = \delta = 0.2$**,** $s = 0.1$**, Pr**$= 2$ **and** $R = 5$

profile decreases as the value of radiation parameter increases. Increase in R causes the fluid temperature to increase as well. This makes the heat transfer rate of the fluid increases, and thus makes the thermal boundary layer becomes thinner.

The effect of Schmidt number Sc on the fluid concentration distribution ϕ is presented in Figure 7.5(a). It can be shown from Figure 7.5(a) that as Sc increases, the concentration of

Table 7.2: The physical properties for selected fluid

Fluid	Pr	T_∞(°C)	ν (cm^2/s)
Gaseous ammonia	1.5-2	25	0.145

the fluid increases at the region $0 < \eta \lesssim 2.1$, but slightly decreases for the region $\eta > 2.1$. Since Schmidt number is defined as the ratio of momentum diffusivity and mass diffusivity, it means that the increase of the ratio of momentum diffusivity and mass diffusivity resulted in a thinner boundary layer of mass transfer. Figure 7.5(b) presented the variation of fluid concentration distribution ϕ with different values of chemical reaction parameter K. Based on Figure 7.5(b), as the value of K increases, the fluid concentration profile increases with the influence of suction and the fact that the fluid past through a horizontal wedge. This means that as K increases, the fluid reacts chemically with the surface of the wedge, increases its concentration. In turns, it resulted in the thicker concentration boundary layer.

The dimensional form for several different types of system are presented for a better understanding on the results produced earlier. Table 7.2 presented the physical properties of fluid used to demonstrate the system in real-world situation. Figure 7.6 showed the heat map of gaseous ammonia at a constant T_∞, U_∞, β, m, s, γ, R and δ, with $T_w = 55$°C for Figure 7.6(a) and $T_w = 115$°C for Figure 7.6(b). It can be seen from Figure 7.6 that the thermal boundary layer for $T_w = 55$°C is thinner than $T_w = 155$°C. Based on the Figure 7.6, for the lower wall temperature, the heat from the wall needed to dissipate is low, which corresponds to the thinner thermal boundary layer flow. It can be concluded that as the wall temperature increases, the thermal boundary layer increases, which means the heat dissipation efficiency decreases.

Figure 7.7(a) showed the heat map of gaseous ammonia with the radiation parameter, $R = 1.5$, while Figure 7.7(b) showed the heat map of gaseous ammonia with the radiation parameter, $R = 5$, both at constant T_∞, T_w, U_∞, β, m, s, γ and δ. Based on Figure 7.7,

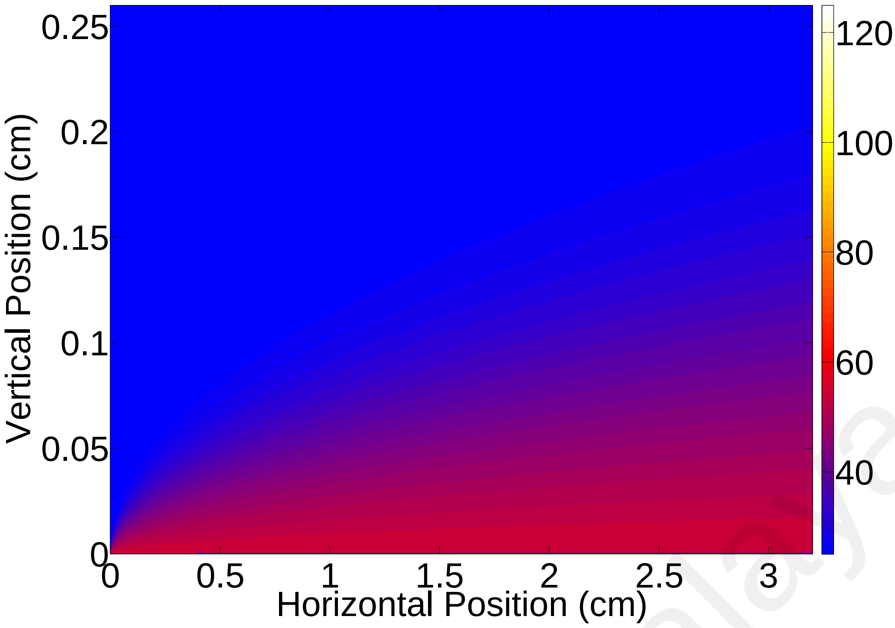

(a)

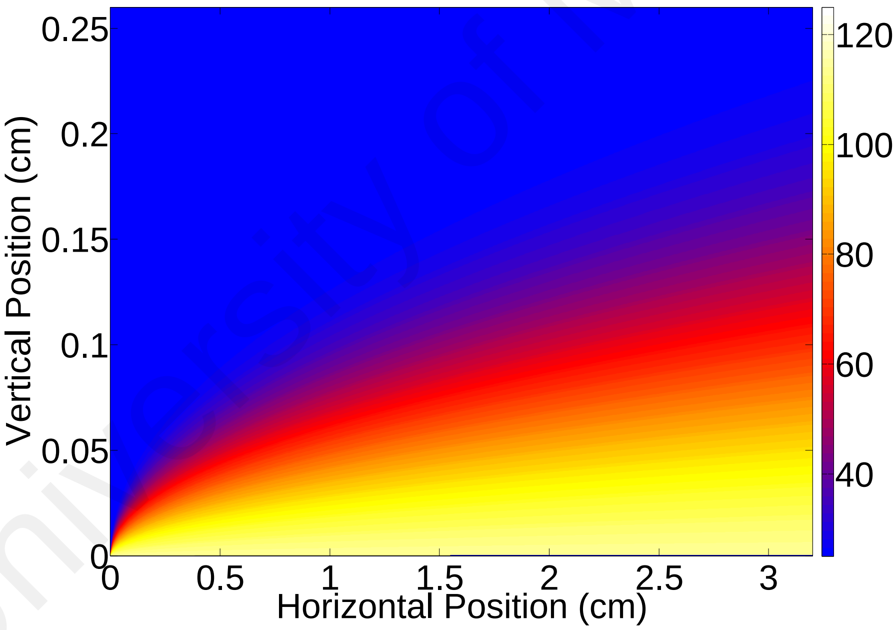

(b)

Figure 7.6: The heat map of gaseous ammonia with: (a) $T_w = 55°$**C; (b)** $T_w = 115°$**C; at** $T_\infty = 25°$**C with** $U_\infty = 100$ **cm/s,** $m = 0.0141$**,** $s = 0.1$**,** $R = 7$ **and** $\beta = \gamma = \delta = 0.2$

the thermal boundary layer for $R = 1.5$ is much thicker than the thermal boundary layer for $R = 5$. Since the heat transfer through radiation is much quicker because it does not require any medium to transfer heat, the presence of heat radiation parameter R increases the efficiency of the heat dissipation from the wall in the fluid. It can be concluded that

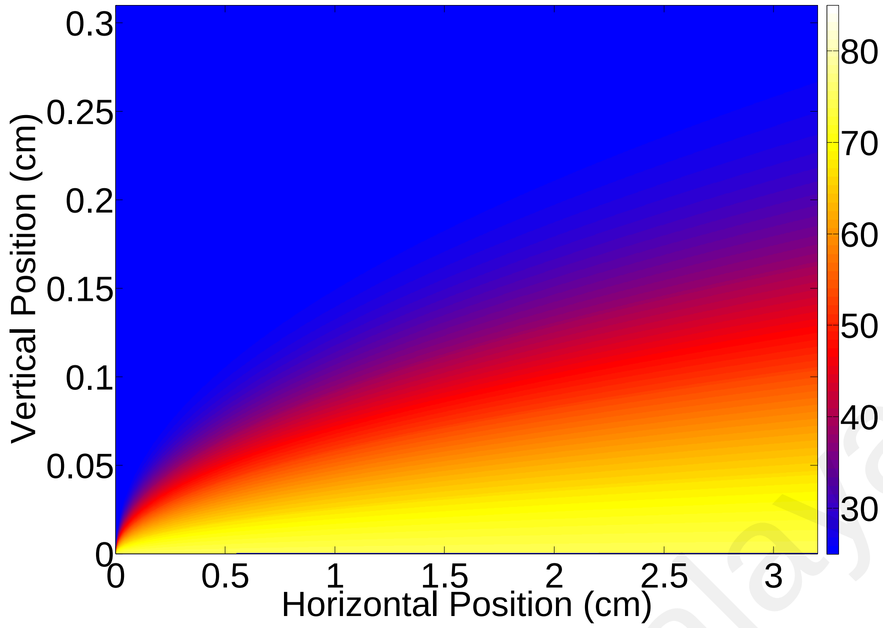

(a)

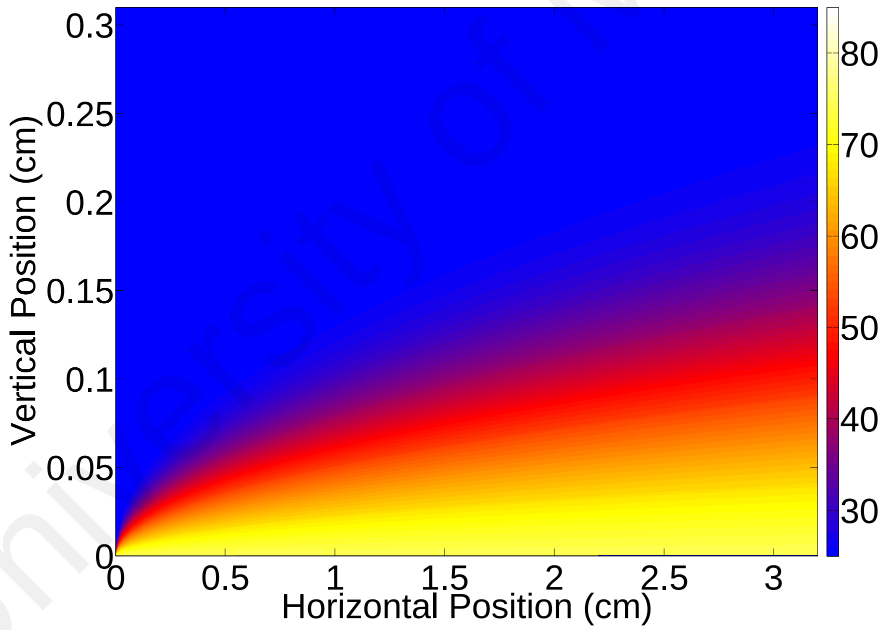

(b)

Figure 7.7: The heat map of gaseous ammonia with: (a) $R = 1.5$**; (b)** $R = 5$**; at** $T_\infty = 25°$**C with** $T_w = 55°$**C,** $U_\infty = 100$ **cm/s,** $m = 0.0141$**,** $s = 0.1$ **and** $\beta = \gamma = \delta = 0.2$

the increase of R increases the heat transfer rate, thus decreases the thickness of thermal boundary layer. This fact corresponds to the results produced in Figure 7.4(b).

Figure 7.8(a) presented the heat map of gaseous ammonia with the fluid free stream velocity $U_\infty = 50$ cm/s, while Figure 7.8(b) presented the heat map of gaseous ammonia

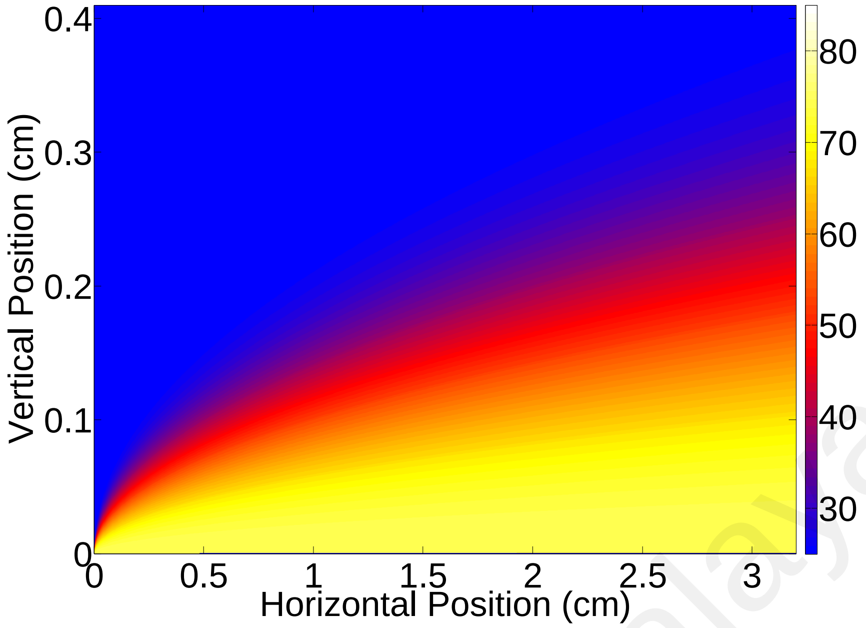

(a)

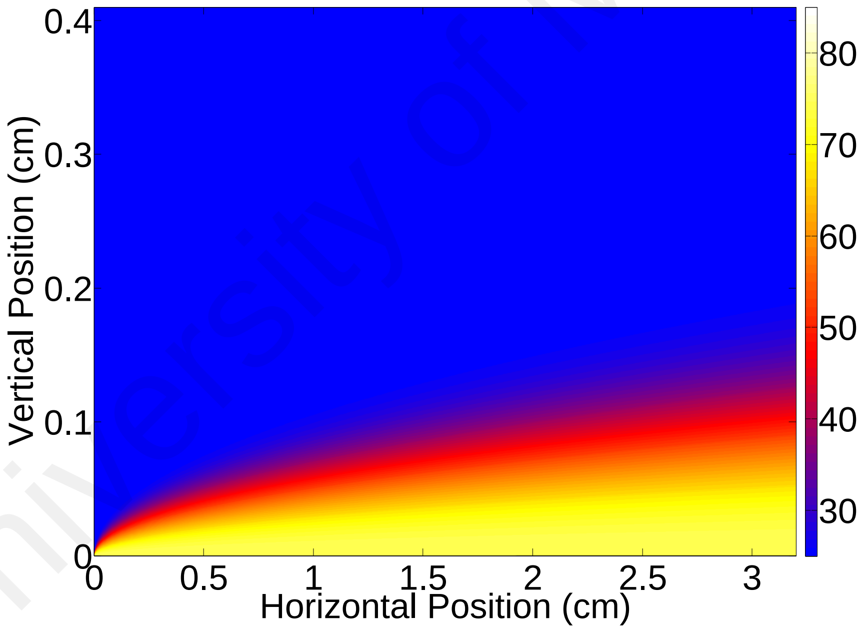

(b)

Figure 7.8: The heat map of gaseous ammonia with: (a) $U_\infty = 50$ **cm/s; (b)** $U_\infty = 200$ **cm/s; at** $T_\infty = 25°$**C with** $T_w = 55°$**C,** $m = 0.0141$**,** $s = 0$**,** $R = 7$ **and** $\beta = \gamma = \delta = 0.2$

with $U_\infty = 200$ cm/s, both at constant T_∞, T_w, β, m, s, γ, R and δ. Based on Figure 7.8, the thermal boundary layer for $U_\infty = 200$ cm/s is much thinner than the thermal boundary layer for $U_\infty = 50$ cm/s. This means that the higher the free stream velocity U_∞, the faster the heat transfer rate from the wall in the fluid. As the fluid moves faster, it can carry the heat from the wall in a faster rate, thus the heat can dissipate faster. This concludes that the heat dissipation efficiency increases as U_∞ increases.

CHAPTER 8: CONCLUSIONS AND RECOMMENDATIONS

8.1 Conclusions

This Masters' dissertation addresses the convective heat transfer of Cattaneo-Christov heat flux model over a wedge. A general introduction to boundary layer flow and fluid dynamics is covered in Chapter 1. Some backgrounds on the general theory of fluid dynamics, boundary layer flow, upper-convected Maxwell fluid model, Carreau fluid model and mass transfer are stated with several examples of the application of heat transfer mode and types of convection. Cattaneo-Christov heat flux model is also discussed in brief which is the generalisation of Fourier's law of heat conduction. In Chapter 2, a comprehensive and extensive literature study on boundary layer flow over a horizontal plate and a horizontal wedge are presented. This literature review is important in driving the flows of the study done in this dissertation. The past study of boundary layer flow with Cattaneo-Christov heat flux model also discussed in detail in this chapter. Several boundary layer flow effects are also emphasized here, namely magnetohydrodynamic, suction/injection, heat generation/absorption, heat radiation and chemical reaction. In Chapter 3, the derivation of the governing equations of the boundary layer flow is presented in detail. It started with the small area within the fluid boundary layer and the derivation of the equation are explained throughout the chapter. The application of stream function, similarity solution, local similarity solution and the local skin-friction coefficient, Nusselt number and Sherwood number are followed. At the end of the chapter, the numerical method used to solve the governed equations is stated with some code validations to validate the computation done.

In Chapter 4, the numerical analysis of mass and heat transfer for Sakiadis and Blasius flows of UCM fluid with Cattaneo-Christov heat flux model over a horizontal plate are discussed. It can be concluded that the fluid velocity decreases as the Deborah number β

increases for Sakiadis flow, while it remains constant for increasing Deborah number γ, Prandtl number and Schmidt number. This is because of only β presents in the momentum equation. It also found that the fluid temperature profile decreases with the increase of Prandtl number and Deborah number γ for both Sakiadis and Blasius flows. It is also worth noted that the fluid temperature distribution for Sakiadis flow is lower that Blasius flow. The fluid concentration distribution is found to be decreasing when Schmidt number increases for both Sakiadis and Blasius flows, although the concentration profile for Blasius flow decreases slower than Sakiadis flow.

The numerical study of mass and heat transfer for Sakiadis flow of magnetohydrodynamic (MHD) Carreau fluid over a horizontal plate using Cattaneo-Christov heat flux model are presented in Chapter 5. There are some conclusions can be drawn from the work done in this chapter such as the fluid velocity profile decreases when Weissenberg number increases but fluid velocity profile increases slightly when the power-law index increases under the influence of magnetic field. The velocity profile remains unchanged for variation of Prandtl number, Schmidt number and local Deborah number γ since these parameters do not present in the momentum equation. The fluid temperature distribution increases with the increase of Weissenberg and local Deborah number γ but decreases with the increase of power-law index and Prandtl number. It also can be seen that the fluid concentration increases when Weissenberg number increases but decreases when power-law index and Schmidt number increase.

In Chapter 6 and Chapter 7, the investigation of the convective boundary layer of UCM fluid over a horizontal wedge using Cattaneo-Christov heat flux model in the presence of suction, chemical reaction, heat generation/absorption and heat radiation are presented. Chapter 6 discussed the boundary layer flow with heat transfer, suction and heat generation/absorption, while Chapter 7 discussed the extension of the first problem by including mass transfer, heat generation and heat radiation effects. It can be concluded that the fluid velocity distribution increases with the increase of wedge angle and suction, while it decreases with the increases of local Deborah number β. From the study, it can be seen that the fluid temperature profile increase when local Deborah number β and γ, and heat generation increase, but the fluid temperature profile decreases when wedge angle, suction, Prandtl number and heat radiation increase. This means that there are many influences that can slow down the heat transfer in the fluid. It also worth noting that the fluid concentration distribution increases with the increase of local Deborah number β, Schmidt number and chemical reaction parameter but the increase of wedge angle and suction decrease the fluid concentration profile.

8.2 Recommendations for Future Study

As for the continuation of the present work, the following future studies are suggested,

1. The study of boundary layer flow over a wedge can be extended by using different fluid models such as Casson fluid model and Williamson fluid model.
2. The usage of Cattaneo-Christov heat flux model to study the heat transfer over a wedge can be expanded and the results can be compared with the same heat transfer study using classical Fourier's law.
3. The inclusion of Soret and Dufour effects, thermophoresis and magnetohydrodynamic into the boundary layer flow over a wedge may be done in the future.
4. The study of boundary layer flow over a wedge can be extended with different fluid characteristics such as Darcy-Forchheimer flow, unsteady flow and slip velocity.

REFERENCES

Abbasbandy, S., & Hayat, T. (2009). Solution of the MHD Falkner-Skan flow by homotopy analysis method. *Communications in Nonlinear Science and Numerical Simulation*, *14*, 3591–3598.

Abbasi, F., Mustafa, M., Shehzad, S., Alhuthali, M., & Hayat, T. (2015). Analytical study of Cattaneo-Christov heat flux model for a boundary layer flow of Oldroyd-B fluid. *Chinese Physics B*, *25*(1), 1–6.

Ahmad, H., Javed, T., & Ghaffari, A. (2016). Radiation effect on mixed convection boundary layer flow of a viscoelastic fluid over a horizontal circular cylinder with constant heat flux. *Journal of Applied Fluid Mechanics*, *9*(3), 1167–1174.

Alfvén, H. (1942). Existence of electromagnetic-hydrodynamic waves. *Nature*, *150*(3805), 405–406.

Ali, H., & Masood, K. (2016). Impact of heat transfer analysis on Carreau fluid flow past a static and moving wedge. *Thermal Science*, *20*, 169.

Alizadeh, E., Farhadi, M., Sedighi, K., Ebrahimi-Kebria, H. R., & Ghafourian, A. (2009). Solution of the Falkner-Skan equation for wedge by Adomian Decomposition Method. *Communications in Nonlinear Science and Numerical Simulation*, *14*(3), 724–733.

Amoura, M., Zeraibi, N., & Benzaoui, A. (2014). Mixed Convection Flow of Non-Newtonian Carreau Fluid : Effect of Viscous Dissipation. In *International conference on heat transfer, fluid mechanics and thermodynamics* (pp. 200–205). Orlando, Florida: Taylor and Francis Group.

Animasaun, I. (2014). Effects of thermophoresis, variable viscosity and thermal conductivity on free convective heat and mass transfer of non-Darcian MHD dissipative Casson fluid flow with suction and *n*-th order of chemical reaction. *Journal of the Nigerian Mathematical Society*, *34*(1), 11–31.

Ara, A., Khan, N. A., Khan, H., & Sultan, F. (2014). Radiation effect on boundary layer flow of an Eyring-Powell fluid over an exponentially shrinking sheet. *Ain Shams Engineering Journal*, *5*(4), 1337–1342.

Awais, M., Hayat, T., Irum, S., & Alsaedi, A. (2015). Heat generation/absorption effects in a boundary layer stretched flow of Maxwell nanofluid: analytic and numeric solutions. *PLoS ONE*, *10*(6), 1–18.

Aziz, A. (2009). A similarity solution for laminar thermal boundary layer over a flat plate with a convective surface boundary condition. *Communications in Nonlinear Science and Numerical Simulation*, *14*(4), 1064–1068.

Bhattacharyya, K. (2011). Boundary layer flow with diffusion and first-order chemical reaction over a porous flat plate subject to suction/injection and with variable wall concentration. *Chemical Engineering Research Bulletin*, *15*(1), 6–11.

Blasius, H. (1908). *Grenzschichten in flüssigkeiten mit kleiner reibung* (Unpublished doctoral dissertation). University of Gottingen.

Boger, D. (1977). Demonstration of upper and lower Newtonian fluid behaviour in pseudoplastic fluid. *Nature*, *265*, 126–128.

Bogue, D. C., & Doughty, J. O. (1966). Comparison of constitutive equations for viscoelastic fluids. *Industrial and Engineering Chemistry Fundamentals*, *5*(2), 243–252.

Brodie, P., & Banks, W. H. H. (1986). Further properties of the Falkner-Skan equation. *Acta Mechanica*, *65*, 205–211.

Burden, R. L., & Faires, J. D. (2011). *Numerical Analysis* (Ninth ed.). Boston, USA: Cengage Learning.

Bush, M. B., & Phan-Thien, N. (1984). Drag force on a sphere in creeping motion through a Carreau model fluid. *Journal of Non-Newtonian Fluid Mechanics*, *16*(3), 303–313.

Carragher, P., & Crane, L. J. (1982). Heat transfer on a continuous stretching sheet. *Journal of Applied Mathematics and Mechanics*, *62*(10), 564–565.

Carreau, P. J. (1972). Rheological equations from molecular network theories. *Transactions of the Society of Rheology*, *16*(1), 99–127.

Casanellas, L., & Ortín, J. (2011). Laminar oscillatory flow of Maxwell and Oldroyd-B fluids: Theoretical analysis. *Journal of Non-Newtonian Fluid Mechanics*, *166*(23-24), 1315–1326.

Cattaneo, C. (1948). Sulla Conduzione del Calore. *Atti del Seminario Matematico e Fisico dell' Universitá di Modena*, *3*, 83–101.

Chakrabarti, A., & Gupta, A. S. (1979). Hydromagnetic flow and heat transfer over a stretching sheet. *Quarterly of Applied Mathematics*, *1*(2), 73–78.

Chambré, P. L., & Acrivos, A. (1956). On chemical surface reactions in laminar boundary layer flows. *Journal of Applied Physics*, *27*(11), 1322–1328.

Chamkha, A. J. (1997). Non-Darcy fully developed mixed convection in a porous medium channel with heat generation/absorption and hydromagnetic effects. *Numerical Heat Transfer; Part A: Applications: An International Journal of Computation and Methodology*, *32*(6), 653–675.

Chamkha, A. J., Al-Mudhaf, A. F., & Pop, I. (2006). Effect of heat generation or absorption on thermophoretic free convection boundary layer from a vertical flat plate embedded in a porous medium. *International Communications in Heat and Mass Transfer*, *33*(9), 1096–1102.

Chen, K. K., & Libby, P. A. (1968). Boundary layers with small departures from the Falkner-Skan profile. *Journal of Fluid Mechanics*, *33*(2), 273–282.

Chhabra, R. P. (2010). Non-Newtonian fluids: An introduction. *Rheology of Complex Fluids*, 3–34.

Chiam, T. C. (1995). Hydromagnetic flow over a surface stretching sheet with a power-law velocity. *International Journal of Engineering Science*, *33*(3), 429–435.

Choi, J. J., Rusak, Z., & Tichy, J. A. (1999). Maxwell fluid suction flow in a channel. *Journal of Non-Newtonian Fluid Mechanics*, *85*(2-3), 165–187.

Christensen, R. M. (1982). *Theory of Viscoelasticity: An Introduction* (Second ed.). New York, USA: Academic Press.

Christov, C. I. (2009). On frame indifferent formulation of the Maxwell-Cattaneo model of finite-speed heat conduction. *Mechanics Research Communications*, *36*(4), 481–486.

Coward, A. V., & Renardy, Y. Y. (1997). Thin film core-annular flow of upper-convected Maxwell liquids. *Journal of Non-Newtonian Fluid Mechanics*, *70*, 155–183.

Crane, L. J. (1970). Flow past a stretching plate. *Zeitschrift für Angewandte Mathematik und Physik*, *21*(4), 645–647.

Devi, S. P., & Thiyagarajan, M. (2006). Steady nonlinear hydromagnetic flow and heat transfer over a stretching surface of variable temperature. *Heat and Mass Transfer*, *42*(8), 671–677.

Evans, J. D., & Hagen, T. (2008). Viscoelastic sink flow in a wedge for the UCM and Oldroyd-B models. *Journal of Non-Newtonian Fluid Mechanics*, *154*(1), 39–46.

Falkner, V., & Skan, S. (1931, November). Solutions of the boundary-layer equations. *The London, Edinburgh and Dublin Philosophical Magazine and Journal of Science Series 7*, *12*(80), 865–896.

Fang, T., & Zhang, J. (2008). An exact analytical solution of the Falkner-Skan equation with mass transfer and wall stretching. *International Journal of Non-Linear Mechanics*, *43*(9), 1000–1006.

Fang, T., Zhang, J., & Yao, S. (2009). Slip MHD viscous flow over a stretching sheet - An exact solution. *Communications in Nonlinear Science and Numerical Simulation*, *14*(11), 3731–3737.

Fetecau, C., Athar, M., & Fetecau, C. (2009). Unsteady flow of a generalized Maxwell fluid with fractional derivative due to a constantly accelerating plate. *Computers and Mathematics with Applications*, *57*(4), 596–603.

Fick, A. (1855). Ueber Diffusion. *Annalen der Physik und Chemie*, *170*(1), 59–86.

Fourier, J.-B.-J. (1822). *Théorie Analytique de la Chaleur*. Paris, France: Libraire pour les Mathématiques, l'Architecture Hydraulique el la Marine.

Ganapathirao, M., Ravindran, R., & Pop, I. (2013). Non-uniform slot suction (injection) on an unsteady mixed convection flow over a wedge with chemical reaction and heat generation or absorption. *International Journal of Heat and Mass Transfer*, *67*, 1054–1061.

Han, S., Zheng, L., Li, C., & Zhang, X. (2014). Coupled flow and heat transfer in viscoelastic fluid with Cattaneo-Christov heat flux model. *Applied Mathematics Letters*, *38*, 87–93.

Hartmann, J., & Lazarus, F. (1937). Experimental investigations on the flow of mercury in a homogeneous magnetic field. *Kongelige danske videnskabernes selskab. Matematisk-Fysiske Meddelelser*, *15*(7), 6–7.

Hartree, D. R. (1937). On an equation occurring in Falkner and Skan's approximate treatment of the equations of the boundary layer. In *Mathematical proceedings of the cambridge philosophical society* (Vol. 33, pp. 223–239). Cambridge, England: Cambridge University Press.

Hayat, T., Abbas, Z., Javed, T., & Sajid, M. (2009). Three-dimensional rotating flow induced by a shrinking sheet for suction. *Chaos, Solitons and Fractals*, *39*(4), 1615–1626.

Hayat, T., Farooq, M., Iqbal, Z., & Alsaedi, A. (2012). Mixed convection Falkner–Skan flow of a Maxwell fluid. *Journal of Heat Transfer*, *134*(11), 114504.

Hayat, T., Javed, T., & Abbas, Z. (2008). Slip flow and heat transfer of a second grade fluid past a stretching sheet through a porous space. *International Journal of Heat and Mass Transfer*, *51*(17), 4528–4534.

Hayat, T., Muhammad, T., Al-Mezal, S., & Liao, S. (2016a). Darcy-Forchheimer flow with variable thermal conductivity and Cattaneo-Christov heat flux. *International Journal of Numerical Methods for Heat and Fluid Flow*, *26*(8), 2355–2369.

Hayat, T., Waqas, M., Shehzad, S. A., & Alsaedi, A. (2016b). Stretched flow of Carreau nanofluid with convective boundary condition. *Pramana - Journal of Physics*, *86*(1), 3–17.

Hossain, M. A., & Takhar, H. S. (1996). Radiation effect on mixed convection along a vertical plate with uniform surface temperature. *Heat and Mass Transfer*, *31*(4), 243–248.

Howarth, L. (1949). On the solution of the laminar boundary layer equations. In *Proceedings of the royal society a* (Vol. 4, pp. 149–154). Cambridge, England: Royal Society Publishing.

Jamaludin, A., Nazar, R., & Shafie, S. (2017). Boundary layer flow and heat transfer in a viscous fluid over a stretching sheet with viscous dissipation, internal heat generation and prescribed heat flux. In *Proceedings of the 24th national symposium on mathematical sciences* (Vol. 1870, p. 040029). Terengganu, Malaysia: AIP Publishing.

Javed, T., Abbas, Z., Sajid, M., & Ali, N. (2011). Heat transfer analysis for a hydromagnetic viscous fluid over a non-linear shrinking sheet. *International Journal of Heat and Mass Transfer*, *54*(9), 2034–2042.

Kandasamy, R., Abd, W., & Khamis, A. (2006). Effects of chemical reaction, heat and mass transfer on boundary layer flow over a porous wedge with heat radiation in the presence of suction or injection. *Theoretical and Applied Mechanics*, *33*(2), 123–148.

Kasim, A. R. M., Mohammad, N. F., & Shafie, S. (2012). Effect of heat generation on free convection boundary layer flow of a viscoelastic fluid past a horizontal circular cylinder with constant surface heat flux. In *The 5th international conference on research and education in mathematics* (Vol. 286, pp. 286–292). Bandung, Indonesia: AIP Publishing.

Kasmani, R., Sivasankaran, S., & Siri, Z. (2014). Convective heat transfer of nanofluid past a wedge in the presence of heat generation / absorption with suction / injection. In *Proceedings of the 21st national symposium on mathematical sciences* (Vol. 1605, pp. 506–511). Penang, Malaysia: AIP Publishing.

Kays, W. M., & Crawford, M. E. (1993). *Convective Heat and Mass Transfer* (Third ed.). New Jersey, USA: McGraw-Hill.

Khan, M., & Hashim. (2015). Boundary layer flow and heat transfer to Carreau fluid over a nonlinear stretching sheet. *AIP Advances*, *5*(10), 107293.

Khan, M., Karim, I., Islam, M., & Wahiduzzaman, M. (2014). MHD boundary layer radiative, heat generating and chemical reacting flow past a wedge moving in a nanofluid. *Nano Convergence*, *1*(1), 1–13.

Khan, M., Malik, M. Y., Salahuddin, T., & Khan, I. (2016). Heat transfer squeezed flow of Carreau fluid over a sensor surface with variable thermal conductivity: A numerical study. *Results in Physics*, *6*, 940–945.

Khan, M. I., Waqas, M., Hayat, T., Khan, M. I., & Alsaedi, A. (2017). Chemically reactive flow of upper-convected Maxwell fluid with Cattaneo–Christov heat flux model. *Journal of the Brazilian Society of Mechanical Sciences and Engineering*, *39*(11), 4571–4578.

Khan, W. A., & Pop, I. (2013). Boundary layer flow past a wedge moving in a nanofluid. *Mathematical Problems in Engineering*, *2013*, 637285.

Khan, Y. (2014). Two-dimensional boundary layer flow of chemical reaction MHD fluid over a shrinking sheet with suction and injection. *Journal of Aerospace Engineering*, *27*(3), 04014019.

Krishnamurthy, M. R., Gireesha, B. J., Prasannakumara, B. C., & Gorla, R. S. R. (2016). Thermal radiation and chemical reaction effects on boundary layer slip flow and melting heat transfer of nanofluid induced by a nonlinear stretching sheet. *Nonlinear Engineering*, *5*(3), 147–159.

Krishnaprakas, C. K., Narayana, K. B., & Dutta, P. (2000). Radiation in boundary layer flow of an absorbing, emitting and anisotropically scattering fluid. *International Journal of Numerical Methods for Heat and Fluid Flow*, *10*(5), 530–540.

Kumar, H. (2011). Heat transfer over a stretching porous sheet subjected to power law heat flux in presence of heat source. *Thermal Science*, *15*(SUPPL.2), 187–194.

Layek, G. C., Mukhopadhyay, S., & Samad, S. A. (2007). Heat and mass transfer analysis for boundary layer stagnation-point flow towards a heated porous stretching sheet with heat absorption/generation and suction/blowing. *International Communications in Heat and Mass Transfer*, *34*(3), 347–356.

Libby, P. A., & Liu, T. M. (1967). Further solutions of the Falkner-Skan equation. *American Institute of Aeronautics and Astronautics Journal*, *5*(5), 1040–1042.

Lock, R. C. (1951). The velocity distribution in the laminar boundary layer between parallel streams. *Quarterly Journal of Mechanical and Applied Mathematics*, *4*(1), 42–63.

Macosco, C. W. (1994). *Rheology: Principles, Measurements and Applications*. New York, USA: Wiley-VCH.

Magyari, E., & Keller, B. (2000). Exact solutions for self-similar boundary-layer flows induced by permeable stretching walls. *European Journal of Mechanics, B/Fluids*, *19*(1), 109–122.

Mahmoud, M. A., & Megahed, A. M. (2009). Effects of viscous dissipation and heat generation (absorption) in a thermal boundary layer of a non-Newtonian fluid over a continuously moving permeable flat plate. *Journal of Applied Mechanics and Technical Physics*, *50*(5), 819–825.

Majeed, A., Zeeshan, A., & Ellahi, R. (2017). Chemical reaction and heat transfer on boundary layer Maxwell Ferro-fluid flow under magnetic dipole with Soret and suction effects. *Engineering Science and Technology, an International Journal*, *20*(3), 1122–1128.

Maleque, K. A. (2013). Effects of chemical reaction and heat generation on MHD boundary layer flow of a moving vertical plate with suction and dissipation. *International Scholarly Research Notice Thermodynamics*, *8*(4), 284637.

Maxwell, J. (1867). On the dynamical theory of gases. *Philosophical Transactions*, *96*, 49–88.

Meister, B. J., & Biggs, R. D. (1969). Prediction of the first normal stress difference in polymer solutions. *American Institute of Chemical Engineers Journal*, *15*(5), 643–653.

Mohamed, M., Salleh, M., Md Noar, N., & Ishak, A. (2017). Effect of thermal radiation on laminar boundary layer flow over a permeable flat plate with Newtonian heating. *Journal of Physics: Conference Series*, *890*(1), 1–6.

Muhaimin, Kandasamy, R., & Hashim, I. (2010). Effect of chemical reaction, heat and mass transfer on nonlinear boundary layer past a porous shrinking sheet in the presence of suction. *Nuclear Engineering and Design*, *240*(5), 933–939.

Muhaimin, Kandasamy, R., & Khamis, A. B. (2008). Effects of heat and mass transfer on nonlinear MHD boundary layer flow over a shrinking sheet in the presence of suction. *Applied Mathematics and Mechanics (English Edition)*, *29*(10), 1309–1317.

Mukhopadhyay, S. (2012). Heat transfer analysis of the unsteady flow of a Maxwell fluid over a stretching surface in the presence of a heat source/sink. *Chinese Physics Letters*, *29*(5), 54703.

Mushtaq, A., Abbasbandy, S., Mustafa, M., Hayat, T., & Alsaedi, A. (2016). Numerical solution for Sakiadis flow of upper-convected Maxwell fluid using Cattaneo-Christov heat flux model. *AIP Advances*, *6*(1), 015208.

Nadeem, S., Riaz, A., Ellahi, R., & Akbar, N. S. (2013). Effects of heat and mass transfer on peristaltic flow of Carreau fluid in a vertical annulus. *Applied Nanoscience*, *4*(4), 393–404.

Olajuwon, B. I. (2011). Convection heat and mass transfer in a hydromagnetic Carreau fluid past a vertical porous plate in presence of thermal radiation and thermal diffusion. *Thermal Science*, *15*(Suppl.2), 241–252.

Oldroyd, J. G. (1950). On the formulation of rheological equations of state. *Proceedings of the Royal Society A: Mathematical, Physical and Engineering Sciences*, *200*(1063), 523–541.

Pandey, P. K. (2017). A numerical method for the solution of general third order boundary value problem. *Bulletin of the International Mathematical Virtual Institute*, *7*, 129–138.

Pantokratoras, A. (2006). The Falkner-Skan flow with constant wall temperature and variable viscosity. *International Journal of Thermal Sciences*, *45*(4), 378–389.

Prandtl, L. (1904). Über flüssigkeitsbeweigung bei sehr kleiner reibung. *Internationalen Methmatker Kongresses zu Heidelberg*, *3*, 484–491.

Qasim, M., & Noreen, S. (2013). Falkner-Skan flow of a Maxwell fluid with heat transfer and magnetic field. *International Journal of Engineering Mathematics*, *2013*, 692827.

Rajagopal, K. R., Gupta, A. S., & Na, T. Y. (1983). A note on the Falkner-Skan flows of a non-Newtonian fluid. *International Journal of Non-Linear Mechanics*, *18*(4), 313–320.

Ramesh, G. K., & Gireesha, B. J. (2014). Influence of heat source/sink on a Maxwell fluid over a stretching surface with convective boundary condition in the presence of nanoparticles. *Ain Shams Engineering Journal*, *5*(3), 991–998.

Rashidi, M. M., & Mohimanian, S. A. (2010). Analytic approximate solutions for unsteady boundary-layer flow and heat transfer due to a stretching sheet by homotopy analysis method. *Nonlinear Analysis: Modelling and Control*, *15*(1), 83–95.

Sahi, R. K., Jator, S. N., & Khan, N. A. (2013). Continuous fourth derivative method for third order boundary value problems. *International Journal of Pure and Applied Mathematics*, *85*(5), 907–923.

Sakiadis, B. C. (1961). Boundary layer behavior on continuous solid surfaces. *American Institute of Chemical Engineers Journal*, *7*(1), 26–28.

Salama, A. A., & Mansour, A. A. (2005). Fourth-order finite-difference method for third-order boundary-value problems. *Numerical Heat Transfer, Part B: Fundamentals*, *47*(4), 383–401.

Sarpkaya, T. (1961). Flow of non-Newtonian fluids in a magnetic field. *American Institute of Chemical Engineers Journal*, *7*(2), 324–328.

Schlichting, H., & Gersten, K. (2017). *Boundary-Layer Theory* (Ninth ed.). Berlin, Germany: Springer.

Shateyi, S. (2013). A new numerical approach to MHD flow of a Maxwell fluid past a vertical stretching sheet in the presence of thermophoresis and chemical reaction. *Boundary Value Problems*, *196*, 1–14.

Shehzad, S. A. (2012). Boundary layer flow of Maxwell fluid with power law heat flux and heat source. *International Journal of Numerical Methods for Heat & Fluid Flow*, *23*(7), 1225–1241.

Shehzad, S. A., Abbasi, F. M., Hayat, T., & Ahmad, B. (2016). Cattaneo-Christov heat flux model for third-grade fluid flow towards exponentially stretching sheet. *Applied Mathematics and Mechanics (English Edition)*, *37*(6), 761–768.

Shehzad, S. A., Hayat, T., Qasim, M., & Asghar, S. (2013). Effects of mass transfer on MHD flow of Casson fluid with chemical reaction and suction. *Brazilian Journal of Chemical Engineering*, *30*(1), 187–195.

Singh, V., & Agarwal, S. (2013). Flow and heat transfer of Maxwell fluid with variable viscosity and thermal conductivity over an exponentially stretching sheet. *American Journal of Fluid Dynamics*, *3*(4), 87–95.

Spriggs, T. W., Huppler, J. D., & Bird, R. B. (1966). An experimental appraisal of viscoelastic models. *Transactions of the Society of Rheology*, *10*(1), 191–213.

Stewartson, K. (1954). Further solutions of the Falkner-Skan equation. In *Mathematical proceedings of the cambridge philosophical society* (Vol. 50, pp. 454–465). Cambridge, England: Cambridge University Press.

Sui, J., Zheng, L., & Zhang, X. (2016). Boundary layer heat and mass transfer with Cattaneo-Christov double-diffusion in upper-convected Maxwell nanofluid past a stretching sheet with slip velocity. *International Journal of Thermal Sciences*, *104*, 461–468.

Tsai, R. (1999). A simple approach for evaluating the effect of wall suction and thermophoresis on aerosol particle deposition from a laminar flow over a flat plate. *International Communications in Heat and Mass Transfer*, *26*(2), 249–257.

Utreja, L. R., & Chung, T. J. (1989). Combined convection-conduction- radiation boundary layer flows using optimal control penalty finite elements. *Journal of Heat Transfer*, *111*, 433–437.

Utz, W. R. (1977). Existence of solutions of a generalized Blasius equation. *Journal of Mathematical Analysis and Applications*, *66*(1), 55–59.

Vajravelu, K., & Nayfeh, J. (1992). Hydromagnetic convection at a cone and a wedge. *International Communications in Heat and Mass Transfer*, *19*(5), 701–710.

Vieru, D., Fetecau, C., & Fetecau, C. (2008). Flow of a viscoelastic fluid with the fractional Maxwell model between two side walls perpendicular to a plate. *Applied Mathematics and Computation*, *200*(1), 459–464.

Waini, I., Zainal, N., & Khashi'ie, N. (2017). Aligned Magnetic Field Effects on Flow and Heat Transfer of the Upper-Convected Maxwell Fluid over a Stretching/Shrinking Sheet. In *International conference on engineering technology 2016* (Vol. 97, p. 01078). Ho Chi Minh City, Vietnam: EDP Sciences.

Waqas, M., Hayat, T., Farooq, M., Shehzad, S. A., & Alsaedi, A. (2016). Cattaneo-Christov heat flux model for flow of variable thermal conductivity generalized Burgers' fluid. *Journal of Molecular Liquids*, *220*, 642–648.

Yacob, N. A., Ishak, A., & Pop, I. (2011). Falkner–Skan problem for a static or moving wedge in nanofluids. *International Journal of Thermal Sciences*, *50*(2), 133–139.

Yao, S., Fang, T., & Zhong, Y. (2011). Heat transfer of a generalized stretching/shrinking wall problem with convective boundary conditions. *Communications in Nonlinear Science and Numerical Simulation*, *16*(2), 752–760.

Yih, K. A. (1998). Uniform suction/blowing effect on forced convection about a wedge: Uniform heat flux. *Acta Mechanica*, *128*, 173–181.